VOL. 11 NO. 5 MAY 1966
PUBLISHED MONTHLY

Journal of

ELECTROANALYTICAL CHEMISTRY

International Journal Dealing with all Aspects of Electroanalytical Chemistry, Including Fundamental Electrochemistry

E L S E V I E R

GENERAL INFORMATION

See also Suggestions and Instructions to Authors which will be sent free, on request to the Publishers.

Types of contributions

(a) Original research work not previously published in other periodicals.
(b) Reviews on recent developments in various fields.
(c) Short communications.
(d) Bibliographical notes and book reviews.

Languages

Papers will be published in English, French or German.

Submission of papers

Papers should be sent to one of the following Editors:
Professor J. O'M. Bockris, John Harrison Laboratory of Chemistry, University of Pennsylvania, Philadelphia 4, Pa., U.S.A.
Dr. R. Parsons, Department of Chemistry, The University, Bristol 8, England.
Professor C. N. Reilley, Department of Chemistry, University of North Carolina, Chapel Hill, N.C., U.S.A.

Authors should preferably submit two copies in double-spaced typing on pages of uniform size. Legends for figures should be typed on a separate page. The figures should be in a form suitable for reproduction, drawn in Indian ink on drawing paper or tracing paper, with lettering etc. in thin pencil. The sheets of drawing or tracing paper should preferably be of the same dimensions as those on which the article is typed. Photographs should be submitted as clear black and white prints on glossy paper.
All references should be given at the end of the paper. They should be numbered and the numbers should appear in the text at the appropriate places.
A summary of 50 to 200 words should be included.

Reprints

Twenty-five reprints will be supplied free of charge. Additional reprints can be ordered at quoted prices. They must be ordered on order forms which are sent together with the proofs.

Publication

The *Journal of Electroanalytical Chemistry* appears monthly and has six issues per volume and two volumes per year, each of approx. 500 pages.

Subscription price (post free): £ 12.12.0 or $ 35.00 or Dfl. 126.00 per year; £ 6.6.0 or $ 17.50 or Dfl. 63.00 per volume.
Additional cost for copies by air mail available on request.
For advertising rates apply to the publishers.

Subscriptions

Subscriptions should be sent to:

ELSEVIER PUBLISHING COMPANY, P.O. Box 211, Amsterdam, The Netherlands.

UNE NOUVELLE TECHNIQUE DE L'ELECTROLYSE: L'ELECTRODE A CONVECTION THERMIQUE. APPLICATION AUX METHODES ELECTROCHIMIQUES D'ANALYSE

L. DUCRET ET C. CORNET

Service de Chimie Analytique, Département P.C.M. Centre National d'Etudes des Télécommunications, Issy les Moulineaux, Seine (France)

(Reçu le 2 juillet, 1965)

Ière PARTIE: L'ÉLECTRODE À CONVECTION THERMIQUE (1)

Les méthodes électrochimiques d'analyse utilisent couramment le phénomène de convection et presque exclusivement la convection mécanique. La solution et l'électrode indicatrice sont donc toujours en mouvement relatif. Si l'électrode est fixe, la solution est animée d'une vitesse aussi constante que possible, au contraire si la solution est immobile, les diverses électrodes utilisées sont animées de mouvements périodiques: électrodes solides vibrantes ou tournantes, électrode liquide comme l'électrode à gouttes de mercure dont le volume varie en fonction du temps. La reproductibilité de la courbe, $i=f(E)$ (i, courant d'électrolyse; E, potentiel de l'électrode indicatrice) dépend beaucoup de la stabilité et de la reproductibilité du mode de convection utilisé. Nous avons pensé qu'il était possible de substituer la convection thermique à la convection mécanique, en créant entre une électrode indicatrice fixe et une solution initialement immobile un gradient de température convenable et constant par chauffage ou refroidissement de l'électrode. S'il est difficile pratiquement de soustraire des calories de manière continue et mesurable, il est par contre très simple de fournir des quantités de chaleur connues en utilisant l'effet Joule. C'est donc finalement le chauffage électrique de l'électrode que nous avons retenu de préférence à l'écoulement continu et régulier d'un fluide à l'intérieur d'une électrode creuse.

1. APPAREILLAGE

Circuit d'électrolyse

C'est un montage classique à trois électrodes utilisant un potentiostat et un voltmètre électronique (Fig. 1).

Electrodes

Nous avons étudié deux types différents d'électrode à convection thermique.

(a) Electrode à circulation de liquide. L'électrode (Fig. 2) est un tube de platine à 10% de rhodium de 12 cm de longueur, de diamètre extérieur 1.5 mm et de diamètre intérieur 1 mm. Ce tube est recourbé en forme de U. Ses extrémités présentent des renflements qui permettent leur raccordement au circuit de circulation.

En fonctionnement, l'intérieur de l'électrode est parcouru par un liquide dont la température est supérieure ou inférieure à celle de la solution.

(b) Electrode à chauffage électrique. L'électrode est chauffée par effet Joule. C'est par exemple un fil de platine de quelques millimètres et de faible diamètre

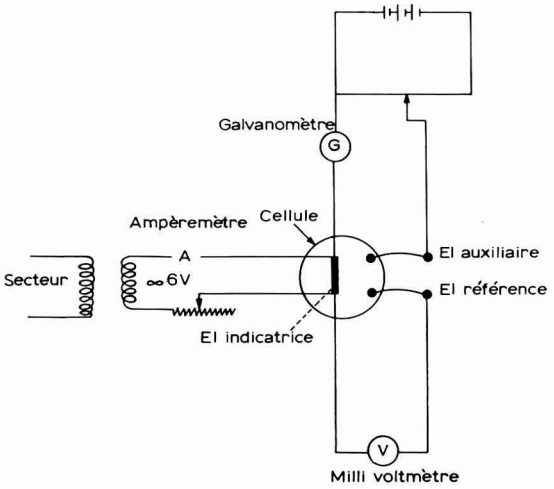

Fig. 1. Schéma du circuit d'électrolyse.

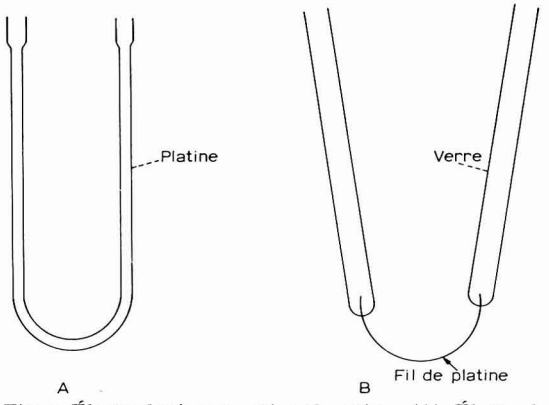

Fig. 2. Électrodes à convection thermique (A), Électrode à circulation de liquide; (B), Électrode à chauffage électrique.

(0.2–0.6 mm) soudé à deux tubes de verre remplis de mercure dans lequel viendront plonger les deux conducteurs du circuit de chauffage (Fig. 2).

Cellule d'électrolyse

C'est une cellule type Métrohm à 5 sorties rodées. Elle est thermostatée dans une cuve à eau, régulée par une résistance chauffante commandée par un thermomètre à contact. La cellule est construite en verre mince pour faciliter les échanges thermiques.

Barbotage d'azote

Les solutions sont débarrassées de l'oxygène dissous par un barbotage d'azote R de 15 min. Un serpentin immergé dans la cuve thermostatée réchauffe le gaz à la température de la solution.

II. ÉTUDE DE L'INFLUENCE DE LA CONVECTION THERMIQUE SUR LA DENSITÉ DU COURANT D'ÉLECTROLYSE

Soit Q le nombre de calories cédées par l'électrode en une seconde et S la surface de cette électrode.

Le tracé d'une série de courbes intensité–potentiel à l'aide d'un système rédox rapide, permet d'étudier l'influence de Q/S cal cm^{-2} sec^{-1} (ou Q/S W cm^{-2}) sur la densité du courant limite de diffusion.

Ces courbes ont été tracées avec les deux types d'électrodes précédemment décrits.

A. Convection thermique par circulation de liquide

(a) Par chauffage de l'électrode

Etalonnage de l'électrode. L'étalonnage de l'électrode permet d'établir la correspondance entre Q/S et Δt (Δt représente la différence de température entre la solution et le liquide traversant l'électrode).

Nous avons procédé par calorimétrie.

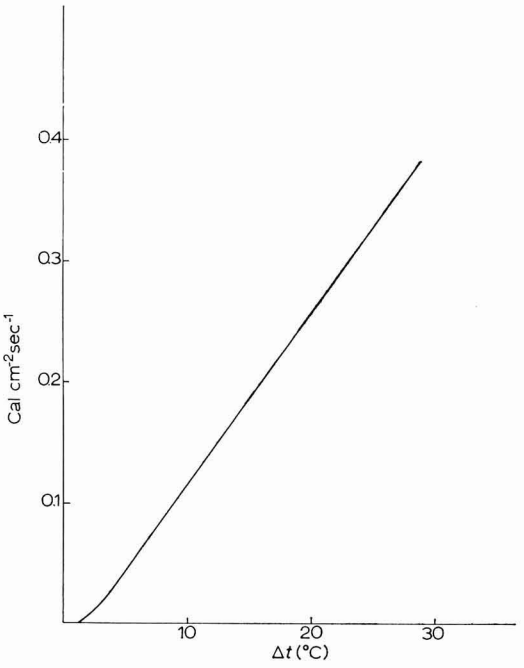

Fig. 3. Courbe d'étalonnage.

Le calorimètre est un vase de Dewar de 100 ml, calorifugé par de la laine de verre. Le couvercle en mousse expansée est percé pour le passage du thermomètre et des canalisations d'entrée et de sortie du liquide de circulation.

L'élévation de la température de l'eau du calorimètre doit être faible par rapport à Δt, afin que la quantité de chaleur Q/S ne varie pas au cours de l'expérience. Un thermomètre au 1/100 a été utilisé.

Un bac à eau alimente l'électrode. Une distance invariable de 50 cm sépare son niveau de celui du calorimètre.

La durée de l'expérience est courte. Une variation du niveau de l'eau dans le bac d'alimentation apporterait une modification du débit.

Dans la cellule d'électrolyse, un gradient de température s'établit entre l'électrode et la solution. Les conditions d'étalonnage devant être identiques aux conditions d'utilisation, la solution ne sera pas agitée pendant l'expérience. Nous ne procéderons à l'homogénéisation que par la suite.

Mode opératoire. 100 ml d'eau sont placés dans le calorimètre. L'électrode y est immergée. Son bord supérieur affleure juste la surface et à l'équilibre on relève la température initiale t_1 de la solution. L'eau du bac de circulation a été thermostatée à la température t_2 telle que $t_2 - t_1 = \Delta t$. Le chronomètre est déclanché à l'instant précis ou le circuit d'eau est ouvert dans l'électrode. De même l'eau est chassée de l'intérieur de celle-ci à l'expiration du temps prévu pour l'expérience. Sa durée est établie par tâtonnement. Elle doit être conforme aux conditions précédemment exposées. La température finale de la solution est relevée après agitation et homogénéisation. L'équilibre est atteint en une minute. Le refroidissement dû à la déperdition de chaleur dans le calorimètre ne dépasse pas 1/100 de degré par minute. L'élévation

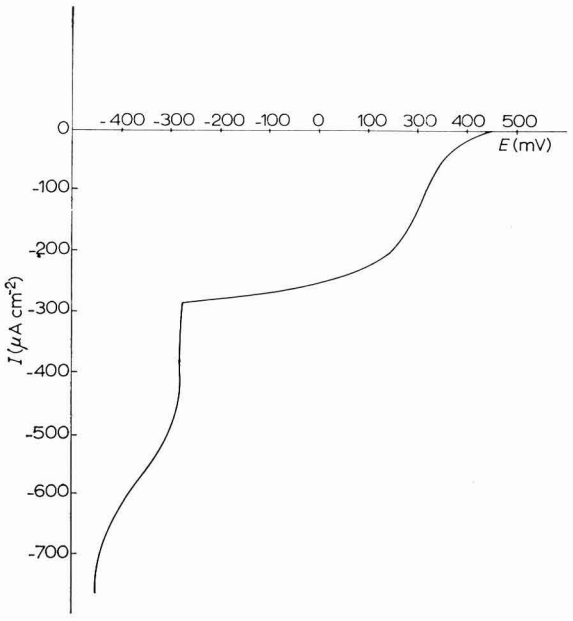

Fig. 4. Réduction de Cu^{2+} sur l'électrode de Pt poli.

de température de l'eau étant en général voisine de 1°, aucune correction n'a été apportée à la lecture directe du thermomètre. A partir de ces résultats nous avons pu tracer la courbe d'étalonnage (Fig. 3).

Tracé des courbes intensité–potentiel. Pour limiter sa surface, une partie de l'électrode a été recouverte d'un vernis qui empêche les réactions électrochimiques et rend négligeables les échanges thermiques avec la solution.

Nous avons utilisé une solution de chlorure cuivrique à la concentration $5 \cdot 10^{-3}$ *M* en milieu HCl *N*. L'oxygène dissous se réduit au même potentiel que le cuivre. Un barbotage d'azote de 15 min l'élimine.

L'ion cuivrique se réduit à l'électrode de convection thermique suivant la réaction:

$$Cu^{2+} + \bar{e} + 2\ Cl^- \rightarrow CuCl_2^-$$

Dans le compartiment séparé une anode de graphite plonge dans le même électrolyte.

Mode opératoire. 60 ml de solution sont placés dans la cellule immergée dans le bac thermostaté à la température $t_1 = 20°$. Après le barbotage d'azote, le liquide de chauffage dont la température est t_2 commence à circuler dans l'électrode. L'établissement de la convection thermique n'est pas instantanée. L'expérience montre que les courants sont stables après 2 min. La courbe intensité–potentiel (Fig. 4) est tracée point par point en explorant le domaine de potentiel s'étendant de +400 à −300 mV (électrode au calomel saturé).

Tracé de la courbe $i = f(Q/S)$. La température t_1 de la solution cuivrique est

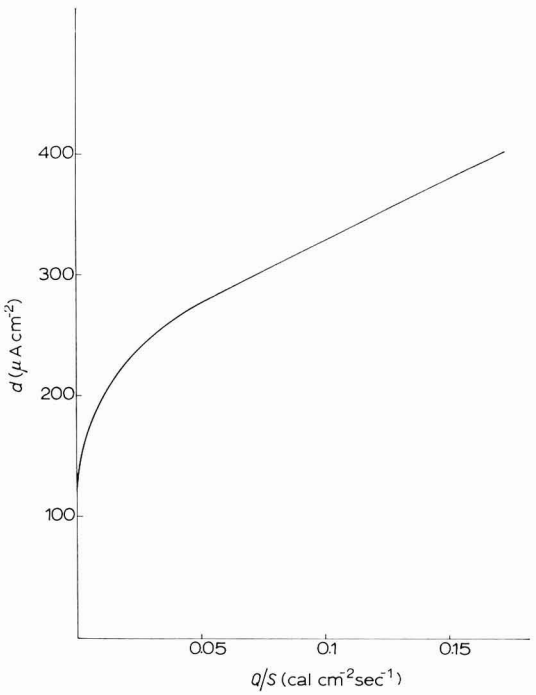

Fig. 5. Courbe $d = f(Q/S)$ par chauffage de l'électrode.

maintenue constante. Des courbes intensité–potentiel sont tracées pour diverses valeurs de la température t_2 du liquide de circulation. Le palier du courant limite de diffusion se place entre -50 et -250 mV. Arbitrairement le potentiel de -200 mV est choisi pour la mesure de l'intensité. La courbe de la Fig. 5 représente la variation de la densité du courant lorsque Q/S varie entre 0 et 0.3 cal cm^{-2} sec^{-1}. L'expérience

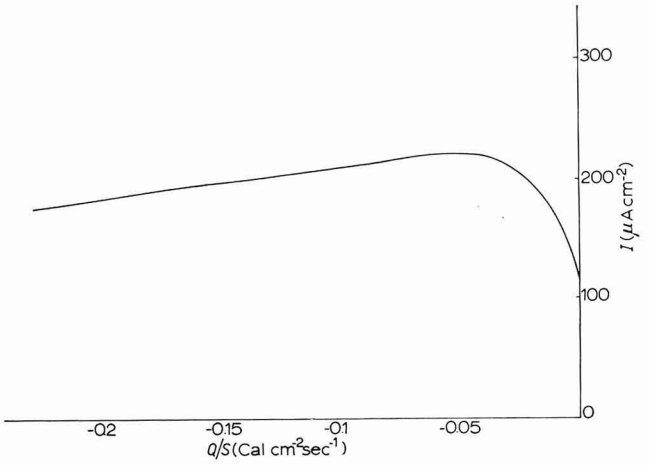

Fig. 6. Courbe de $d = f(Q/S)$ par refroidissement de l'électrode.

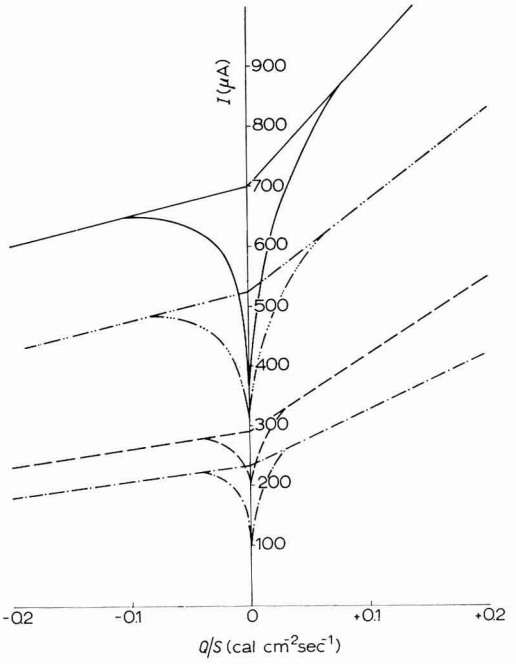

Fig. 7. Courbe de $i = f(Q/S)$ à différentes températures de solution. (——) 50°, (—··—) 40°, (— — —) 30°, (—·—) 20°.

montre qu'une bonne reproductibilité des mesures associée à une excellente stabilité du courant d'électrolyse est obtenue lorsque l'expression Q/S atteint 0.06 cal cm^{-2} sec^{-1}.

(b) Par refroidissement de l'électrode

Un courant de convection prend naissance dès qu'il existe un gradient de température entre la solution et l'électrode. Ce résultat doit être obtenu quelque soit son signe.

C'est ce que nous avons essayé de vérifier: dans une première expérience, l'eau traversant l'électrode circule à des températures inférieures à celle de la solution qui reste à 20°.

Le même mode opératoire à été utilisé. Nous avons ainsi tracé la courbe (Fig. 6) de la densité du courant limite de diffusion en fonction de Q/S.

(c) A diverses températures de la solution

Dans les mêmes conditions une série de courbes a été tracée pour des valeurs de Q/S comprises entre -0.3 et 0.3 cal cm^{-2} sec^{-1} à diverses températures t_1 de la solution cuivrique.

Les résultats sont représentés sur la Fig. 7.

Remarque

Le point de congélation de l'eau limite l'étude vers les basses températures. Une circulation d'alcool a été essayée. Mais ce solvant ayant un coefficient d'échange thermique bien inférieur à celui de l'eau, il est nécessaire d'introduire une différence de température, Δt, deux fois plus importante pour obtenir une même valeur de Q/S. Dans ces conditions on constate rapidement un givrage sur l'électrode et toute mesure devient impossible.

L'étude a été également limitée à 50°. A cette température, pour une valeur de Q/S de 0.3 cal cm^{-2} sec^{-1} l'eau de circulation est à 70°. La dilatation de l'électrode de Pt n'est plus négligeable et provoque des fissures dans le vernis qui la recouvre partiellement.

B. Convection thermique par effet Joule

En vue d'une utilisation pratique de l'électrode à convection thermique, il est préférable de disposer d'une source de calories plus facilement réglable et plus souple que la circulation d'un liquide à l'intérieur de l'électrode. Le chauffage par effet Joule a été employé. L'électrode est décrite précédemment (Fig. 2).

Chauffage en courant continu. L'électrode est alimentée par une batterie de 6 V. Un rhéostat permet de règler l'intensité.

La quantité de chaleur cédée par l'électrode par seconde est

$$Q = \frac{RI^2}{J} = \frac{\varrho l I^2}{Js}$$

ou l représente le longueur utile de l'électrode, s sa section et ϱ sa résistivité.

Si d est le diamètre de l'électrode

$$Q = \frac{4\varrho l I^2}{J\pi \cdot d^2}$$

L'expression Q/S s'écrit en exprimant le diamètre en centimètres et l'intensité en ampères

$$\frac{Q}{S} = \frac{4\varrho}{J\pi^2} \cdot \frac{I^2}{d^3}$$

Pour le platine, cette expression peut s'écrire pratiquement:

$$\frac{Q}{S} = 10^{-6} \cdot \frac{I^2}{d^3}$$

Les résultats obtenus par circulation de liquide ont montré qu'une quantité de chaleur minimum de 0.06 cal cm^{-2} sec^{-1} est nécessaire pour obtenir une convection suffisante. Une valeur supérieure à ce minimum est obtenue en utilisant par exemple un courant de 3A et une électrode de platine de 1.6 cm de longueur et 0.4 mm de diamètre. La valeur de l'expression Q/S est alors de 0.14 cal cm^{-2} sec^{-1}.

La surface de l'électrode étant voisine de 0.2 cm^2, la quantité de chaleur cédée à la solution est de 0.028 cal sec^{-1}. Le volume de la solution étant de 60 ml, l'apport des calories nécessaires à la convection pour la durée d'une expérience est donc négligeable.

Avec cette électrode alimentée en courant continu, nous avons tracé la courbe intensité–potentiel de la réduction du cérium cérique à la concentration $5 \cdot 10^{-3}$ M en milieu sulfurique normal. Le pont d'agar–agar au chlorure de potassium reliant la solution à l'électrode de référence, a été remplacé par un pont d'agar–agar au sulfate.

Nous avons ainsi obtenu la courbe 1 de la Fig. 8. Dans ces conditions, l'expé-

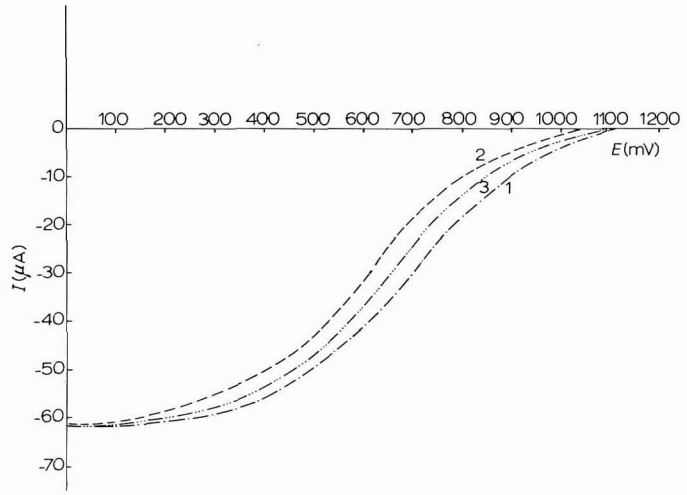

Fig. 8. Courbes de réduction de Ce^{4+} ($5 \cdot 10^{-3}$ N) en fonction de la nature du courant de chauffage. (1), courant continu; (2), courant continu; (3) courant alternatif.

rience montre que pour un potentiel imposé à l'électrode, le courant d'électrolyse atteint son équilibre en moins de 10 sec et reste ensuite parfaitement stable dans le temps. La reproductibilité est excellente: 0.3% pour un courant de 50 μA.

La courbe 2 de la Fig. 8 a été obtenue en inversant le sens du courant de chauffage. Les deux courbes sont identiques mais déplacées par translation de 100

mV. Ce décalage est dû à la chute ohmique entre les deux extrémités de l'électrode.

Remarque. En prenant pour le platine une résistivité de $1.2 \times 10^{-5}\ \Omega cm^{-1}$, le calcul de la chute ohmique dans l'électrode donne 46 mV. En inversant le sens du courant l'écart entre les deux courbes serait de 92 mV. L'incertitude sur la valeur de ϱ permet d'admettre la valeur de 100 mV trouvée expérimentalement.

Chauffage en courant alternatif. La batterie d'alimentation est remplacée par un transformateur qui délivre une tension alternative de 6 V. La courbe intensité–potentiel obtenue dans ces conditions est la courbe 3 de la Fig. 8. Elle se place exactement entre les courbes 1 et 2. Nous pouvons en déduire que l'électrode alimentée en courant alternatif se comporte comme une surface statistiquement équipotentielle.

Ce système de chauffage a été adopté pour tous les essais suivants.

Les remarques précédentes concernant la stabilité et la reproductibilité du courant d'électrolyse sont valables pour ce mode de chauffage.

Essais avec des électrodes de platine de différents diamètres

En utilisant le système rédox $Cu^{2+}/CuCl_2^-$, une série de courbes densité de courant en fonction de Q/S, a été tracée avec des électrodes de platine poli de différents diamètres. Elles doivent nous permettre de déterminer avec quelle précision la formule $Q/S = 10^{-6} I^2/d^3$ peut être appliquée.

Nous avons obtenu la courbe (Fig. 9) pour des fils de platine de 0.3, 0.4 et 0.5

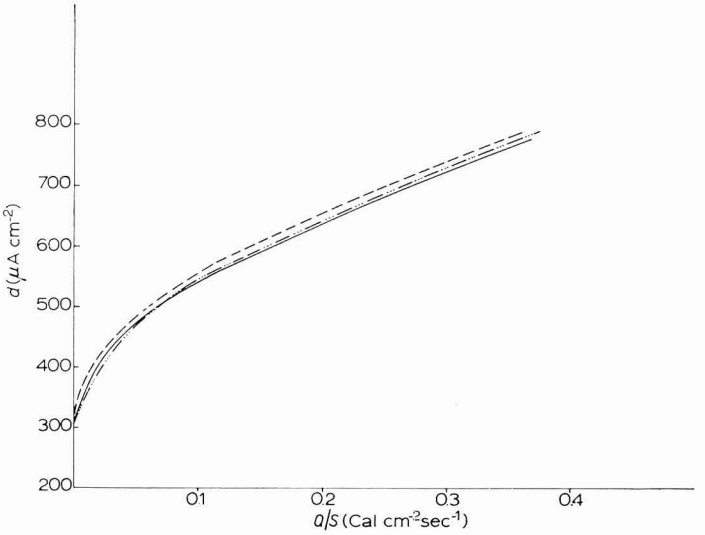

Fig. 9. Courbes $d = f(Q/S)$ avec différents diamètres d'électrodes. (·····), 0.3; (– –), 0.4; (—), 0.5 mm.

mm de diamètre. Ces courbes sont très rapprochées les unes des autres et les faibles écarts existants proviennent d'une précision insuffisante dans la détermination du diamètre exact des fils. L'erreur est d'autant plus grande que dans la formule d est élevé au cube. La précision sur la détermination de l'intensité du courant de chauffage est bonne.

Les résultats de la Fig. 9 montrent que la formule est utilisable et que Q/S

peut être déterminé sans courbe d'étalonnage par une simple mesure du diamètre du fil et un choix convenable de l'intensité du courant de chauffage.

Essais avec différents systèmes électrochimiques

Avec une électrode donnée nous avons tracé les courbes de la densité de courant en fonction de Q/S pour différents systèmes électrochimiques rapides.

La Fig. 10 représente les courbes obtenues pour la réduction d'une solution de

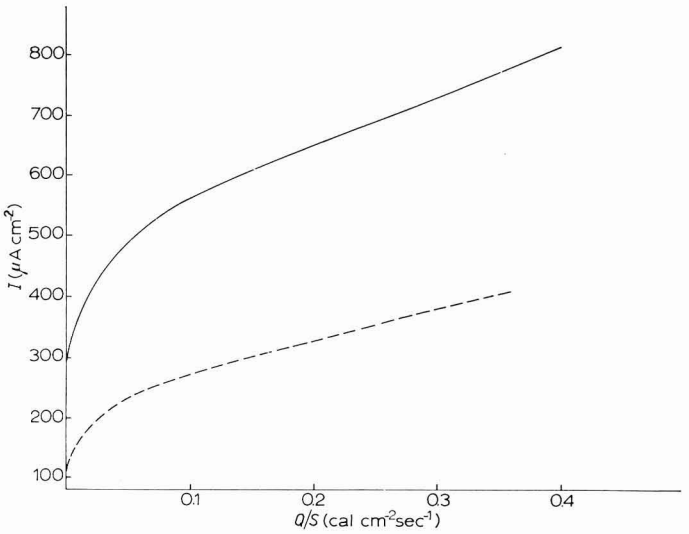

Fig. 10. Courbes $i = f(Q/S)$ pour Cu^{2+}, $5 \cdot 10^{-3}$ N, (—); Ce^{4+}, $5 \cdot 10^{-3}$ N, (– –). Electrode 0.4 mm diamètre.

chlorure cuivrique à la concentration $5 \cdot 10^{-3}$ M et la réduction d'une solution de cérium cérique de même concentration.

Les densités de courant sont différentes, mais la forme générale des courbes reste inchangée.

III. CONCLUSION

Les courbes de la densité de courant en fonction de Q/S présentent la même forme quelque soit l'électrode, le mode de chauffage ou le système électrochimique utilisé.

Chaque courbe présente deux parties distinctes (Fig. 7):

(i) Pour les valeurs de Q/S inférieures à 0.06 cal cm^{-2} sec^{-1} la densité du courant limite de diffusion croît d'autant plus rapidement que Q/S est petit.

(ii) Pour des valeurs de Q/S supérieures à 0.06 cal cm^{-2} sec^{-1}, la densité du courant limite de diffusion croît linéairement avec Q/S.

Les courbes obtenues par refroidissement de l'électrode présentent également ces deux zones:

(i) Une partie non linéaire où la densité de courant croît d'une manière analogue à la première fraction de la courbe obtenue par chauffage.

(ii) Une partie également linéaire mais où la densité de courant décroît quand $-Q/S$ augmente.

Comparons ces deux courbes avec celles obtenues par agitation mécanique.

Les courbes de la densité de courant en fonction de l'intensité d'une agitation mécanique quelconque présentent une première partie rapidement croissante en tous points analogue à celle obtenue par convection thermique. La deuxième partie est une droite horizontale où la densité de courant est indépendante de l'agitation.

Nous pouvons en déduire que les parties de courbes comprises entre -0.06 et $+0.06$ cal cm^{-2} sec^{-1} représentent la variation de la densité de courant due principalement à la convection. En dehors de ces limites la pente des parties linéaires est positive, négative ou nulle suivant que l'électrode est chauffée, refroidie ou reste à la température constante. Cette partie de la courbe représente donc la variation de la densité de courant en fonction du gradient de température autour de l'électrode.

Extrapolons à $Q/S=0$, les parties linéaires de la Fig. 7. Nous constatons que pour chaque température de la solution, les deux portions de droite pour Q/S positif et négatif sont concourantes quand $Q/S=0$. En effet, en ce point, le gradient de tem-

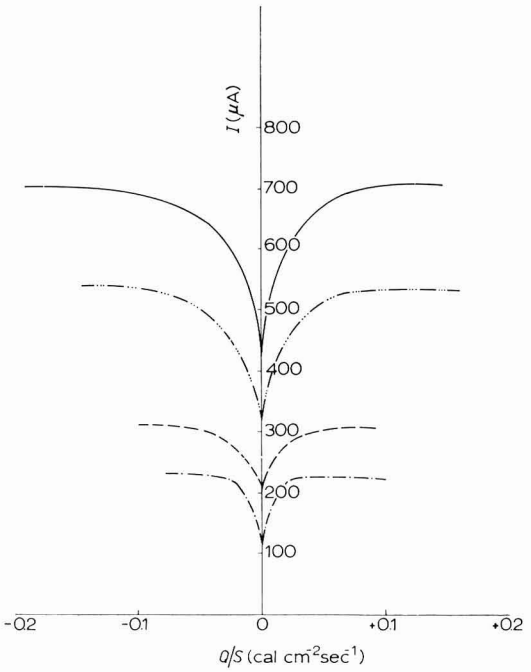

Fig. 11. Courbe $i = f(Q/S)$ à différentes températures de solution; (----), 20°; (——), 30°; (·····), 40°; (—), 50°.

pérature entre la solution et l'électrode est nul. Les parties non linéaires des courbes Q/S sont donc la somme de deux composantes: la convection et l'effet thermique.

Eliminons l'action du gradient de température par soustraction de celui-ci sur les ordonnées. Nous obtenons la Fig. 11 analogue aux courbes observées pour la convection mécanique.

Dans tous les cas un apport de chaleur de 0.1 cal cm^{-2} sec^{-1} est largement suffisant pour assurer un courant de convection stable et reproductible.

2ème PARTIE: ÉTUDE DE DIVERSES ÉLECTRODES ET DE QUELQUES SYSTÈMES REDOX

1. ÉLECTRODE DE PLATINE PLATINÉ

L'électrode est un fil de platine de 1.7 cm de longueur et de 0.5 mm de diamètre, soudé à ses extrémités à deux tubes de verre suivant le modèle représenté Fig. 2.

L'électrode est platinée par électrolyse pendant 5 min avec une densité de courant de 0.06 A cm^{-2}. L'anode est une capsule de platine poli.

La composition du bain est la suivante: 30 ml d'eau, 1 g de tétrachlorure de platine, 8 mg d'acétate de plomb.

La surface réelle d'une électrode de platine platiné n'est pas connue. On sait qu'elle est grande par rapport à la surface de l'électrode de platine poli servant de support. Il est dès lors impossible de calculer la quantité de chaleur nécéssaire à la convection par centimètre carré d'électrode et par seconde.

Comme pour l'électrode de platine poli correspondante, des courbes intensité–potentiel ont été tracées en utilisant une solution $5 \cdot 10^{-3}$ M de chlorure cuivrique en milieu HCl N.

Le palier du courant limite de diffusion se situe entre $+100$ et -50 mV (par rapport à l'électrode au calomel saturée) (Fig. 12). Au potentiel zéro pris arbitrairement la variation du courant de diffusion en fonction de l'intensité du courant de chauffage est identique à celle obtenue avec la même électrode polie.

Dans ces conditions, la formule: $Q/S = 10^{-6} I^2/d^3$ a été appliquée à l'électrode platinée. Ici d représente le diamètre de l'électrode support de platine poli et I l'intensité du courant de chauffage. Les courbes Q/S en fonction de l'intensité du courant d'électrolyse ont été tracées à la même échelle sur la Fig. 13 pour la même

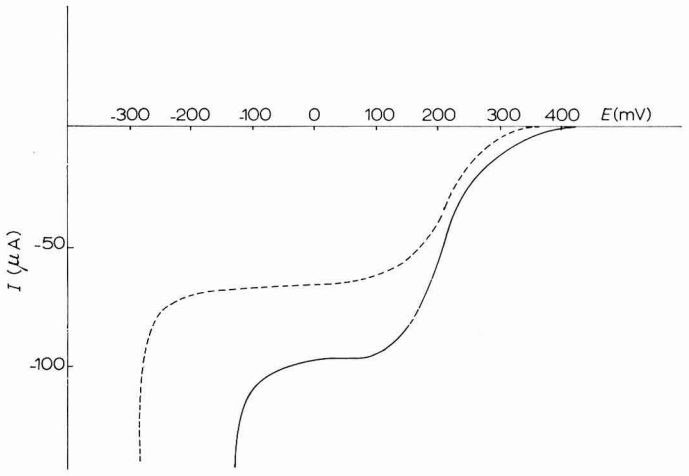

Fig. 12. Réduction de Cu^{2+} sur platine poli (– –); platine platiné (—). Electrode 0.4 mm diamètre.

électrode de platine poli et platiné. Elles montrent que pour une même solution, l'intensité du courant d'électrolyse est plus grande sur platine platiné, mais que la quantité Q/S nécessaire pour assurer une convection convenable est identique.

Tracé des courbes intensité–potentiel de réduction de l'eau et de ses ions

Il est possible (2) de mettre en évidence la réduction successive des ions hydrogène et de l'eau suivant les réactions:

$$2\,H^+ + 2\,\bar{e} \rightleftharpoons H_2\nearrow$$

et

$$2\,H_2O + 2\,\bar{e} \rightleftharpoons H_2\nearrow + 2OH^-$$

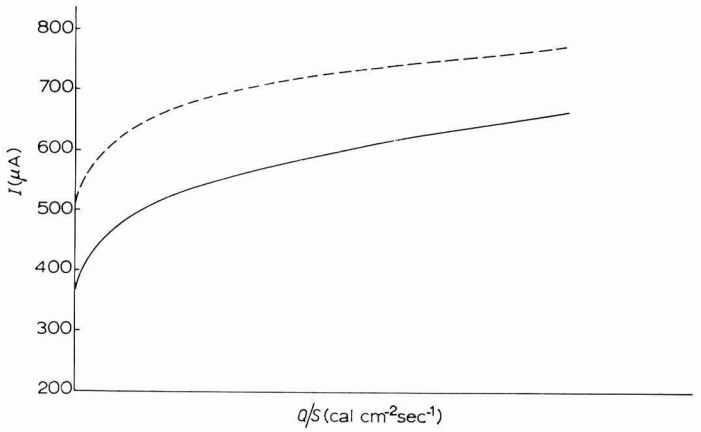

Fig. 13. Courbe de $i=f(Q/S)$ sur électrode de platine poli (—); platiné (---).

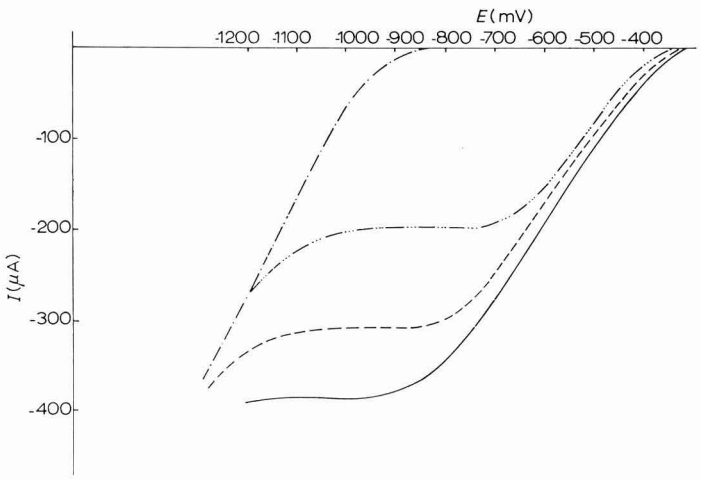

Fig. 14. Réduction de H^+ et de H_2O sur platine platiné. (-·-·), KCl, 1 N seul; (-···-), KCl, 1 N + H^+; $2.5 \cdot 10^{-3}$ N; (---), KCl, 1 N + H^+, $4 \cdot 10^{-3}$ N; (—), KCl, 1 N + H^+, $5 \cdot 10^{-3}$ N.

Avec les méthodes de convection habituellement utilisées, le tracé de la courbe représentant la réduction des ions de l'eau est en général difficile par suite de l'instabilité du courant d'électrolyse. Avec l'électrode de convection thermique l'équilibre est atteint rapidement, le courant d'électrolyse est stable à un potentiel donné et la reproductibilité satisfaisante. Nous avons tracé, par exemple (Fig. 14), les courbes intensité–potentiel de solutions de HCl aux concentrations $2.5 \cdot 10^{-3}$ N, $4 \cdot 10^{-3}$ N et $5 \cdot 10^{-3}$ N en présence de KCl N. Ces courbes présentent un palier du courant limite de diffusion dont la hauteur est proportionelle à la concentration des ions hydrogène : l'erreur relative est voisine de 1.5%.

Remarque

Toutes les courbes de la Fig. 14 ont été tracées avec le même platinage de l'électrode. Des courbes identiques avec la même électrode replatinée font apparaître de légères fluctuations dans la hauteur des paliers de diffusion. La méthode de platinage n'est certainement pas très reproductible et la surface de l'électrode doit varier d'un platinage à l'autre.

II. ÉLECTRODE DE GRAPHITE

L'électrode est un cylindre de graphite pur pour spectrographie de 2 cm de longueur et de 2 mm de diamètre. Ses extrémités sont serties à l'intérieur de manchons en laiton isolés de la solution par une couche d'araldite D. Des fils de cuivre soudés sur les manchons et recouverts de vernis assurent les contacts électriques. La résistance de l'électrode est voisine de 0.076 Ω ; sa surface 1.26 cm^2. Un courant de 3 A est nécessaire pour que l'électrode libère plus de 0.1 cal cm^{-2} sec^{-1}.

Cette électrode a été utilisée pour tracer les courbes intensité–potentiel de réduction des ions Cu^{2+} en milieu HCl N suivant la réaction :

$$Cu^{2+} + 1\ \bar{e} + 2\ Cl^- \rightleftharpoons CuCl_2^-$$

Avant chaque essai l'oxygène dissous est chassé par un barbotage d'azote R.

Les courbes de la Fig. 15 ont été tracées à partir de solutions de $CuCl_2$ 10^{-3}, $2 \cdot 10^{-3}$ et $5 \cdot 10^{-3}$ N en milieu HCl N ; le palier du courant limite de diffusion apparaît entre −300 et 100 mV (par rapport au calomel saturé). Il est proportionnel aux concentrations.

Les courbes intensité–potentiel de la Fig. 15 ont été tracées en partant des potentiels électronégatifs vers les potentiels électropositifs. Au potentiel de départ de −600 mV, un dégagement d'hydrogène est visible sur l'électrode. Les courbes tracées dans le sens opposé sont déformées et leur pente est importante. Il est probable que l'électrode contient de l'oxygène occlus dont la vague se superpose à celle des ions cuivriques. Le dégagement d'hydrogène chasse l'oxygène retenu dans les pores de l'électrode et à ce potentiel les dernières traces d'oxygène sont rapidement réduites.

III. ÉLECTRODES AMALGAMÉES

En raison des difficultés technologiques, nous n'avons pas tenté la fabrication

d'une électrode de mercure à convection thermique.

Deux types d'électrodes amalgamées ont été essayés.

1. Electrode d'or

Une électrode d'or amalgamé a été étudiée. Elle est fragile, et son état de surface se modifie rapidement. Les résultats ne sont pas reproductibles et l'électrode n'est pratiquement pas utilisable.

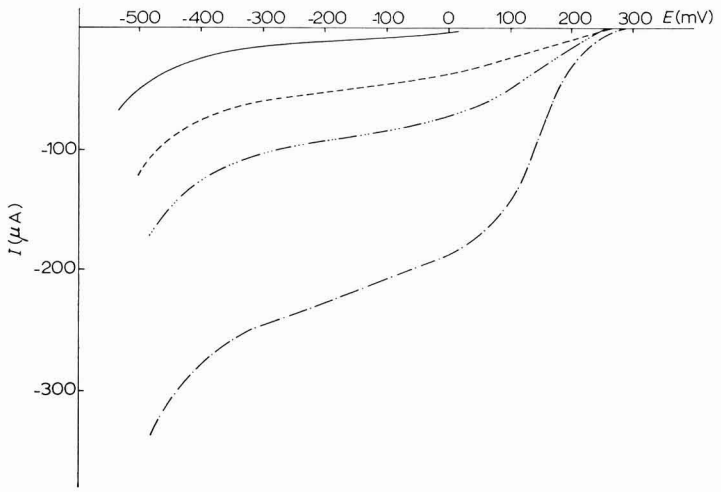

Fig. 15. Réduction de Cu^{2+} dans HCl, 1 N, sur un électrode de graphite (—), HCl seul; (– –), Cu^{2+}, 10^{-3} N; (·····), Cu^{2+}, $2 \cdot 10^{-3}$ N; (·–·–), Cu^{2+}, $5 \cdot 10^{-3}$ N.

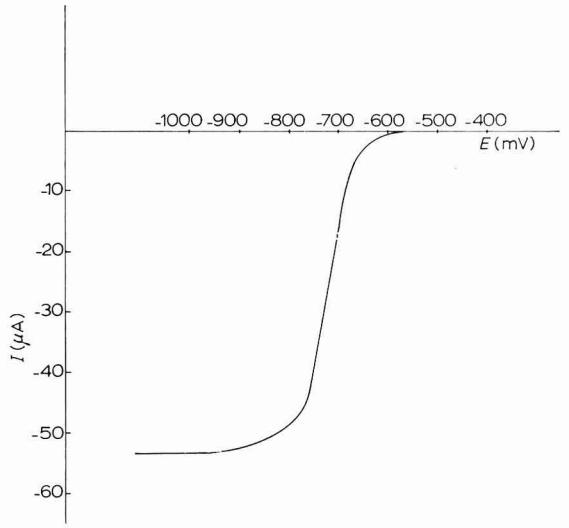

Fig. 16. Réduction des ions cadmium, 10^{-3} N, sur électrode recouverte de mercure.

2. Electrode de platine recouverte de mercure

L'électrode est du type décrit Fig. 2. Le fil de platine a 0.3 mm de diamètre et 2 cm de longueur.

La seule méthode qui donne des dépôts de mercure adhérents et des résultats reproductibles est celle décrite par GARDINER, MARPLE ET ROGERS[3].

Mode opératoire. Pendant 5 min une différence de potentiel de 3 V est imposée entre l'électrode et une capsule de platine servant d'anode. L'électrolyte est une solution de nitrate mercurique.

Au début de l'électrolyse, le fil de platine est le siège d' un intense dégagement d'hydrogène qui disparaît après recouvrement total de l'électrode par le mercure. Le mercure en excès apparaît sous forme de fines gouttelettes qui sont enlevées par contact avec un fil de cuivre amalgamé. L'électrode est alors rincée abondamment à l'eau.

Courbe intensité–potentiel du cadmium et du plomb. La courbe de réduction d'une solution de sulfate de cadmium à la concentration 10^{-3} N dans KCl 0.1 N est représentée (Fig. 16). L'oxygène dissous a été chassé par barbotage d'azote R. Sur un total de huit essais l'erreur maximum sur la hauteur du palier de diffusion est de 2 μA. Le potentiel de demi-vague (−0.625 mV) est reproductible à ± 5 mV près. Les courbes de réduction du plomb à la concentration 10^{-4} N dans une solution de KCl 0.1 N présentent la même reproductibilité.

Pour ces deux métaux la hauteur du palier de diffusion est proportionnelle à la concentration.

CONCLUSION

L'électrode à convection thermique alimentée par effet Joule est utilisable quelque soit le matériau conducteur choisi comme électrode.

Les courbes intensité–potentiel sont reproductibles.

A un potentiel imposé, le courant d'électrolyse est stable et l'équilibre est atteint après quelques secondes. Cependant les densités de courant des paliers de diffusion sont légèrement plus faibles que sur une électrode vibrante.

3ème PARTIE. COULOMÉTRIE À POTENTIEL CONSTANT

On sait que l'intensité du courant d'électrolyse au cours d'une coulométrie à potentiel constant, varie théoriquement suivant une loi exponentielle $i = i_0 e^{-kt}$. La quantité totale d'électricité mise en jeu est

$$q = \int_0^\infty i \mathrm{d}t = \frac{i_0}{k}$$

en désignant par i_0 le courant initial. Les paramètres, i_0 et k, peuvent être déterminés facilement en traçant la droite $\log i = \log i_0 - (\log e)\, kt$. Toutefois ce procédé qui a été décrit par MACNEVIN ET BAKER[4] semble rencontrer de sérieuses difficultés lorsqu'il est appliqué au dosage de faibles quantités en utilisant les procédés classiques d'électrolyse et d'agitation mécanique. L'expérience montre que la décroissance exponentielle du courant n'est pas suivie d'une façon suffisamment rigoureuse. Aussi les techniques actuelles emploient des coulomètres intégrateurs. De plus l'influence

du courant résiduel qui peut devenir prépondérante en fin de dosage apporte une difficulté supplémentaire. On est donc amené à faire un essai "à blanc" pour déterminer la quantité d'électricité correspondant au courant résiduel pendant la durée de l'électrolyse. Nous avons pensé que les propriétés de l'électrode à convection thermique permettaient d'utiliser les conclusions théoriques. Le dosage par électrolyse à potentiel constant se résume alors au tracé de la droite $\log i = \log i_0 - (\log e)\, kt$ pendant les premières minutes de l'opération, ce qui permet de déterminer facilement par le calcul les valeurs de i_0 et de k. De plus l'influence du courant résiduel peut être rendue négligeable si les conditions opératoires sont choisies pour que le courant initial soit élevé.

I. ÉLECTRODE ET CELLULE D'ÉLECTROLYSE

Electrode

L'électrode est un cylindre de platine à 10% de rhodium, de 16.55 mm de diamètre extérieur et de 21.5 mm de hauteur. Sa surface apparente est de 11.2 cm². Un fil de platine soudé sur ce tube, relie l'électrode au circuit extérieur (photo).

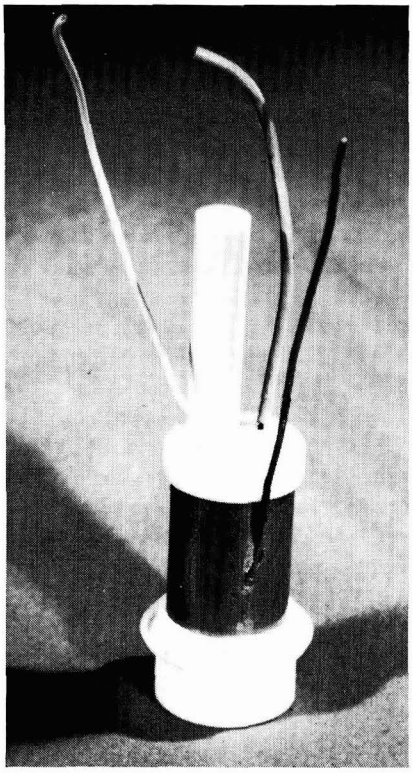

Le chauffage est indirect. Il est assuré par une résistance de 2.1 Ω constituée par un fil de 16 cm de longueur et de 13.5 Ω de résistance au mètre. Ce fil est bobiné sur un mandrin en Téflon. L'ensemble est placé au centre du cylindre de platine dont

le fond est obturé par une plaque de Téflon. Le volume intérieur est de 3.2 ml. Il est rempli d'un liquide organique comme le xylène qui assure la transmission de la chaleur. L'électrode est fermée par un couvercle de Téflon. Une cheminée également en Téflon permet le remplissage et la dilatation du liquide. Les fils d'alimentation de la résistance de chauffage traversent le couvercle par deux passages étanches.

Nous avons établi précédemment qu'un apport de 0.1 cal cm^{-2} sec^{-1} était nécessaire pour assurer une convection efficace. L'électrode utilisée doit donc libérer environ 1.1 cal sec^{-1} ce qui entraîne un courant de chauffage de 1.5 A.

Cellule d'électrolyse

L'utilisation d'une électrode de convection thermique de grande surface pose le problème de l'évacuation de la chaleur libérée. La cellule d'électrolyse est donc un récipient à double paroi. De l'eau provenant d'un bac thermostaté en assure le refroidissement.

Etude de la convection dans la cellule

Nous avons pensé que des particules métalliques offrant le moins d'inertie possible pourraient matérialiser les courants de convection. Une suspension de poudre d'aluminium dans de l'eau contenant quelques gouttes d'un corps tensio-actif a été utilisée.

La cellule est éclairée par un projecteur et un écran de velours noir empêche la réflexion de la lumière parasite. L'électrode est largement recouverte de liquide. Après le temps de mise en équilibre de la convection (2 min) nous avons constaté en suivant le trajet suivi par les particules métalliques:

(a) Que le volume de la solution située au-dessous de l'électrode n'était pratiquement pas atteint par la convection.

(b) Que la solution recouvrant l'électrode était le siège d' un intense mouvement turbulent.

(c) Que le volume de la solution placée entre l'électrode et la paroi de la cellule était animée d'un mouvement laminaire ascendant le long de l'électrode et descendant le long de la paroi froide.

(d) Qu'une distance trop importante entre l'électrode et cette paroi donnait naissance à une zone stationnaire comprise entre les deux courants laminaires (Fig. 17A). Pour éliminer le volume de solution situé au dessous de l'électrode qui n'est pas atteint par la convection, le fond (en Téflon) de l'électrode a été élargi pour faire joint avec les parois de la cellule (voir photo). Nous avons constaté que cette modification n'apportait aucune perturbation à la forme des courants de convection.

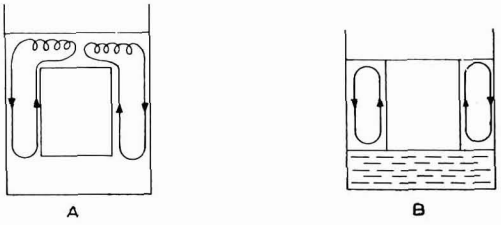

Fig. 17. Convection dans la cellule de coulométrie. Schéma des courants de convection à l'intérieur de la cellule.

Dans un autre essai, le niveau de la solution est ajusté au bord supérieur de l'électrode. Dans ces conditions, la convection est uniquement laminaire (Fig. 17B).

Au cours de ces essais, nous avons constaté que sur l'électrode comme sur la paroi froide, l'épaisseur des courants laminaires de convection est de 0.3 cm environ. La distance séparant les deux parois ne devra donc pas dépasser 0.6 cm.

La cellule utilisée est un cylindre en verre à double paroi. Son diamètre intérieur est 2.4 cm et sa hauteur 6 cm. Le diamètre de l'électrode étant de 1.6 cm la source chaude est donc séparée de la source froide par 0.4 cm. La cellule remplie de solution jusqu'au bord supérieur de l'électrode a une capacité de 5 ml.

Sur le côté de la cellule et à mi-hauteur de l'électrode une ouverture permet d'adapter un compartiment séparé. Ce compartiment est un tube coudé fermé par un verre fritté de résistance voisine de 9000 Ω.

Une électrode de platine ou de graphite de 1 cm^2 joue le rôle d'électrode auxiliaire. Un bouchon en chlorure de polyvinyle ferme la cellule.

II. RÉSULTATS EXPÉRIMENTAUX

Appareillage

Un potentiostat à réponse rapide Tacussel type PRT 2000, fixe le potentiel qui est mesuré avec précision à l'aide d'un millivoltmètre électronique type S3. L'électrode de référence est une électrode au calomel saturée. Un galvanomètre SEFRAM mesure les intensités comprises entre 0.1 et 3000 μA.

1. Dosage coulométrique des ions Cu^{2+}

La courbe intensité–potentiel de réduction des ions cuivriques Cu^{2+} en milieu HCl 1 *N* présente un palier de diffusion entre −50 et −250 mV (Fig. 4). Nous avons choisi arbitrairement le potentiel de −100 mV et le potentiostat est réglé sur cette valeur avant le début de l'électrolyse.

La réaction de réduction est la suivante:

$$Cu^{2+} + 1\ \bar{e} + 2\ Cl^- \rightleftharpoons CuCl_2^-$$

Mode opératoire. A l'aide d'une burette, on introduit dans la cellule 5 ou 6 ml d'une solution titrée de chlorure cuivrique dilué dans de l'acide chlorhydrique *N* qui sert d'électrolyte indifférent. Les masses de cuivre mises en jeu sont comprises entre 1.27 et 1.92 mg. La même solution est placée dans le compartiment séparé.

Le barbotage d'azote R et le chauffage de l'électrode sont mis en marche. Le courant d'azote est arrêté après 10 min. L'expérience montre que l'équilibre thermique de l'ensemble est atteint 2 min plus tard.

Les intensités sont relevées toutes les minutes. Dans ces conditions l'expérience montre que les courbes: logarithme de l'intensité en fonction du temps sont des droites (Fig. 18).

Résultats. Six mesures effectuées sur une masse de cuivre de 1.92 mg donnent une erreur moyenne de −1% avec une erreur maximum de −1.5% pour 1.27 mg, 4 mesures donnent une erreur moyenne de −1.5% avec une erreur maximum de −2%.

Ces erreurs sont systématiquement par défaut. Elles proviennent vraisemblablement de la construction de la cellule expérimentale. En effet une faible partie de la solution (0.05 ml) retenue dans la jonction entre la cellule et le compartiment

séparé, ne participe pas à l'électrolyse. Une jonction par rodage éliminerait certainement cette erreur.

2. Dosage coulométrique des ions Fe^{2+}

Une solution titrée environ 0.1 *N* de fer ferreux a été préparée par pesée de sel de Mohr.

Une solution de H_2SO_4 *N* sert d'électrolyte indifférent. La courbe intensité–potentiel d'oxydation du fer ferreux (Fig. 19) présente un palier de diffusion entre

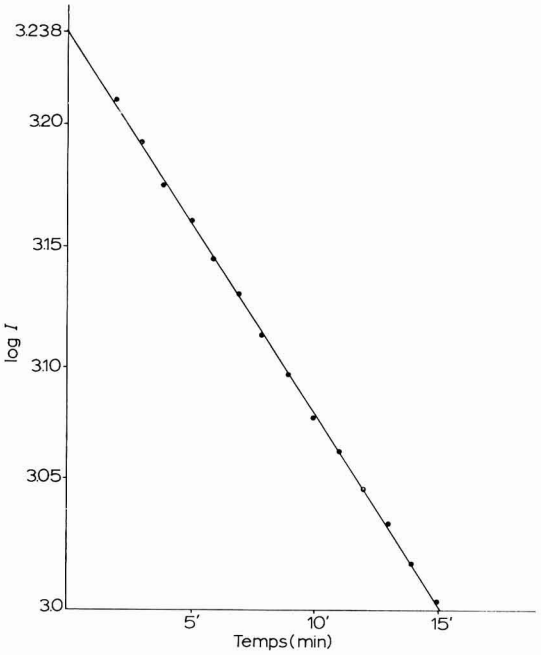

Fig. 18. Coulométrie de Cu^{2+}. Courbe de $\log i = f(t)$.

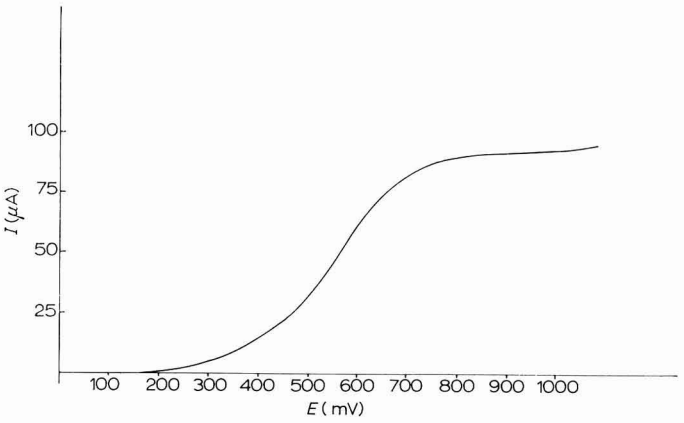

Fig. 19. Oxydation d'une solution de Fe^{2+}, $4 \cdot 10^{-3}$ *N* dans H_2SO_4 sur un électrode de platine poli.

+750 et +1050 mV (par rapport au calomel). Arbitrairement le potentiel a été fixé à +900 mV.

Nous avons constaté expérimentalement que l'introduction directe d'une solution très diluée de fer ferreux dans l'électrolyte amenait d'importantes erreurs par défaut. En effet, l'oxydation de telles solutions par l'oxygène de l'air est rapide et le contact prolongé avec l'électrode de platine accélère peut-être le phénomène. Dans la cellule, l'électrolyte indifférent sera débarrassé de l'oxygène dissous et placé en régime de convection thermique. L'introduction d'une faible quantité d'une solution de fer ferreux environ 0.1 *N* s'effectuera immédiatement avant l'électrolyse. Une ultra micro burette au 1/1000 de ml est utilisée.

Mode opératoire. 6 ml de H_2SO_4 *N* sont placés dans la cellule. Après barbotage d'azote et mise en équilibre thermique de la solution, l'électrolyte indifférent est électrolysé à un potentiel de +900 mV (par rapport au calomel). Le courant résiduel passe de 30 à 10 μA en quelques minutes puis reste stable. Le volume désiré de la solution de fer ferreux est injecté dans la cellule. En 2 min la convection thermique rend la solution homogène et la coulométrie s'effectue dans les mêmes conditions que pour les ions cuivriques.

Résultats. Pour une masse de fer voisine de 1.5 mg, les erreurs sont du même ordre de grandeur et dans le même sens que pour le dosage des ions cuivriques.

Les remarques faites précédemment restent valables.

3. Détermination du nombre d'électrons mis en jeu dans une réaction électrochimique

Le dosage coulométrique d'une quantité connue d'une substance électroactive permet de connaître le nombre d'électrons mis en jeu au cours d'une réaction électrochimique.

Nous avons tenté d'appliquer cette méthode à la coulométrie d'une quantité connue d'acide ascorbique. Les variations du potentiel de demi-vague en fonction du pH ont été étudiées par KOLTHOFF ET LAITINEN[5].

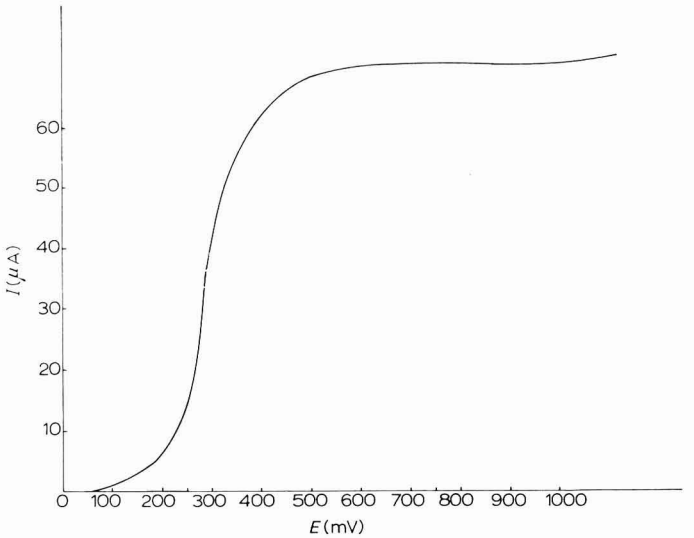

Fig. 20. Courbe $i=f(E)$ d'oxydation de l'acide ascorbique, 5.10^{-3} *N*, sur électrode de platine poli.

Le tampon métaphosphorique N de pH $=3.4$ semble convenir. Il a été utilisé comme électrolyte indifférent.

La courbe intensité–potentiel (Fig. 20) présente un palier d'oxydation de l'acide ascorbique compris entre $+550$ et 1100 mV (par rapport à une électrode au calomel saturé). Arbitrairement le potentiel de coulométrie a été fixé à 800 mV.

Une oxydation des impuretés de l'électrolyte indifférent est nécessaire. Au potentiel choisi sa durée est d'environ 1 h. Le courant résiduel se stabilise à 2.5 μA par centimètre carré d'électrode. La solution traitée peut alors être conservée sans modification pendant plusieurs jours.

Les solutions aqueuses d'acide ascorbique s'oxydent très rapidement à l'air. Toutes les manipulations s'effectueront sous courant d'azote.

Mode opératoire. Par pesée, environ 12 mg d'acide ascorbique sont introduits dans une fiole jaugée de 25 ml.

La fiole est remplie de tampon métaphosphorique N préalablement électrolysé et débarrassé d'oxygène par barbotage d'azote. Après dissolution et homogénéisation, 6 ml de solution sont immédiatement prélevés et placés dans la cellule sous balayage d'azote. La coulométrie est effectuée à $+800$ mV.

Résultats. Soit X le nombre de coulombs par électron mis en jeu dans la réaction d'oxydation.

$$X = \frac{FP}{M}$$

ou F représente le faraday, M la masse moléculaire de l'acide ascorbique et P la prise d'essai exprimées en g.

Si Y est le nombre de coulombs déterminé par coulométrie, le nombre d'électrons n mis en jeu est $n = Y/X$.

Y	X	n
3.16	1.63	1.94
3.10	1.63	1.90
2.94	1.53	1.92

Ces résultats montrent que n est égal à 2.

Remarque. A l'erreur par défaut signalée précédemment, vient s'ajouter une faible oxydation de la solution d'acide ascorbique au cours des manipulations malgré les précautions opératoires observées.

RÉSUMÉ

Dans cette nouvelle technique de l'électrolyse, la convection mécanique généralement utilisée dans les méthodes électrochimiques d'analyse est remplacée par une convection thermique obtenue en créant un gradient de température entre une électrode fixe et une solution initialement immobile. Le chauffage de l'électrode par effet Joule est le moyen pratique le plus simple de réaliser cette convection. L'expérience montre que ce mode de convection permet une excellente reproductibilité des résultats et confère au courant d'électrolyse à potentiel imposé une grande stabilité dans le temps. Les applications de cette technique décrites dans ce mémoire

sont principalement le tracé des courbes intensité–potentiel de divers systèmes oxydo-réducteurs et la description d'une coulométrie à potentiel constant par le simple tracé de la droite $\log i = f(t)$.

SUMMARY

In this new electrolysis technique, the mechanical stirring generally used in electrochemical methods of analysis is replaced by thermal stirring obtained by creating a temperature gradient between a stationary electrode and an initially immobile solution. The heating of the electrode by the Joule Effect is the simplest means of realising this. Experience has shown that this method of stirring gives excellent reproducibility of results and confers great stability on the electrolysis current of the imposed potential. The applications of this technique that spring to mind are mainly, the following of intensity–potential curves of various oxidation–reduction systems and the graphical representation of coulometry at constant potential by the simple plot of $\log i = f(t)$.

BIBLIOGRAPHIE

1 L. DUCRET, *Compt. Rend.*, 13 (1961) 1948.
2 J. COUPEZ, *Anal. Chem. Acta*, 16 (1957) 582.
3 K. W. GARDINER ET L. B. ROGERS, *Anal. Chem.*, 25 (1953) 1393; T. L. MARPLE ET L. B. ROGERS, *Anal. Chem.*, 25 (1953) 1351.
4 W. M. MACNEVIN ET B. B. BAKER, *Anal. Chem.*, 24 (1952) 986.
5 I. M. KOLTHOFF ET J. J. LINGANE, *Polarography*, Interscience Publishers Inc., New York, London, 1952, p. 729.

RATE STUDIES ON THE IODINATION OF TETRAORGANOLEAD COMPOUNDS

L. RICCOBONI, G. PILLONI, G. PLAZZOGNA AND G. TAGLIAVINI
Istituto di Chimica Analitica, Universitá di Padova (Italy)
(Received June 8th, 1965)

INTRODUCTION

Biamperometric titrations of organo-lead and -tin compounds with electrolytically-generated halogens have been described in previous papers[1-3].

In the present work, the indication current due to the I_3^-/I^- redox system was recorded continuously in order to obtain plots indicating the course of the reaction between I_3^- species and tetraorganolead compounds. The method is the same as one already described, *i.e.*, an application of the conventional dropping-mercury electrode[4]. This technique is limited to conducting solutions, but in some cases, when moderately rapid reactions occur[5-7], it is a useful alternative to spectrophotometric methods.

Iodination of tetraalkyllead compounds takes place in polar solvents in which the equilibrium $I_3^- \rightleftharpoons I_2 + I^-$ exists. Hence, the reaction:

$$R_4Pb + I_2 \rightarrow R_3Pb^+I^- + RI$$

may be followed by observing the decrease in current generated by the I_3^-/I^- system.

This paper refers to rate data on the iodination of tetramethyl-, tetraethyl- and tetrapropyl-lead in methanol, ethanol, *n*-propanol and acetonitrile, and is a preliminary contribution to the investigation of electrophilic substitution at the saturated carbon centre of organolead substrates. Such data will also indicate whether two compounds of this kind, when present together, can be titrated separately. The examination of the following mixtures has already been described[1,2,27]: Et_6Pb_2–Et_4Pb, Me_6Sn_2–Me_4Sn and Ph_6Sn_2–$Ph_3SnSnMe_3$.

Because of the extremely high reactivity of one component relative to the other, the technique of biamperometric titration could be employed in these cases.

EXPERIMENTAL

Reagents

Absolute methanol, ethanol and *n*-propanol were treated with magnesium activated with iodine under reflux and then fractionally distilled[8]. Acetonitrile was dried over phosphorous pentoxide[9] and re-distilled. Anhydrous sodium perchlorate was dried in a vacuum oven at 90° and stored over anhydrous magnesium perchlorate. Anhydrous sodium iodide (Merck reagent) was used without further purification. Tetramethyllead and tetraethyllead were kindly supplied by S.L.O.I. (Bologna,

Italy). They were purified by distillation in nitrogen[10]. $(CH_3)_4Pb$, b.p. 110–112° at 760 mm; $(C_2H_5)_4Pb$, b.p. 78–79° at 12 mm. Tetrapropyllead was prepared by the Gruttner and Kraus method[11] (b.p. 124–127° at 13 mm).

Solutions of organolead compounds of approximately 10^{-2}–10^{-3} *M* were prepared and standardized by the procedure previously described[3].

Procedure

The cell, and the arrangement of the indicator and generator electrodes used in this work, are shown in Fig. 1. The anodic compartment A, surrounded by the jacket I, is maintained at a constant temperature by circulating water. The generator and indicator circuits have been described in previous papers[1,2]. The anodic and cathodic (C) compartments are separated by a sintered-glass disc. For a typical kinetic run, compartment A was filled with a measured volume of sodium iodide–sodium perchlorate solution of known concentration. Sodium perchlorate solution was present in the cathodic compartment, C.

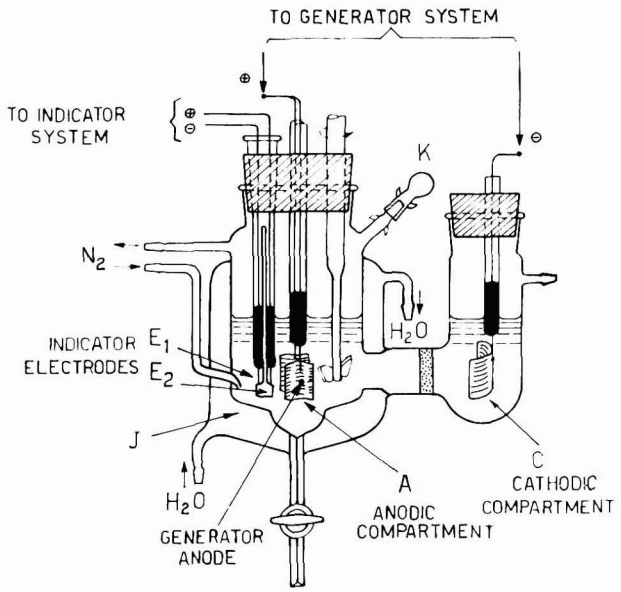

Fig. 1. Cell for kinetic measurements using a pair of indicator electrodes.

The anodic solution was then degassed with dry nitrogen. After the temperature had reached the desired value and the amperometric recording system was switched on, iodine generation was started at an appropriate constant current (5–10 mA) for a known time (40–150 sec). In order to obtain a linear dependence of the indicator current with the I_3^- concentration, it was important to use uniform stirring, at a speed which could be adjusted by means of a stroboscopic disc illuminated by a neon bulb; a stirred speed of 1,000 rev./min, was maintained. A known volume of standardized tetralkyllead solution was injected into the anode compartment through K.

One of the several kinetic plots (indicator current *vs.* time), obtained by means of a galvanometer (sensitivity $1.45 \cdot 10^{-9}$ A/mm min) and a recording device consisting of a cylinder carrying a roll of photographic paper, is given in Fig. 2. At every twentieth revolution of the cylinder, the lighting of a lamp was recorded as a thin line on the photographic roll. The interval between two vertical lines was therefore a measure of the cylinder speed. Since only three different cylinder speeds were used, kinetic plots could be obtained in which the interval between two vertical lines was 42, 83 or 165 sec.

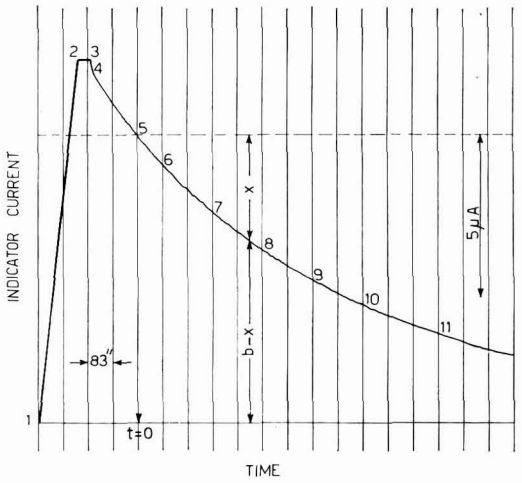

Fig. 2. Example of a kinetic plot: reaction, $Me_4Pb + I_2$, in ethanol: 0.037 *M* NaI : 0.163 *M* $NaClO_4$ at 25° (*cf.* Table 1).

Points 1, 2, 3, 4, and 5 in Fig. 2 represent the various experimental steps; 1 represents the galvanometer zero position, before iodine generation; 1–2 represents the increase in the indicator current (11.10 μA) caused by the electrolytically-generated iodine (generator current 8.70 mA; generation time 135 sec). At point 3, the organolead sample was injected. In this case, 2 ml of a $1.5 \cdot 10^{-2}$ *M* tetramethyl-lead solution was mixed with 68 ml of a $3.82 \cdot 10^{-2}$ *M* NaI solution brought to an ionic strength of 0.2 *M* by means of $NaClO_4$. The indicator current, on mixing, falls slightly due to dilution; this is represented by the interval 3–4. Although point 4 can be considered as the effective beginning of the kinetic plot, for precision purposes, point 5 was taken as zero time. The data were treated as described below.

Calculation of rate constants

The reactions were run under second-order conditions with reactant solution concentrations of approximately 10^{-4} *M* and a R_4Pb/I_2 ratio of 1 to 15. The data were treated according to the following integrated second-order rate equation:

$$k_{obs} = \frac{2.303}{t(a-b)} \log \frac{b}{a} \frac{(a-x)}{(b-x)} . \qquad (1)$$

The experimental rate equation was assumed to be

$$v = k_{obs}[R_4Pb]\,[I_3^-] \tag{2}$$

where a and b are $[R_4Pb]$ and $[I_3^-]$, respectively at zero time (Fig. 2, point 5), and $(b-x)$ is the concentration of I_3^- at time t. Since the equilibrium constants for the reaction,

$$I_3^- \rightleftarrows I_2 + I^- \tag{3}$$

in the solvents examined are about 10^{-5}–10^{-8}, and the minimum concentration of iodide was $3 \cdot 10^{-2}\ M$, it can be assumed that all the iodine generated is present as I_3^-.

The calculated values of k_{obs} (l mole^{-1} sec^{-1}) were in good agreement within 1.5%. Reproducibility was approximately 2%. Table 1 lists the data obtained for one run, the kinetic plot of which is given in Fig. 2, as an example.

TABLE 1

REACTION, $(CH_3)_4Pb + I_2$, IN ETHANOL : 0.037 M NaI : 0.163 M $NaClO_4$ AT 25°
$a = [Me_4Pb] = 4.28 \cdot 10^{-4}$; $b = [I_3^-] = 8.69 \cdot 10^{-5}$

Time (sec)	$\frac{2.303}{t(a-b)}$	$(b-x) \cdot 10^5$	$x \cdot 10^5$	$(a-x) \cdot 10^5$	k_{obs}
83	81.265	6.366	0.694	40.510	3.05
249	27.088	5.159	1.901	39.303	3.13
415	16.253	4.224	2.836	38.368	3.12
581	11.609	3.500	3.560	37.643	3.08
747	9.029	2.896	4.164	37.040	3.08
996	6.772	2.172	4.888	36.316	3.09
				Average value	3.09 ± 0.04

RESULTS AND DISCUSSION

The nature of iodine solutions

The choice of solvent for the reaction

$$R_4Pb + I_2 \rightarrow R_3PbI + RI \tag{4}$$

is important[3,25,26]. In the present work, the nature of the solvents used is such that iodine is complexed with them:

$$I_2 + S \rightleftarrows I_2.S \tag{5}$$

where S stands for the solvent. On the other hand, under these experimental conditions, equilibrium (3) is also established. Therefore, some experimental work on systems (3) and (5), for which data were not available in literature, has been carried out. Numerical values of the equilibrium constants

$$K_s = \frac{[I_2.S]}{[I_2][S]} \tag{6}$$

and

$$K = \frac{[I_2][I^-]}{[I_3^-]} \tag{7}$$

are given in Tables 2 and 3, respectively. Table 2 lists previously published values for

alcohols[12,13], together with the value determined for acetonitrile. Absorption maxima of iodine solutions are also reported.

Samples of I_2 solutions in mixtures of CCl_4 and acetonitrile were prepared and their absorbance band heights measured at wave-lengths of 517 mμ and 456 mμ. These two wave-lengths correspond to uncombined and combined iodine, respectively. Table 3 shows the K-values obtained in ethanol and n-propanol by Job's method of continuous variation[14,15]. For these systems, u.v. spectra show two isosbestic points, at 232 mμ and 268 mμ. They correspond to the conjugate redox pairs, I_3^-/I^- and I_3^-/I_2, respectively. Data for methanol[6] and acetonitrile[16] were available.

TABLE 2

EQUILIBRIUM CONSTANTS K_S (MOLE FRACTION UNITS) FOR THE REACTION, $I_2 + S \rightleftharpoons I_2S$ IN CCl_4 AT 25°

S	K_S	*Absorption maximum (mμ)*	*Ref.*
Methanol	4.65	440	12
Ethanol	4.00	443	12
Propanol	6.25	440	13
Acetonitrile	5.51	456	this work
Solvent carbon tetrachloride	—	517	this work

TABLE 3

EQUILIBRIUM CONSTANTS FOR THE SODIUM IODIDE COMPLEXES WITH IODINE IN ETHANOL AND n-PROPANOL ($I_3^- \rightleftharpoons I^- + I_2$)

$C = [I_2] + [I^-]$; $t = 25°$; $\lambda = 360$ mμ

Solvent	$C \cdot 10^4$	$K \cdot 10^5$	*Ref.*
Ethanol	1.0	2.95	this work
	2.0	3.04	
	2.5	3.06	
	10.0	2.98	
	Average value	3.01 ± 0.05	
n-Propanol	2.0	4.01	this work
	5.0	4.00	
	10.0	4.09	
	15.0	3.98	
	Average value	4.02 ± 0.04	
Methanol	—	6.54	6
Acetonitrile	—	0.004	16

The diagrams in Figs. 3 and 4 show the behaviour of absorbance, ΔA *vs.* $X = [I_2/(I_2 + NaI)]$ for ethanol and propanol, respectively, at four different concentrations and at constant $\lambda = 360$ mμ.

In these diagrams, ΔA is the difference between the experimentally-determined optical density (A_{obs}) and the optical density (A_c) which the solution would theoretic-

ally have had if there has been no reaction on mixing the components. Because the optical density of alcoholic iodine solutions varies considerably with time[17], the A_c-values were extrapolated to zero time from a series of values obtained at known time intervals.

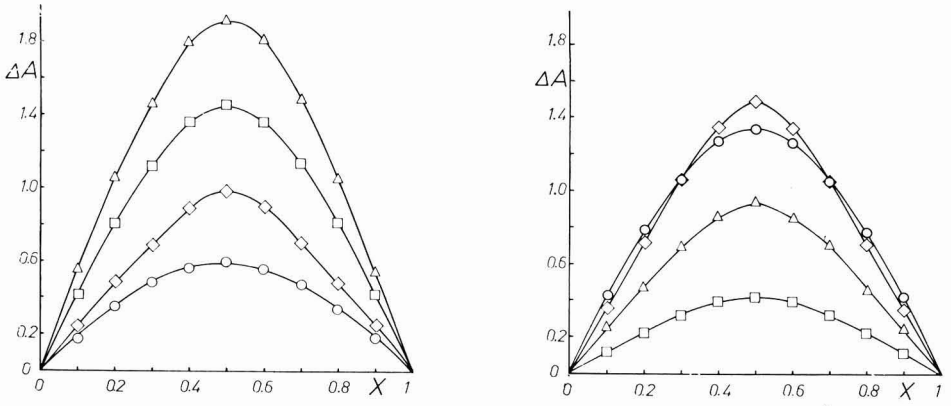

Fig. 3. Job's plot for ethanol solns. of NaI + I_2 at 25° at different concns. (λ = 360 mμ; $\varepsilon_{I_3^-}$ = 25,000). ○, 1 · 10^{-4} M; □, 2 · 10^{-4} M; △, 2.5 · 10^{-4} M; ◇, 10 · 10^{-4} M. Cell width for ○, □, △, 10 mm; for ◇, 1 mm.

Fig. 4. Job's plot for *n*-propanol solns. of NaI + I_2 at 25° at different concns. (λ = 360 mμ, $\varepsilon_{I_3^-}$ = 25,000). ○, 2 · 10^{-4} M; □, 5 · 10^{-4} M; △, 10 · 10^{-4} M; ◇, 15 · 10^{-4} M. Cell width for ○, 10 mm; for □, △, ◇, 1 mm.

The K-values given in Table 3 were calculated from the difference between theoretical and experimental absorbance maxima using known procedures[18]. The smaller value of K for acetonitrile, in comparison with the values for the other solvents, must be attributed to the much weaker solvation of the I^- ions in the former solvent than in the three alcohols[19,20]. Furthermore, I_3^- ions in acetonitrile are known to be particularly stable[16,21].

Kinetic data

According to NASIELSKI *et al.*[6] three equations should be considered:

$$v = k_1[R_4Pb][I_2][I^-] \quad (8)$$

$$v = k_2[R_4Pb][I_2] \quad (9)$$

$$v = k_3[R_4Pb][I_3^-] \quad (10)$$

By taking into account relations (2) and (7), and assuming that the rates of the forward and reverse reactions concerning the I_3^- complex are faster than the iodination rates of the organolead compounds, the following relation,

$$k_{obs} = k_1K + k_2K/[I^-] + k_3 \quad (11)$$

can be derived from eqns. (8), (9) and (10).

Relation (11) implies that k_{obs} must be linearly related to $1/[I^-]$. Table 4 shows the k_{obs}-values for tetramethyllead, obtained by varying the iodide concentration in the solvents used. The total salt concentration was kept constant by adding appropri-

TABLE 4

EFFECT OF VARYING I^- CONCENTRATION

Reaction, $Me_4Pb + I_2$, at 25°

Acetonitrile $\mu = 0.194$		*Methanol* $\mu = 0.194$		*Ethanol* $\mu = 0.194$		*n-Propanol* $\mu = 0.057$	
$[I^-]$	k_{obs}	$[I^-]$	k_{obs}	$[I^-]$	k_{obs}	$[I^-]$	k_{obs}
0.029	0.47	—	—	—	—	0.029	2.22
—	—	—	—	0.037	3.09	—	—
0.043	0.33	0.043	17.75	0.043	2.67	0.043	1.51
—	—	0.051	14.91	—	—	—	—
—	—	—	—	0.057	2.02	0.057	1.14
—	—	0.071	10.56	—	—	—	—
—	—	—	—	0.091	1.26	—	—
0.097	0.15	0.097	7.97	—	—	—	—
—	—	0.114	7.13	—	—	—	—
—	—	0.194	3.97	—	—	—	—

ate amounts of sodium perchlorate. Since all the plots of k_{obs} *vs.* $1/[I^-]$ are straight lines through the origin (Fig. 5), it may be concluded that only kinetic pathway (9) is open. Therefore eqn. (11) becomes:

$$k_{obs} = k_2 K/[I^-] \tag{12}$$

and

$$k_2 = k_{obs}[I^-]/K \tag{13}$$

This result agrees perfectly with the findings on the iodination of organotin compounds.[6]

Table 5 lists the results, at 25°, obtained for all compounds examined; k_2

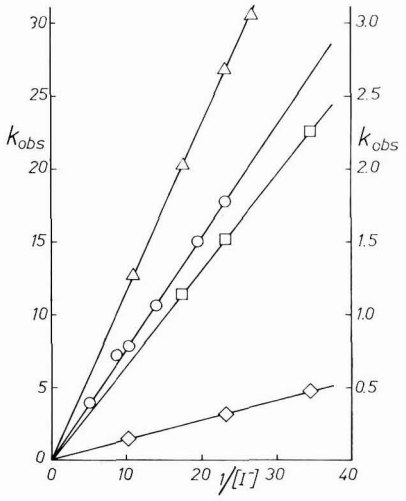

Fig. 5. Effect of iodide concn. on k_{obs}, for tetramethyllead in various solvents: ○, in methanol (k_{obs} on the left); △, ethanol; □, *n*-propanol; ◇, acetonitrile (k_{obs}-values on the right).

values ($l\,mole^{-1}\,sec^{-1}$) are also reported. In addition, the salt effect has been examined for tetramethyllead in the solvents used. k_{obs}-values relative to the various ionic strengths are given in Table 6; a positive salt effect is indicated.

TABLE 5

IODINATION OF TETRAALKYLLEAD COMPOUNDS AT 25° IN SOLVENT: 0.057 *M* NaI

Compound	*Acetonitrile*		*Methanol*		*Ethanol*		*n-Propanol*	
	k_{obs}	$k_2 \cdot 10^{-5}$	k_{obs}	$k_2 \cdot 10^{-3}$	k_{obs}	$k_2 \cdot 10^{-3}$	k_{obs}	$k_2 \cdot 10^{-3}$
Me_4Pb	0.168	2.41	10.80	9.41	1.48	2.80	1.14	1.61
Et_4Pb	0.065	0.93	4.20	3.66	0.704	1.33	0.517	0.73
$n\text{-}Pr_4Pb$	0.014	0.20	1.45	1.26	0.105	0.20	0.071	0.10

TABLE 6

IONIC STRENGTH EFFECT

Reaction $Me_4Pb + I_2$ in solvent: NaI : $NaClO_4$

Ionic strength	*Methanol* $[I^-] = 0.114$		*Ethanol* $[I^-] = 0.057$		*Acetonitrile* $[I^-] = 0.029$	
	k_{obs}	$k_2 \cdot 10^{-3}$	k_{obs}	$k_2 \cdot 10^{-3}$	k_{obs}	$k_2 \cdot 10^{-5}$
0.057	—	—	1.48	2.80	0.33	2.40
0.100	—	—	1.71	3.24	0.39	2.84
0.114	6.42	11.19	—	—	—	—
0.194	7.13	12.43	2.02	3.82	0.47	3.42
0.300	8.18	14.26	—	—	—	—

CONCLUSION

From the experimental data, it is evident that the rates of iodination in each solvent of the organolead compounds examined are quite close. It is clear, therefore, that analyses of compounds of this kind in the presence of one another cannot be achieved by means of biamperometric titration under the experimental conditions used in previous papers[1,2,27]. Nevertheless, on the basis of the rate constants (k_{obs}) determined, the system might be analysed by the differential rate method[31].

From the kinetic point of view, it may be concluded from the results that an S_E2-type electrophilic substitution takes place at the saturated carbon centre

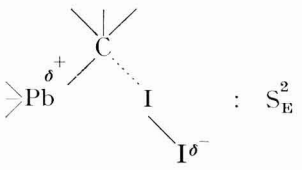

This is closely analogous to the conclusions reached by GIELEN AND NASIELSKI on the

cleavage by electrophilic reagents of Sn–C bonds in tetraorganotin compounds[22]. We reject the idea of the four-centre or cyclic transition state:

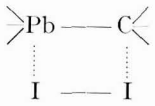

S_F^2

in view of the insignificant contribution of I^- and I_3^- species, for which no evidence of nucleophilic assistance has been found. On the other hand, the discovery of a positive salt effect agrees with a polar transition state such as S_E2 as opposed to the S_F2 four-center intermediate. The values of relative reactivities of R_4Pb compounds (Table 7), cannot be explained by taking into account only the solvation state of iodine in these solvents and assuming[12,23,24] a different polarization $I^+ - I^-$.

TABLE 7

RELATIVE REACTIVITIES

Compound	*Acetonitrile*	*Methanol*	*Ethanol*	*n-Propanol*
Me_4Pb	150	6	1.7	1
Et_4Pb	130	5	1.8	1
n-Pr_4Pb	200	12	2	1

The greater reactivity in acetonitrile may be due to greater solvation, and therefore increased stability, of the polar transition-state complex. In this connection it should be noted that exceptional solvation of heavy metal ions by acetonitrile has already been verified[21,30]. In addition, a dipolar aprotic solvent such as acetonitrile, stabilizes large polarizable anions such as I_3^-, which can be regarded as the transition state for displacement by I^- of I^+ at a univalent iodine atom[28,29]. Taking this into consideration, the following sequence of reactivity in all solvents:

$$Me_4Pb > Et_4Pb > n\text{-}Pr_4Pb\ ,$$

could be accounted for by assuming a balance of polar and steric effects of the R-groups attached to the lead atom, while the decrease in the reactivity of each substrate in acetonitrile, methanol, ethanol and n-propanol, in that order, could be dependent on the different degrees of solvation of the transition-state complex.

Further work on the electrophilic substitution on the carbon centre using tetraorganolead compounds, is obviously needed, and additional kinetic measurements are in preparation in this Institute.

ACKNOWLEDGEMENT

The authors thank Dr. COSTANZO BERNARDIN who participated in the early stage of the work. This investigation was supported by Consiglio Nazionale delle Ricerche (Roma, Italia).

SUMMARY

The analytical technique of biamperometric titration, has been utilized to obtain kinetic data in different polar solvents on the reaction,

$$R_4Pb + I_2 = R_3Pb^+I^- + RI ,$$

where R is CH_3, C_2H_5 or n-C_3H_7 .

REFERENCES

1 G. TAGLIAVINI, U. BELLUCO AND L. RICCOBONI, *Ric. Sci.*, 31 (1961) 338.
2 G. TAGLIAVINI AND G. PLAZZOGNA, *Ric. Sci.*, 32 (1962) 356.
3 G. PILLONI AND G. PLAZZOGNA, *Ric. Sci.*, 34 (1964) 27.
4 I. KOLTHOFF AND J. LINGANE, *Polarography*, Interscience Publishers Inc., New York, 1941, 2nd ed., 1952; G. SEMERANO, L. RICCOBONI AND A. FOFFANI, *Gazz. Chim. Ital.*, 79 (1949) 395; L. RICCOBONI, A. FOFFANI AND E. VECCHI, *ibid.*, 79 (1949) 418, 485; L. RICCOBONI, *Cronache di Chimica*, 4 (1964) 3.
5 D. DELHAYE, J. NASIELSKI AND M. PLANCHON, *Bull. Soc. Chim. Belges*, 69 (1960) 134.
6 M. GIELEN AND J. NASIELSKI, *Bull. Soc. Chim. Belges*, 71 (1962) 32.
7 M. GIELEN AND J. NASIELSKI, *Bull. Soc. Chim. Belges*, 71 (1962) 601.
8 H. LUND AND J. BJERRUM, *Chem. Ber.*, 64 (1931) 210.
9 G. L. LEWIS AND C. P. SMYTH, *J. Chem. Phys.*, 7 (1939) 1085.
10 G. TAGLIAVINI, G. SCHIAVON AND U. BELLUCO, *Gazz. Chim. Ital.*, 88 (1958) 746.
11 G. GRUTTNER AND E. KRAUSE, *Ber.*, 49 (1916) 1421.
12 P. A. D. DE MAINE, *J. Chem. Phys.*, 26 (1957) 1192.
13 J. GROH, *Z. Anorg. Allgem. Chem.*, 160 (1927) 287.
14 P. JOB, *Ann. Chim.*, 9 (1928) 113.
15 W. C. VOSBURGH AND G. R. COOPER, *J. Am. Chem. Soc.*, 63 (1941) 437.
16 J. DESBARRES, *Bull. Soc. Chim. France*, (1961) 502.
17 T. C. J. OVENSTON AND W. T. REES, *Anal. Chim. Acta*, 5 (1951) 123.
18 L. RICCOBONI, *Met. Ital.*, 6 (1960) 289.
19 J. E. COATES AND A. G. TAYLOR, *J. Chem. Soc.*, (1936) 1245.
20 J. F. COETZEE, Ph.D. Thesis, University of Minnesota, 1955.
21 I. M. KOLTHOFF AND J. F. COETZEE, *J. Am. Chem. Soc.*, 79 (1957) 1852.
22 M. GIELEN AND J. NASIELSKI, *J. Organometal. Chem.*, 1 (1963) 173.
23 J. KLEINBERG AND A. W. DAVIDSON, *Chem. Rev.*, (1948) 601.
24 P. A. D. DE MAINE, *J. Chem. Phys.*, 26 (1957) 1199.
25 A. J. JAKOBUWITSCH AND I. PETROV, *J. Prakt. Chem.*, 144 (1935) 67.
26 G. CALINGAERT, H. SOROOS AND H. SHAPIRO, *J. Am. Chem. Soc.*, 62 (1940) 1104.
27 G. TAGLIAVINI, *Anal. Chim. Acta*, 34 (1966) 24.
28 J. MILLER AND A. J. PARKER, *J. Am. Chem. Soc.*, 83 (1961) 117.
29 A. J. PARKER, *Quart. Rev. London*, 16 (1962) 163.
30 G. S. HAMMOND, M. F. HAWTHORNE, J. H. WATERS AND B. M. GRAYBILL, *J. Am. Chem. Soc.*, 82 (1960) 704.
31 C. N. REILLEY AND L. J. PAPA, *Anal. Chem.*, 34 (1962) 801.

REVIEW

ELECTRODE KINETIC ASPECTS OF ELECTROCHEMICAL ENERGY CONVERSION

J. O'M. BOCKRIS AND S. SRINIVASAN
The Electrochemistry Laboratory, The University of Pennsylvania, Philadelphia, Pa. 19104 (U.S.A.)
(Received July 13th, 1965)

1. INTRODUCTION

The distinctive feature of electrochemical energy conversion is the direct conversion of the chemical energy of a reaction into electrical energy without going through the intermediary of heat, and thus avoiding the Carnot limitation. Since it should be possible, theoretically, to obtain electrical energy to the extent of the free energy change of the chemical reaction, the overall thermal efficiencies expected are nearly 100% (since $\Delta G^0 \simeq \Delta H^0$ for most chemical reactions as seen from Table 1). The

TABLE 1

STANDARD FREE ENERGY AND ENTHALPY CHANGES, AND THEORETICAL THERMAL EFFICIENCIES FOR SOME FUEL-CELL REACTIONS

Reaction	$-\Delta G^0$	$-\Delta H^0$	*Thermal eff.*	E^0
1. $H_2 + \frac{1}{2} O_2 \rightarrow H_2O$	56.69	68.32	0.830	1.229
2. $CH_4 + 2 O_2 \rightarrow CO_2 + 2 H_2O$	195.50	212.80	0.919	1.060
3. $C_3H_8 + SO_2 \rightarrow 3 CO_2 + 4 H_2O$	503.90	530.61	0.950	1.093
4. $C_{10}H_{22} + \frac{31}{2} O_2 \rightarrow 5 CO_2 + 11 H_2O$	1574.42	1632.35	0.965	1.102
5. $CH_3OH + \frac{2}{3} O_2 \rightarrow CO_2 + 2 H_2O$	168.95	182.61	0.925	1.222
6. $C + \frac{1}{2} O_2 \rightarrow CO$	32.81	26.42	1.242	0.712
7. $CO + \frac{1}{2} O_2 \rightarrow CO_2$	61.45	67.63	0.909	1.333
8. $H_2 + Br_2 \rightarrow 2 HBr$	24.57	28.90	0.850	1.066

oxidation of carbon to carbon monoxide is an interesting reaction since the theoretical thermal efficiency exceeds 100%, which is, as expected when there is an increase in the number of molecules in the gas phase during the reaction, causing a positive entropy change for the reaction. However, the observed efficiencies of most electrochemical energy converters are considerably lower than expected due to a slowness of one or more of the intermediate steps of the overall reaction.

The kinetic processes that occur in an electrochemical energy converter are:

(i) Dissolution of reactants in the electrolyte.

(ii) Diffusion of dissolved reactant to the electrode.

(iii) Adsorption of reactant on electrode from solution.
(iv) Charge transfer from reactant in solution, or in the adsorbed state, to the electrode.
(v) Diffusion of products away from the electrode.
(vi) Transfer of conducting ions through the electrolyte.
(vii) Transfer of electrons from one electrode to the other through the external load.

The importance of a knowledge of electrode kinetics is apparent in the analysis of the rates of the above steps. Hitherto, electrode kinetics has been applied—if somewhat sporadically—to electrochemical reactors but never in a form particularly calculated for them. Here, we try to present some aspects of electrochemical conversion particularly relevant to converters.

2. THEORETICAL EXPRESSIONS FOR THE TERMINAL CELL POTENTIAL, ENERGY CONVERSION EFFICIENCY AND POWER OF ELECTROCHEMICAL REACTORS

(i) *General*

Experimental (and largely engineering) work in electrochemical reactors has now been in progress for about seven years and several collections of papers in this field have been published. It is remarkable that, hitherto, no theoretical formulation has been made of the energy conversion efficiency or power of an electrochemical converter in terms of the parameters that determine it. Reference has frequently been made, in a qualitative fashion, to the overpotentials which compose the "internal resistance" of the electrochemical cell. However, either:

(a) These contributions to the ultimate electrical potential available are often given simply in terms of the parameters for (α) driven, and (β) single electrodes; and when one takes into account the fact that the basic electrochemical generator *must* have two electrodes, and work spontaneously, certain fundamental differences arise which have not before been manifest. The distinctions have great importance for the future of electrochemical engineering—they give the connecting link between engineering (as well as design considerations) and the "atomic-molecular" factors which control the rate-determining steps of energy conversion and power, *i.e.*, those at the interfaces.

(b) Alternatively, the formulations made to date have been concerned too much with purely *electrical* considerations of circuitry.

An attempt is made here to formulate the basic equations that govern the functioning of electrochemical converters, with the simplification that reactions occur at planar surfaces, to avoid the mathematical complexities of the porous surfaces.

(ii) *Fundamental differences between driven cells and spontaneously-acting ones*

In the history of the recent interest in electrochemical energy conversion, attention was paid, perhaps too strongly, to the differences between driven and spontaneously-acting electrochemical devices; very little connection was made between the functioning of fuel cells and the electrode kinetic behavior observed at individual electrodes under conditions in which the current across the electrode–solution interface was controlled by some other power source. During the last three to

four years, the connections of electrochemical energy conversion processes to electrode kinetics at individual interfaces became clear, and now there is perhaps even too much identification of the driven with the spontaneously-acting surfaces.

Although there is a large degree of truth in the view that in electrochemical reactors there simply functions the electrode reactions, made familiar in the last few years, "the other way round", yet the differences should be formulated. At the same time, the rechargeable battery will be taken into account. It is noteworthy that the old terminology is probably worth changing as follows:

Fuel cell = Electrochemical electricity producer
Driven cell = Electrochemical substance producer
Secondary battery = Electrochemical electricity storer

The usual grouping with primary and secondary batteries together seems inappropriate: primary cells are simply "fuel cells" in which the fuel is the substance of which the electrodes are made. It is the secondary cell that has a unique character different from the other devices grouped together here. It *stores electricity*, *i.e.*, it accepts it and re-delivers it, the only way, of which we have knowledge at present, of carrying out such storage.

TABLE 2

BASIC SIMILARITIES AND DISSIMILARITIES AMONG THE THREE ELECTROCHEMICAL DEVICES

Electrochemical substance producer (Driven cell)	*Electrochemical electricity producer (Fuel cell)*	*Electrochemical electricity storer (Secondary battery)*
Cathode is negative, anode is positive.	Cathode is positive, anode is negative.	Cathode is positive, anode is negative.
Reaction forced by external power source.	Reaction spontaneous.	Reaction spontaneous. during discharge.
The driving cell is tacit, inexplicit. No load. The thermodynamic potential is not important.	The load is tacit, inexplicit. The thermodynamic potential is the central point.	The load is tacit, inexplicit. The thermodynamic potential is the central point.
Accepts electricity and produces substance.	Accepts substances and produces electricity.	Accepts electricity during charging, gives out electricity during discharging.
In principle, can operate *ad infinitum*.	In principle, can operate *ad infinitum*.	Intrinsically limited to store certain amount of energy.
Can be regarded in terms of single electrodes.	Cannot be regarded in terms of single electrodes.	Cannot be regarded in terms of single electrodes.
The current that is forced through creates the polarization; current determined outside the cell. This causes certain polarization.	The potential drop at the electrode–solution interface is modified by the passage of current as a kind of feed-back. Current determined (partly) inside cell. Stimulated by $E_r - \Sigma\eta$.	The potential drop at the electrode–solution interface is modified by the passage of current as a kind of feed-back.

The similarities and differences of the three types of electrochemical devices are shown in Table 2.

(iii) *The basic relation between current and terminal cell potential, or external load in an electrochemical reactor*

As is seen from Table 2, the current across a driven cell is the result of the overpotentials forced upon electrodes by outside cells. The independent variable is the overpotential. In the reactor, the independent variable is the external load. Thus, the current, I, is given by

$$I = \frac{(e_c - e_a) - IR_i}{R_e} \tag{1}$$

where e is the *net* electrode potential of either cathode or anode (as indicated by the suffices c or a) and is related to the thermodynamically reversible electrode potential (e_r) of the reaction by the equation:

$$e = e_r \pm \eta, \tag{2}$$

where η is the numerical value of the overpotential developed at a given electrode in the generator when current passes across the electrode concerned at a current density, i. The positive sign applies to the anode and the negative sign to the cathode. R_e is the resistance of the external load (the external load may be a variable resistor) and R_i is the internal ohmic resistance of the cell.

Hence, utilizing well-known expressions which relate overpotential to current density, one has:

$$IR_e = \left[E_r - \frac{RT}{\alpha_c F} \ln \frac{I}{A_c i_{o,c}} + \frac{RT}{nF} \ln \left(1 - \frac{I}{A_c i_L}\right) - \frac{RT}{\alpha_a F} \ln \frac{I}{A_a i_{o,a}} + \frac{RT}{n_a F} \ln \left(1 - \frac{I}{A_a i_{L,a}}\right) - IR_i\right] \tag{3}$$

where E_r is the thermodynamic reversible potential of the cell and is given by

$$E_r = e_{r,c} - e_{r,a} \tag{4}$$

i_o, i_L and α, with the appropriate suffices, are the exchange current density, limiting current density and the transfer coefficient of the cathodic or anodic reaction; n is the number of electrons transferred from the cathode to the anode during one act of the overall reaction in the cell, and A_a and A_c are the active areas of the anode and cathode, respectively.

The quantity IR_e is, of course, the potential that the reactor has available for delivering energy to an outside source. It can be called the "Terminal cell potential," (E) and, physically, it is the total thermodynamic potential, the maximum of which the cell (for the given ratio of constituents) is capable, diminished by the internal potential losses, *i.e.*, the overpotentials and the internal ohmic potential, caused by the passage of current between the electrodes in the cell.

Thus, eqn. (3) allows us—if we know the fundamental electrochemical parameters ($i_{o,c}$, $i_{o,a}$, $i_{L,c}$, $i_{L,a}$ and E_r) on which the workings of the cell depend—to calculate the terminal cell potential corresponding to a given current. This calculation

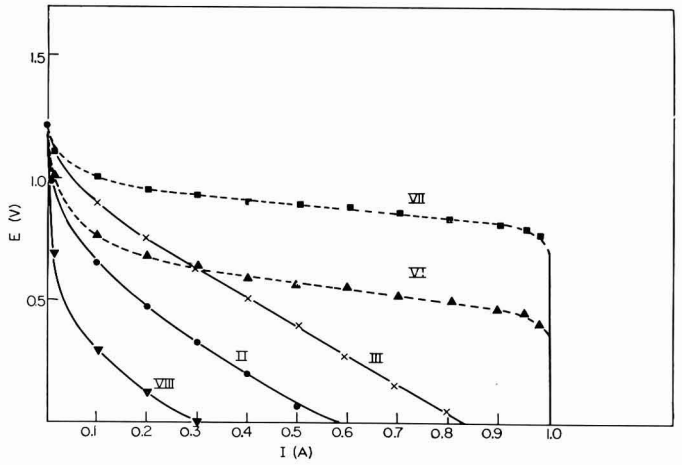
E (V)
1.5
1.0
0.5
VII
VI
II
III
VIII
0.1 0.2 0.3 0.4 0.5 0.6 0.7 0.8 0.9 1.0
I (A)

(1.1)

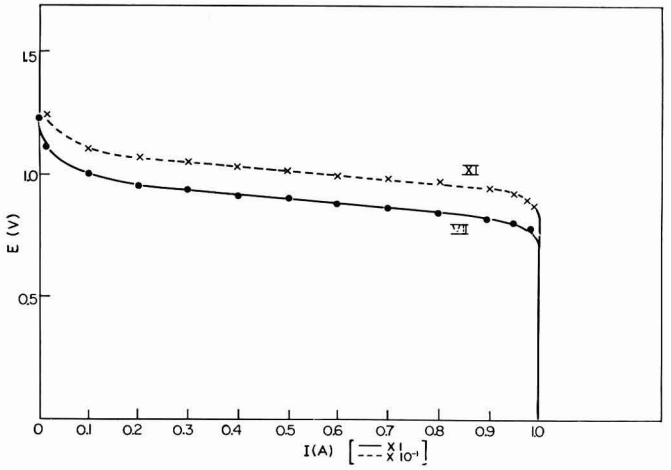
E (V)
1.5
1.0
0.5
XI
VII
0 0.1 0.2 0.3 0.4 0.5 0.6 0.7 0.8 0.9 1.0
I(A) [— x 1 --- x 10⁻¹]

(1.2)

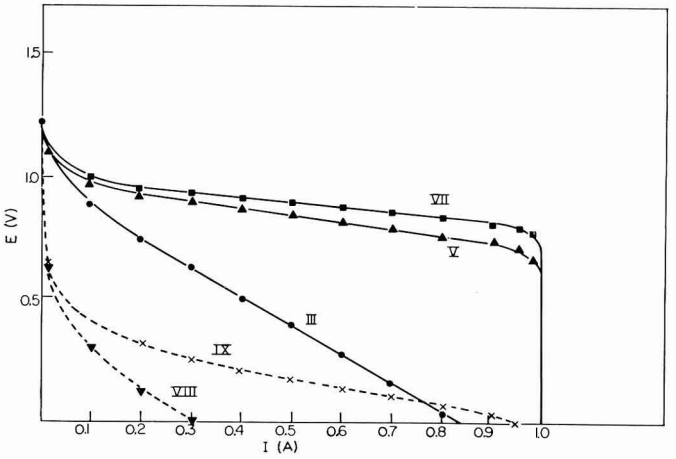
E (V)
1.5
1.0
0.5
VII
V
III
IX
VIII
0.1 0.2 0.3 0.4 0.5 0.6 0.7 0.8 0.9 1.0
I (A)

(1.3)

TABLE 3

KINETIC PARAMETERS USED IN THEORETICAL ANALYSIS OF PERFORMANCE OF ELECTROCHEMICAL REACTOR

Calcn. No.	$Ai_{o,a}$ *(A)*	$Ai_{o,c}$ *(A)*	$Ai_{L,a}$ *(A)*	$Ai_{L,c}$ *(A)*	α_a	α_c	R_i *(Ω)*
I	10^{-3}	10^{-9}	1	1	1/2	1/2	1
II	10^{-3}	10^{-3}	1	1	1/2	1/2	1
III	>1	10^{-3}	1	1	∞	1/2	0.1
IV	10^{-3}	10^{-3}	1	1	1/2	1/2	0.1
V	>1	10^{-3}	1	1	∞	1/2	0.01
VI	10^{-3}	10^{-3}	1	1	1/2	1/2	0.01
VII	>1	10^{-3}	1	1	∞	1/2	0.01
VIII	10^{-3}	10^{-6}	1	1	1/2	1/2	1
IX	10^{-3}	10^{-6}	1	1	1/2	1/2	0.1
X	>1	10^{-6}	1	1	∞	1/2	0.1
XI	>1	10^{-3}	0.1	0.1	∞	1/2	0.01
XII	>1	10^{-6}	0.1	0.1	∞	1/2	1

has been carried out varying the various parameters, as indicated in Table 3. Figure 1.1 shows the effect of variation of Ai_o keeping Ai_L and R_i constant for two extreme values of R_i. It is seen that, initially, there is a marked decrease in E and, thereafter, the E–I relation is nearly linear until the limiting current, if the product Ai_o is fairly high. If Ai_o is low even for one of the electrode reactions, E decreases significantly with I over the whole range. In Fig. 1.2, the effect of variation of Ai_L while Ai_o and R_i are constants, is shown. The range of current is reduced by a decade for a reduction of i_L by a factor of 10. Otherwise, the shape of the E–I curve is essentially a constant. Figure 1.3 shows the marked effect the internal resistance of the cell has on the linear E–I region while maintaining Ai_o and Ai_L as constant. This figure shows the great importance of reducing the internal resistance of the cell. However, as seen from Fig. 1.1, the linear region is practically parallel to the I-axis when $R_i = 0.01\ \Omega$ cm and it can be raised considerably only by increasing the exchange current densities significantly.

(iv) *The differential resistance of an electrochemical reactor*

The expression for $\mathrm{d}E/\mathrm{d}I$ is:

$$\frac{\mathrm{d}E}{\mathrm{d}I} = -\frac{RT}{\alpha_c FI} - \frac{RT}{\alpha_a FI} - \frac{RT}{nF(Ai_{L,c} - I)} - \frac{RT}{nV(Ai_{L,a} - I)} - R_i \qquad (5)$$

$\mathrm{d}E/\mathrm{d}I$ may be called "the differential resistance of the reactor". It is plotted as a function of current density in Figs. 2.1–2.3.

The effect of concentration overpotential on the slope $\mathrm{d}E/\mathrm{d}I$ is seen only close to the limiting current. The importance of the activation overpotential on the slope is quite high in the low current density region. Assuming that $\alpha_c = \alpha_a = 1/2$, and that $I < Ai_L$, the effect of activation overpotential on $\mathrm{d}E/\mathrm{d}I$ is less than 10% of

Fig. 1. Terminal cell potential–current plots (see Table 3 for assumed kinetic parameters).
1.1. Effect of Ai_o on E–I curves at constant values of Ai_L and R_i. (—), $R_i = 1\ \Omega$; (---), $R_i = 0.01\ \Omega$.

1.2. Effect of Ai_L on E–I curves at constant values of Ai_o and R_i.

1.3. Effect of R_i on E–I curves at constant values of Ai_o and Ai_L.

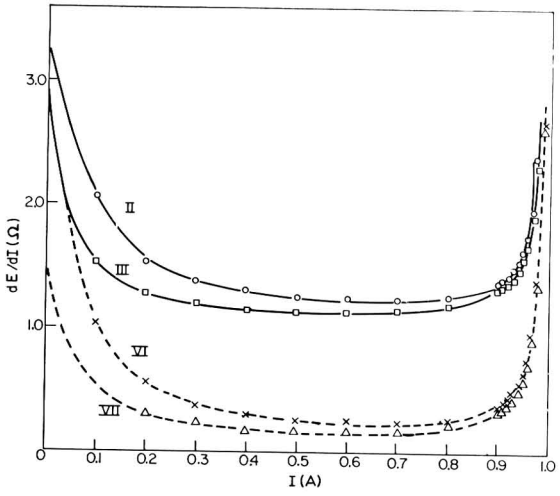

(2.1)

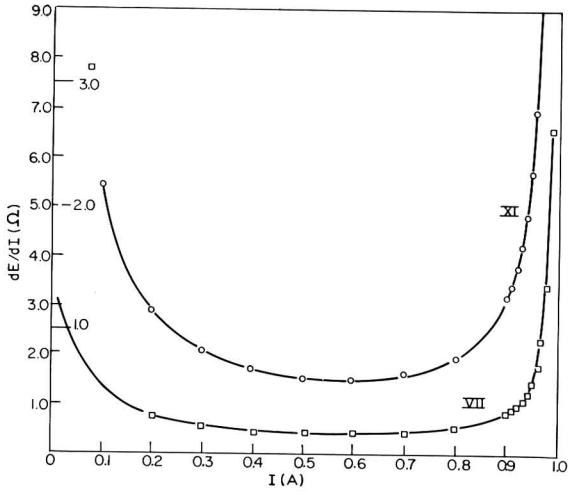

(2.2)

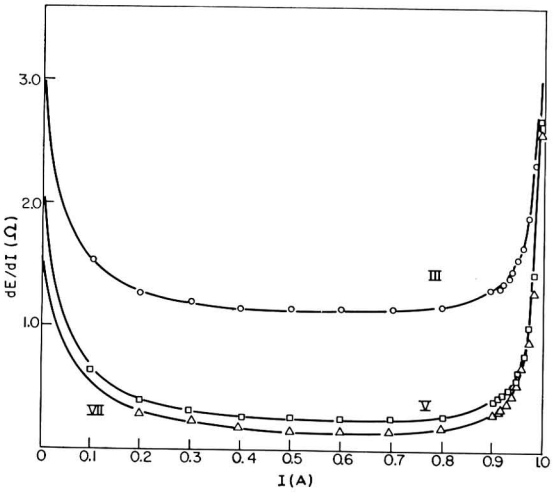

(2.3)

R_i when $IFR_i/RT > 10$. If R_i is unity, this value of I is 0.25 A. This would account for the near constancy of dE/dI observed in a number of the present cases as well as observed experimentally.

(v) *Efficiency of energy conversion*

The overall efficiency (ε_0) of a fuel cell is defined by the equation

$$\varepsilon_0 = \varepsilon_t \varepsilon_p \varepsilon_f \tag{6}$$

where ε_t, ε_p and ε_f are the thermal, voltage and Faradaic efficiencies, respectively. ε_f is the efficiency on a basis of degree of complete conversion of fuel to a certain final reaction product, for example, decane to CO_2. Correspondingly, ε_p and ε_t are given by

$$\varepsilon_p = \frac{E}{E_r} \tag{7}$$

and

$$\varepsilon_t = \frac{\Delta G^0}{\Delta H^0} = -\frac{nFE_r}{\Delta H^0} \tag{8}$$

In the case of most reactions of interest to fuel cells it has been established that ε_f is practically unity and does not vary with current density. Assuming ε_f is unity, and using eqns. (7) and (8) in eqn. (6)

$$\varepsilon_0 = -\frac{nF}{\Delta H^0} E \,. \tag{9}$$

From eqns. (3) and (9) together with

$$E = IR_e \tag{10}$$

it follows that

$$\varepsilon_0 = -\frac{nF}{\Delta H^0}\left[E_r - \frac{RT}{\alpha_c F} \ln \frac{I}{A_c i_{o,c}} + \frac{RT}{nF} \ln \left(1 - \frac{I}{A_c i_{L,c}}\right)\right.$$

$$\left. - \frac{RT}{\alpha_a F} \ln \frac{I}{A_a i_{o,a}} + \frac{RT}{nF} \ln \left(1 - \frac{I}{A_a i_{L,a}}\right) - IR_i\right] \tag{11}$$

It follows from eqn. (11) that ε_0 and E vary in the same way with I.

Plots are given in Figs. 3.1–3.3 of the efficiency as a function of I for various parameters. The efficiency is a maximum when $I = 0$ and decreases monotonously with increasing I.

(vi) *Power in an electrochemical reactor*

The power (P) of an electrochemical reactor is given by

$$P = IE \tag{12}$$

Fig. 2. Differential resistance–current plots. Division into sub-group 2.1–2.3 as in Fig. 1.

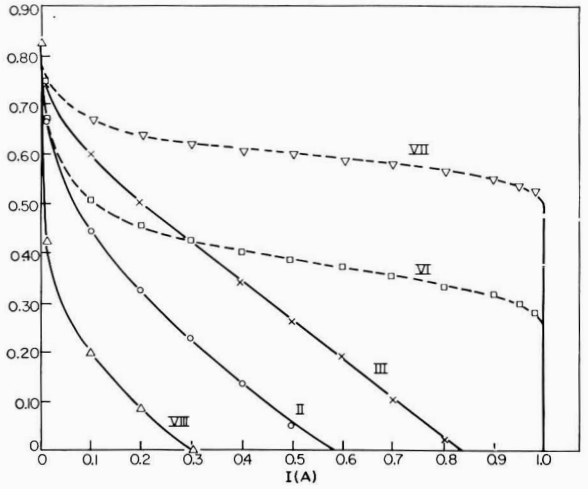
0.90
0.80
0.70
0.60
0.50
0.40
0.30
0.20
0.10
0
0 0.1 0.2 0.3 0.4 0.5 0.6 0.7 0.8 0.9 1.0
I(A)
VII
VI
III
II
VIII

(3.1)

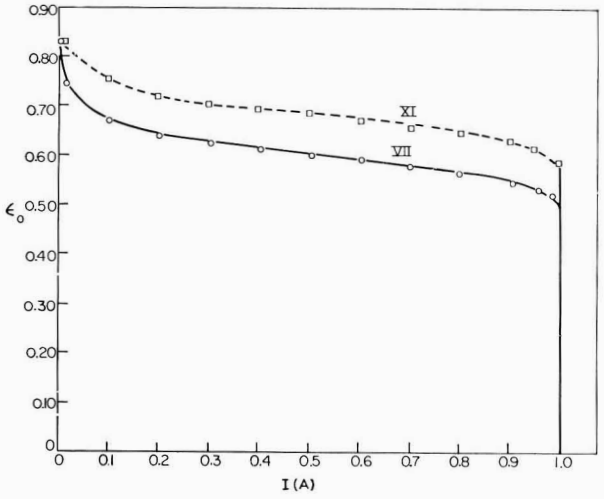
0.90
0.80
0.70
0.60
0.50
0.40
0.30
0.20
0.10
0
ϵ_o
0 0.1 0.2 0.3 0.4 0.5 0.6 0.7 0.8 0.9 1.0
I (A)
XI
VII

(3.2)

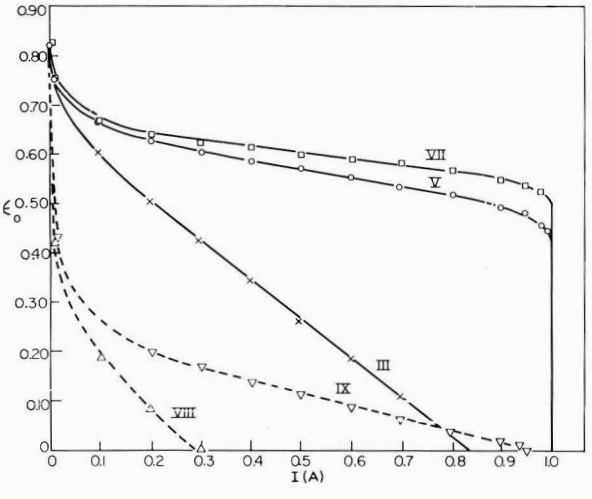
0.90
0.80
0.70
0.60
0.50
0.40
0.30
0.20
0.10
0
ϵ_o
0 0.1 0.2 0.3 0.4 0.5 0.6 0.7 0.8 0.9 1.0
I (A)
VII
V
III
IX
VIII

(3.3)

The units of P are watts if I is in amps and V in volts. Qualitatively, one can examine the nature of the P–I relation. When I is low, E is high and, conversely, when I is high E is low. Thus, the P–I curve should pass through a maximum (Fig. 4.1–4.3). Further, this curve should pass through the origin since when $I=0$, $P=0$. If one compares the P–I and ε_0–I curves, it will be seen that the efficiency is a maximum when $P=0$ and the ε–I curve steadily decreases with increasing I, whereas the P–I curve first increases, passes through a maximum and then decreases to a power of zero when E reaches 0.

Thus, from eqns. (3) and (12), it follows that:

$$P = I\left[E_r - \frac{RT}{\alpha_c F}\ln\frac{I}{A_c i_{o,c}} + \frac{RT}{nF}\ln\left(1 - \frac{I}{A_c i_{L,c}}\right)\right.$$

$$\left. - \frac{RT}{\alpha_a F}\ln\frac{I}{A_a i_{o,a}} + \frac{RT}{nF}\ln\left(1 - \frac{I}{A_a i_{L,a}}\right) - IR_i\right] \qquad (13)$$

The power is plotted as a function of I in Figs. 4.1–4.3 for various parameters. Further, at any particular value of I, the power is significantly increased with increase of Ai_o. P is also increased by decrease of R_i. In most of the cases calculated, *except when the internal resistance is high or when Ai_o, even for one of the electrodes, is low*, the maximum power is close to the limiting current.

A general analytical expression for the potential at which the power is a maximum is difficult to obtain. Here, some limiting cases are given.

(a) *Conditions under which E–I relation is linear.* Under the condition when the electrode reactions are fast, the sum of the activation overpotentials (η_a) at both electrodes varies linearly with the current according to the equation

$$\eta_a = \frac{RT}{nF}\left[\frac{I}{A_a i_{o,a}} + \frac{I}{A_c i_{o,c}}\right] \qquad (14)$$

Further, if $I \ll A_a i_{L,a}$ and $I \ll A_c i_{L,c}$, the total concentration overpotential (η_c) is given by

$$\eta_c = \frac{RT}{nF}\left[\ln\left(1 - \frac{I}{A_c i_{L,c}}\right) + \ln\left(1 - \frac{I}{A_a i_{L,a}}\right)\right]$$

$$\simeq \frac{RT}{nF}\left[\frac{I}{A_c i_{L,c}} + \frac{I}{A_a i_{L,a}}\right] \qquad (15)$$

Thus, all forms of polarization vary linearly with the current and the terminal cell potential is given by

$$E = E_r - IR_t \qquad (16)$$

where

$$R_t = \frac{RT}{nF}\left[\frac{1}{A_c}\left(\frac{1}{i_{o,c}} + \frac{1}{i_{L,c}}\right) + \frac{1}{A_a}\left(\frac{1}{i_{o,a}} + \frac{1}{i_{L,a}}\right)\right] + R_i \qquad (17)$$

R_t is the effective resistance of the cell. For this case, the power is given by

$$P = I(E_r - R_t I) \qquad (18)$$

Fig. 3. Efficiency–current plots. Division into sub-group as in preceding figures.

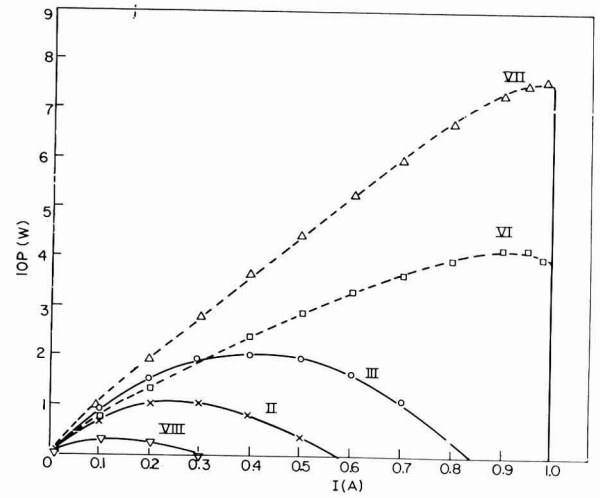
IOP (W)
I(A)
VII
VI
III
II
VIII

(4.1)

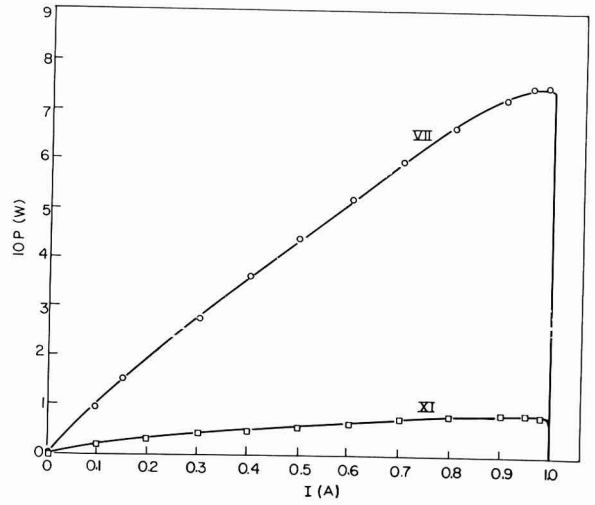
IOP (W)
I (A)
VII
XI

(4.2)

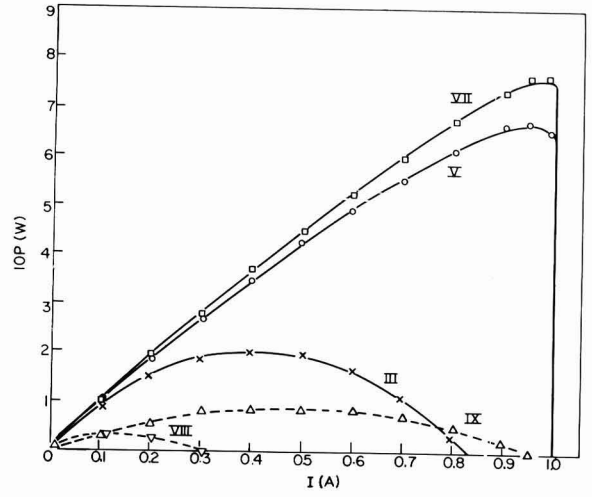
IOP (W)
I (A)
VII
V
III
IX
VIII

(4.3)

from eqns. (12) and (16). The condition for maximum power is

$$dP/dI = E_r - 2\,R_t I_m = 0 \tag{19}$$

i.e.,

$$I_m = E_r/2\,R_t \tag{20}$$

$$P_m = E_r^2/4\,R_t \tag{21}$$

$$E_m = E_r - I_m R_t = E_r/2 \tag{22}$$

From eqn. (19), it is seen that the power is a maximum when the external load is equal to R_t. As seen from eqns. (16) and (20), in order that P_m may be as high as possible, it is necessary for the exchange current densities and the limiting current densities of the relevant reactions to be as high as possible and to have low internal resistances of the cell.

Using eqns. (10) and (16) in eqn. (12), the power may also be expressed in terms of R_i and R_e by the relation

$$P = E_r^2 \frac{R_e}{(R_e + R_i)^2} \tag{23}$$

(b) *Condition under which current–potential relation at each electrode is Tafellian.* The mass transfer and ohmic polarizations are assumed to be negligible. The power–current density relation is given by

$$P = I[E_r - (a_1 + a_2) - (b_1 + b_2) \log I] \tag{24}$$

from eqns. (3) (with $R_i = 0$ and η_e, as expressed by eqn. (15), also as zero) and eqn. (12). In eqn. (24),

$$a_1 = \frac{RT}{\alpha_c F} \ln A_c i_{o,c} \tag{25}$$

$$a_2 = \frac{RT}{\alpha_a F} \ln A_a i_{o,a} \tag{26}$$

$$b_1 = \frac{RT}{\alpha_c F} \tag{27}$$

$$b_2 = \frac{RT}{\alpha_a F} \tag{28}$$

The condition for maximum power is

$$dP/dI = E_r - (a_1 + a_2) - (b_1 + b_2) \log I_m - b_1 + b_2 = 0 \tag{29}$$

i.e.,

$$\log I_m = \frac{E_r - (a_1 + a_2) - (b_1 + b_2)}{b_1 + b_2} \tag{30}$$

$$E_m = (b_1 + b_2) \tag{31}$$

$$P_m = (b_1 + b_2) \exp\left(\frac{E_r - (a_1 + a_2) - (b_1 + b_2)}{b_1 + b_2}\right) \tag{32}$$

Fig. 4. Power–current plots. Division into sub-group as in preceding plots.

Equation (30) shows that log I_m, and hence I_m, increases as the exchange current densities increase, since the latter are related to a_1 and a_2 by eqns. (25) and (26).

(vii) *Some conclusions regarding the factor of importance in electrochemical reactors*

The performance of an electrochemical reactor, both from efficiency and power considerations, depends mainly on the E–I curve. The E–I curve may be broadly divided into three regions. At low values of I there is a marked decrease of E with I. This decrease is due to activation polarization and is greater, the smaller the value of i_oA. At high values of I, E again decreases sharply with the current, becoming zero when $I = Ai_L$ ($a_a i_{L,a}$ or $A_c i_{L,c}$, whichever is smaller). In the intermediate range, the E–I curve is linear if $A_a i_o$ for either of the electrode reactions is not too small and R_i is not negligible. A simple way of examining the relative importance of the various forms of polarization is by assuming the E–I relation is linear (eqn. 16). Combining eqns. (10) and (16)

$$I = \frac{E_r}{R_e + R_t} \tag{33}$$

From eqns. (17) and (33), it follows that for a constant R_e, the current is controlled by the largest of the terms on the right-hand side of eqn. (17). If R_i is fairly small and is not responsible for controlling the rate, the rate may be increased by increasing the relevant i_o, i_L or A. The smallest of the quantities i_o or i_L for either of the electrodes, controls the rate.

The cell potential (E) may also be expressed by

$$E = E_r \frac{R_e}{R_e + R_t} \tag{34}$$

using eqns. (10) and (16).

Suppose R_e is large and also much greater than R_t, then it follows from eqn. (33) that

$$I \simeq E_r/R_e \to 0 \tag{35}$$

and from eqn. (34) that

$$E \simeq E_r \,. \tag{36}$$

If $R_e \ll R_i$, eqn. (33) shows that

$$I \simeq E_r/R_i \tag{37}$$

Further, if $R_i \to 0$, $I \to \infty$; from eqn. (34), it follows that

$$E \simeq E_r(R_e/R_i) \,. \tag{38}$$

and since $R_e \ll R_i$,

$$E \to 0 \,. \tag{39}$$

A similar analysis may be made for increasing the power of a fuel cell, using eqn. (23). If it is assumed that $A_c i_{o,c}$ is the smallest of the quantities in eqn. (17) and that R_i is small, the maximum power (eqn. (21)) is given by

$$P_m = \frac{E_r^2}{4\,RT/A_c i_{o,c}} \tag{40}$$

Thus, P_m increases directly with $A_c i_{o,c}$; $i_{o,c}$ is a measure of the electrocatalytic rate constant for the cathodic reaction. A similar conclusion may be reached when the current–potential relation is not linear and is expressed by an equation of the form of eqn. (3).

3. IMPORTANCE OF ELECTROCATALYSIS IN ELECTROCHEMICAL ENERGY CONVERSION

(i) *General*

The previous sections illustrate that the central problem in electrochemical energy conversion is overpotential reduction at practical current densities. In the case of a number of potential fuel cell reactions (*e.g.*, hydrocarbon oxidation), which are feasible from an economic standpoint, the major portion of the loss in cell potential is due to activation control.

The current–cell potential relation for a hydrocarbon–air fuel cell may be represented by an equation of the form (3). This equation shows that it is necessary to increase the exchange current densities for the oxidation of the hydrocarbon and the reduction of oxygen to improve the performance of this fuel cell. Thus, electrocatalysis is a vital field of study for the further advance of electrochemical energy conversion.

Electrocatalysis is closely related to the field of chemical catalysis but with two major differences—the influence of the electric field, and of the solvent on the rate of the reaction. The additional variable of potential is in many ways an advantage, since the rate of the reaction may be varied over several decades simply by changing the potential at any one temperature. In chemical catalysis, in order to change the rate by several decades, it is necessary to increase the temperature of the reaction by a considerable amount.

One of the problems in electrocatalysis is that electrochemical reactions are generally carried out in aqueous or non-aqueous solution. Thus, it is necessary to elucidate the role of the solvent in the overall reaction. In addition, it is necessary to carry out the reaction under highly purified solutions; otherwise, impurities in the solution may affect the kinetics of the reactions concerned, so that mechanism studies become difficult.

As in chemical catalysis, geometric and electronic factors play an important role in electrocatalysis. Their influence will be seen from the following examples.

(ii) *Hydrogen electrode reaction*

(a) *Effect of work function of the metal.* When the logarithm of the exchange current density (i_o) for the hydrogen evolution reaction is plotted *versus* the work function of the metal, three distinct groups are obtained[1] (Fig. 5). The high overpotential metals belong to one, the medium overpotential metals to another and the low-overpotential metals to a third group. These three groups are associated with the slow discharge, slow electrochemical desorption, and slow recombination mechanisms, respectively.

(b) *Effect of d-band character.* A plot of overpotential at a constant current density *versus* the heat of adsorption of hydrogen on the metal (as % *d*-band character increases, the heat of adsorption decreases) also shows a distinct separation into these two groups[2] (Fig. 6).

The effect of *d*-band character (or *d*-vacancies) on the hydrogen electrode reaction is better seen in the recent work of BOCKRIS, DAMJANOVIC AND JAHAN[3], using Au, Pd (or Pt) and their alloys of varying composition. With increasing Au-content of the alloy, log i_o decreases fairly sharply until 60% Au, whereafter the change in log i_o is considerably slower (Fig. 7). At 60% Au, the *d*-band is completed and no change in activity should be expected above 60%.

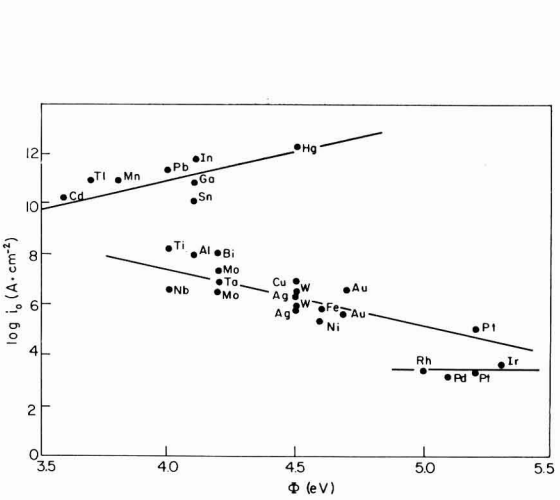

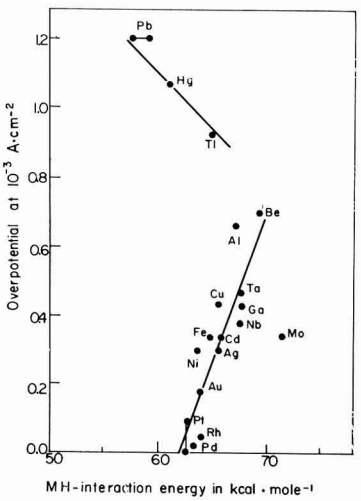

Fig. 5. Log i_o (exchange current density)–work function plot for hydrogen electrode reaction on some metals. Two points for some metal obtained in cases where there is two section Tafel plot.

Fig. 6. Overpotential (η) at a current density of 10^{-3} A cm^{-2} *vs.* strength of M–H band (D_{M-H}) in the hydrogen electrode reaction on some metals.

Further, a plot of log i_o *vs.* the number of unpaired *d*-electrons/atom in these alloys is linear (Fig. 8). This type of relationship was also obtained by CONWAY *et al.*[4], who studied the hydrogen evolution reaction on Cu, Ni and their alloys.

(c) *Geometric factors.* Only a little work has been done to examine the influence of geometric factors. Hydrogen overpotential measurements have been carried out on the various crystal planes of Ni[5]. The (111) plane which is the most densely packed plane has the highest activity. No effect of grain size on the rate of hydrogen evolution on platinized platinum was observed probably because low enough grain sizes were not used[6].

(iii) *Oxygen electrode reaction*

RAO *et al.*[7] measured the maximum oxygen coverages (θ) at one atmosphere pressure on a number of metals, coulometrically. The results show that unpaired *d*-electrons participate directly in the bonding of the metal atom to oxygen (Table 4). Au with no unpaired *d*-electrons has the lowest oxygen coverage, while Ru with the highest number of unpaired electrons has the highest θ. This work was confirmed by the work on Pt–Rh alloys.

The influence of electronic factors on the rate of oxygen electro-reduction was studied on a number of metals and alloys[8]. From the Tafel lines obtained on the

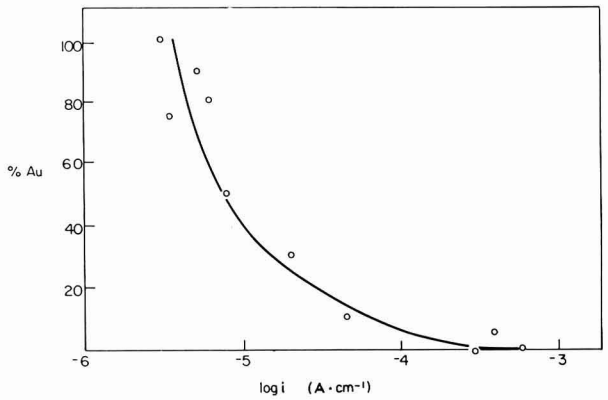

Fig. 7. Dependence of exchange current density for hydrogen evolution on % Au composition in a series of Au–Pd alloys.

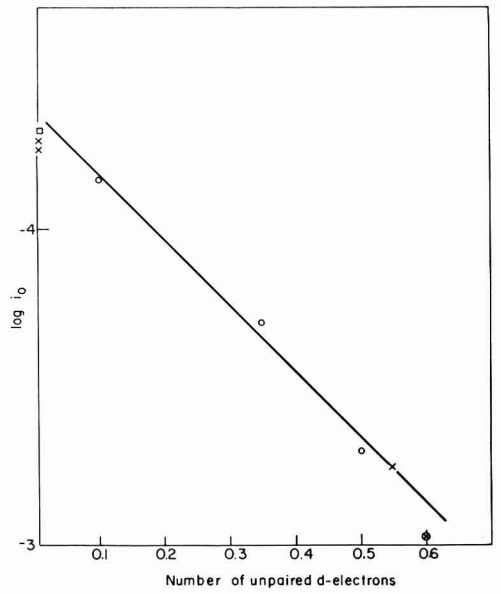

Fig. 8. Dependence of exchange current density on unpaired *d*-electrons for hydrogen electrode reaction. (○), Pd and Pd-alloys; (×), Pt and Pt alloys; (□), Au.

metals Pt, Pd, Ir, Rh and Au (Fig. 9) in acid solutions, it appears that Au with no unpaired *d*-electrons has a significantly lower exchange current density than other metals. Rh and Ir with the same number of unpaired electrons show essentially an identical current–potential behavior. Pd and Pt with practically the same number of unpaired electrons show similar Tafel behavior. The current–potential behavior (Fig. 10) of a series of Au–Pd alloys show that (a) the rest potential decreased from the value of Pd to that for Au, and (b) Au and the alloy containing 75% Au have a considerably higher Tafel slope than Pd and other alloys which have nearly the same

TABLE 4

RELATIONSHIP OF OXYGEN COVERAGES TO NUMBER OF UNPAIRED *d*-ELECTRONS/ATOM FOR THE NOBLE METALS

Metal	*(a) Obs. oxygen coverage ($\mu C\ cm^{-2}$)*	*(b) Calc. oxygen coverage of a monolayer ($\mu C\ cm^{-2}$)*	*(c) Fraction of surface covered by oxygen (θ)*	*(d) No. of unpaired d-electrons/atom*
Pd	110	510	0.22	0.55
Pt	110	500	0.22	0.55–0.6
Pt	135	500	0.27	0.55–0.6
Rh	480	530	0.90	1.7
Ir	440	525	0.84	1.7
Ru	500	530	0.95	2.2
Au	<15		<0.03	0

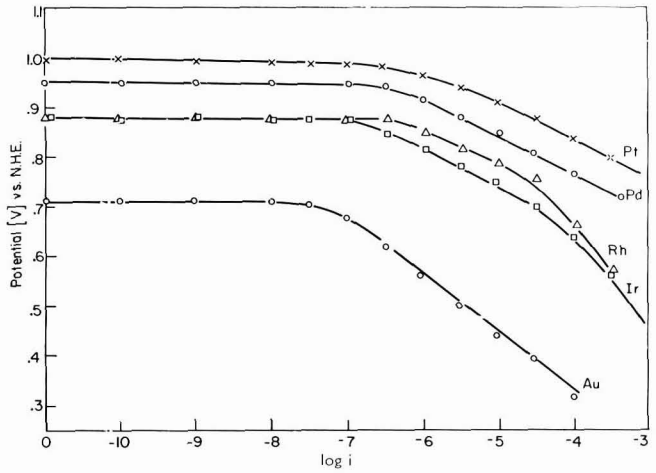

Fig. 9. Tafel lines for the electro-reduction of oxygen on some noble metals.

slopes. Thus, a change in mechanism occurs between 50 and 75% Au, probably at 60% where the *d*-band is completed.

A probable explanation of the influence of the % *d*-vacancy on the electrocatalysis of oxygen reduction is that chemisorbed oxygen is an intermediate in the reaction and that the M-O bond strength varies with the % *d*-vacancy.

(iv) *Electro-organic oxidation*

The first systematic study on electrocatalysis in electro-organic oxidation was carried out by DAHMS AND BOCKRIS[9] (Table 5). Complete oxidation was observed on the platinum metals, whereas there was only partial oxidation on Au and Pd. The explanation suggested was that, due to a lower binding energy between the metal and the organic on Pd and Au than on Pt, Rh and Ir, intermediates are easily desorbed from the surface on the former. A direct correlation between the rate of the reaction at a constant metal–solution potential and the exponential of the work function was also shown.

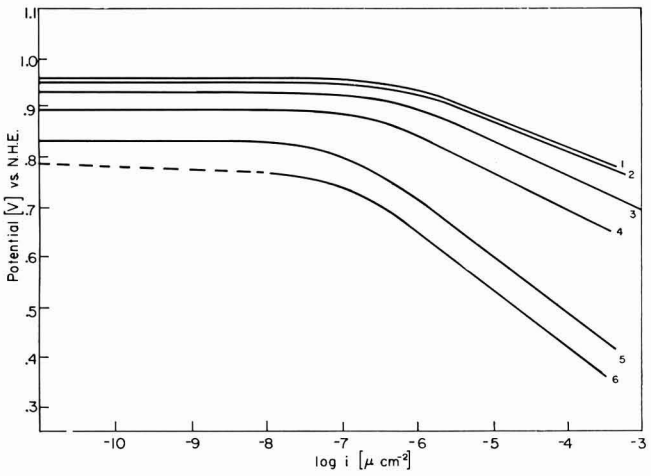

Fig. 10. Tafel lines for the electro-reduction of oxygen on Au, Pd and a series of their alloys. (1), Pd; (2), 90% Pd: 10% Au; (3), 75% Pd: 25% Au; (4), 50% Pd: 50% Au; (5), 75% Pd: 25% Au; (6), Au.

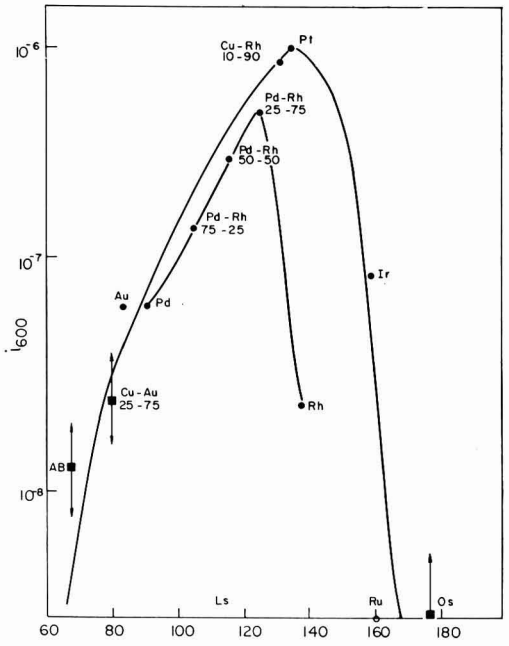

Fig. 11. Relation of current at 600 mV (N.H.E.) in the oxidation of ethylene to the latent heat of sublimation for some metals and alloys.

Recently, a parabolic of relation between the exchange current density for ethylene oxidation at 600 mV (N.H.E.) and the latent heat of sublimation for a number of metals was obtained by KUHN AND BOCKRIS[10] (Fig. 11). It was also shown that by using alloys of two metals but of varying composition, one on the left-hand

TABLE 5

INFLUENCE OF ELECTROCATALYTIC PROPERTIES OF SOME METALS IN THE ELECTRO-OXIDATION OF ETHYLENE

	Reaction product	*Chemical reaction rate at p.z.c.* (A/cm^2)	*pH-dependence* $(dE/dpH)_i$ (*V*)	*Tafel slope* $(dE/d\log i)_{pH}$ (*V*)	*Lattice parameter* *Q*(*Å*)	*Potential of zero charge* (*p.z.c.*) *hydrogen scale* (*V*)	*Vacant d-orbitals/ atom*	*Heat of sublimation* L_S (*kcal* $mole^{-1}$)
Platinum	CO_2	$1 \cdot 10^{-7}$	70	160	3.914	+0.30	0.55	135
Iridium	CO_2	$1 \cdot 10^{-11}$	75	132	3.823	$+0.05 \pm 0.1$	1.5	165
Rhodium	CO_2	$5 \cdot 10^{-11}$	70	155	3.794	0.05 ± 0.1	1.5	138
Gold	No CO_2, aldehydes	$1 \cdot 10^{-11}$	0	72	4.070	+0.30	0	84
Palladium	No CO_2, aldehydes	$7 \cdot 10^{-10}$	0	80–110	3.879	+0.25	0.55	91

side of the peak and the other on the right-hand side of the peak, similar volcano-type relations between activity and alloy composition was observed but with lower peaks. The peak in the first curve was obtained on Pt. Since Pt is too expensive a metal for electrochemical energy conversion, alloys of composition corresponding to the peaks (*e.g.*, as in second curve) may be good substitutes.

From the parabolic relation, it may be inferred that on the left-hand side of the peak, since there is an increase of rate with heat of sublimation, an adsorption process is rate-determining (it may easily be shown by using the Pauling equation that the strength of an adsorbed bond increases with the heat of sublimation) whereas on the right-hand side of the peak, a desorption step controls the rate of the overall reaction.

4. MECHANISM OF OXYGEN DISSOLUTION REACTION

(i) *General*

A knowledge of the mechanism of oxygen dissolution reaction is of fundamental importance in the development of fuels. Practically all fuel-cell systems, except for a few that use the halogens, use air or oxygen as the oxidant*. In the case of the most-advanced fuel-cell system, that uses hydrogen as the fuel and oxygen or air as the oxidant, the polarization losses at the hydrogen electrode are relatively low compared to that at the oxygen or air electrode. Even on open circuit, with platinum which is one of the best catalysts, the potential of the oxygen electrode is about 1 V which represents a loss of about 0.2 V in cell potential or 16% in useful energy. Thus, an improvement in performance of the oxygen electrode, even at low current densities is vital. Such improvements are only possible by a study of the mechanism of the reaction on a number of catalysts. Some aspects of mechanism studies carried out in our laboratory will be treated in the following subsections.

(ii) *Attainment of the reversible potential*

The first time that the reversible potential of 1.23 V was attained on a platinum electrode in sulfuric acid was when the solution was vigorously purified by cathodic and anodic pre-electrolysis and the electrode heated in an oxygen atmosphere prior to the measurement[11]. The potential was stable for only a few hours but could be maintained by continued pre-electrolysis on an auxiliary electrode. WATANABE AND DEVANATHAN[12] found that the reversible potential could also be obtained if the platinum electrode was first pre-anodized, then maintained in an oxygen atmosphere for 24 h above the solution, immersed in the electrolyte and the potential measured. In this case, too, the potential was only stable for a few hours. More recently GENSHAW[13] observed the thermodynamic reversible potential for over 100 h. The solution and the oxygen gas for bubbling through the solution were vigorously purified. A stable reversible potential was also observed by HOARE[14] on a Pt electrode, previously quenched in concentrated HNO_3, and washed with conductivity water.

A recent theoretical analysis[15] shows that the generally observed rest potential of 1 V (N.H.E.) is probably due to a mixed potential caused by oxygen reduction and some impurity oxidation. Such a theory is able to explain the pH and oxygen partial-pressure effects on the rest potential and also the observed shifts of the rest potential

* The use of H_2O_2 and of N_2O_4 as oxidants, though attempted, is quite rare.

towards the thermodynamic reversible potential, depending on the degree of purification of the electrolyte.

(iii) *Nature of the substrate on oxygen electrodes*

As pointed out in the last section, an oxygen-containing species is present on the surface of Pt electrodes on which the reversible potential is obtained. Such a species may also be present on electrodes on which the oxygen dissolution reaction is taking place, although at lower potentials the species may be reduced. Further, by working at potentials below about 1 V, on electrodes where such species were not previously formed, the reduction reaction can be carried out on the bare electrode.

Several methods have been used to examine the nature of the film on oxygen electrodes. Coulometric methods of independent workers[16–18] showed that the coverage–potential relation is linear. The quantity of electricity required for reduction of species formed at higher potentials indicate that oxides are probably present. Direct evidence for the presence of oxide at potentials above 1 V arises from the ellipsometric studies of REDDY *et al.*[19]. No oxides are present below 1 V. Coverages obtained by the ellipsometric and coulometric methods are in excellent agreement above 1 V. Hysteresis behavior in the coverage–potential relation, during oxide formation and reduction, is observed in both methods. Below 1 V, coulometry shows a coverage whereas ellipsometry indicates no film. Thus, only adsorbed oxygen is present below 1 V.

Thus, oxygen evolution occurs only on oxide-covered electrodes, whereas the oxygen reduction may occur on oxide-covered or bare electrodes, depending on the potential as well as on the rates at which oxides form or reduce at this potential. Reduction of the oxide occurs only below 1 V and its rate decreases with increase of potential. At potentials below 1 V, the rate of oxygen reduction is faster on the bare metal than on the oxide[13]. Thus, in an electrochemical energy converter, which uses Pt as the cathode, it is preferable to maintain an oxide-free surface for operating cell potentials of less than 1 V.

(iv) *Overall reaction and its path*

There are two possible overall reactions in the cathodic reduction of oxygen:

$$O_2 + 2\,H^+ + 2\,e_0^- \rightarrow H_2O_2 \qquad (41)$$

$$O_2 + 4\,H^+ + 4\,e_0^- \rightarrow 2\,H_2O \qquad (42)$$

The standard thermodynamic reversible potential for reaction (41) is 0.68 V. However, with decrease of the concentration of H_2O_2 in solution, the reversible potential for this reaction shifts in the anodic direction. From the point of view of efficient electrochemical energy conversion, it is necessary for the overall reaction to be the second one. Further, this reaction may take place either directly or by the first reaction followed by the electrochemical or chemical reduction of H_2O_2 according to the equations

$$H_2O_2 + 2\,H^+ + 2\,e_0 \rightarrow 2\,H_2O \qquad (43)$$

$$2\,H_2O_2 \rightarrow H_2O + \tfrac{1}{2}\,O_2 \qquad (44)$$

Thus, one of the main problems in mechanism determination is the elucidation of both the overall reaction (or reactions) and the path.

NEKRASSOV AND MÜLLER[20] used a rotating-disk electrode with a ring to study the oxygen reduction reaction. Pt was used as the electrode and ring material. It was concluded that H_2O_2 is an intermediate in the reduction of H_2O_2 to O_2. However, the possibility that H_2O_2 is formed in a parallel reaction was not investigated. Recently, GENSHAW *et al.*[21] used the same electrode arrangement to distinguish between these two possibilities. In this method, the oxygen reduction was carried out on the disk. The H_2O_2 formed may be further reduced on the disk or diffuse to the ring where it is oxidized according to the reaction

$$H_2O_2 \rightarrow 2\ H^+ + 2\ e_0 + O_2 \tag{45}$$

The potential of the ring is so maintained that the latter oxidation reaction proceeds at its limiting current density.

The possible reactions at the disk may be represented by[21]

$$O_2 \xrightarrow{i_1} H_2O \tag{46}$$

$$O_2 \xrightarrow{i_2} H_2O_2 \begin{cases} \xrightarrow{i_3} H_2O \\ \xrightarrow{i_4} \text{Diffusion to solution} \end{cases} \tag{47}$$

The currents for the reaction are represented above the respective arrows. The current on the disk (I_d) is hence:

$$I_d = i_1 + i_2 + i_3 \tag{48}$$

The current on the ring (I_r), is proportional to i_4, and may be expressed by

$$I_r = N i_4, \tag{49}$$

where N is a numerical factor that may be calculated.

From Kirchoffs Laws:

$$i_2 = i_3 + i_4 \tag{50}$$

Also writing

$$i_1 = x\ i_2 \tag{51}$$

where $x \geqslant 0$,

$$I_d = x\ i_2 + 2\ i_2 - I_r/N \tag{52}$$

$$i_2 = \frac{I_d + I_r/N}{x+2} \tag{53}$$

The current on the ring may also be expressed by the equation[22]:

$$I_r = \frac{N\ i_2}{1 + k'\omega^{-1/2}} \tag{54}$$

where k' is a measure of the rate constant for the reduction of H_2O_2 at the disk and ω is the speed of rotation.

Using eqns. (53) and (54)[21],

$$\frac{I_d}{I_r} = \frac{x+1}{N} + \frac{x+2}{N} \cdot \frac{k'}{\omega^{1/2}} \tag{55}$$

I_d and I_r are directly measurable. Thus, a plot of I_d/I_r *vs.* $\omega^{-1/2}$ should be a straight line with slope $k'(x+2)/N$ and intercept $(x+1)/N$, and x gives the ratio of rates of H_2O (formed directly) to H_2O_2 formation.

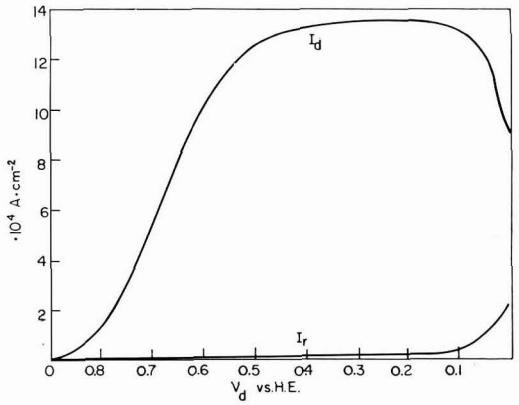

Fig. 12. Disk current (I_d) for O_2 reduction and ring current (I_r) for H_2O_2 oxidation as a function of potential in purified sulfuric acid solution (electrode material, Pt).

It was found that in H_2SO_4, when the solution was pre-electrolyzed using a platinized platinum gauze electrode, maintained at 0.3 V, for about 10 h, the i–V relation on the disk shows a plateau from 0.5 V until about 0.1 V. Below 0.1 V, the current on the disk decreases. The current on the ring remains low until 0.1 V but starts increasing below this potential, indicating H_2O_2 formation (Fig. 12). The sum of the currents on the disk and on the ring below 0.1 V is approximately equal to the limiting current on the disk above 0.1 V. Thus, above 0.1 V, the reaction is predominantly the 4-electron transfer, while below this potential the overall reaction on the disk is essentially the 2-electron transfer reaction to H_2O_2.

In solutions that have not been rigorously purified as stated in the previous paragraph, a plot of I_d *vs.* potential shows a maximum at about 0.6 V after which it decreases sharply (Fig. 13). Further, H_2O_2 is produced at the disk, as indicated by the current on the ring, below 0.8 V. The current on the ring also shows a maximum but at about 0.5 V. The plots of I_d/I_r *vs.* $\omega^{-1/2}$ at various potentials yield parallel straight lines with zero slope (Fig. 14). From the analysis given earlier, it may be concluded that O_2 is reduced to H_2O_2 and H_2O in parallel reactions and that the H_2O_2 is not reduced further on the disk.

It was shown that the deactivation results from the adsorption of impurities on the electrode. The deactivation is initially linear with time and depends on the square-root of the speed of rotation. The current is a minimum at about 0.3 V (Fig. 13) which potential corresponds to the adsorption maximum. Rigorous purification of the solution considerably altered the behavior to that given earlier.

In alkaline solution, it was shown that H_2O_2 is formed as an intermediate. The rate constant k_2 (k' is a measure of k_2) for the H_2O_2 reduction varies linearly with potential over a considerable potential range and then exponentially with potential.

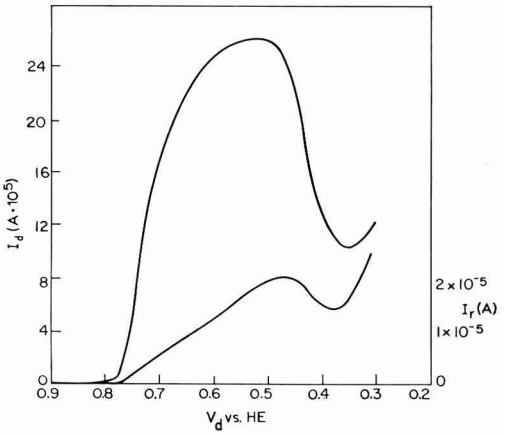

Fig. 13. I_d and I_r *vs.* potential in unpurified H_2SO_4.

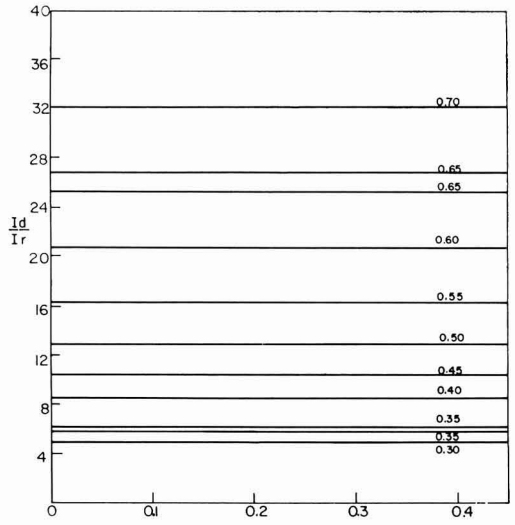

Fig. 14. Ratio of I_d to I_r *vs.* $\omega^{-1/2}$ (ω = angular velocity of rotation of electrode).

5. MECHANISM OF ELECTRO-ORGANIC OXIDATION

(i) *General*

The basic steps in the electro-oxidation of organic compounds (*e.g.*, hydrocarbons, alcohols) are:

(i) Dissolution of reactant in electrolyte.
(ii) Diffusion of dissolved reactant to electrode.
(iii) Adsorption of reactant from solution.
(iv) Electrochemical reaction.
(v) Diffusion of products away from the electrode.

As mentioned earlier, with organic fuels, activation-controlled processes are the main causes for polarization losses. Some new results concerning the adsorption behavior of organic compounds and the mechanism of electro-organic oxidation will be dealt with below.

(ii) *Adsorption behavior of organic compounds*

(a) *Comparison of electroadsorption and adsorption from the gas phase.* Adsorption of organic compounds from solution and from the gas phase differ in the following respects.

(1) Adsorption from the gas phase occurs on the bare metal. Adsorption from solution takes place on a metal covered with solvent molecules. Thus, the latter process is essentially a replacement reaction[23] according to

$$A_{soln} + n\ H_2O_{ads} \rightleftharpoons A_{ads} + n\ H_2O_{soln} \tag{56}$$

(2) From the above difference, it follows that the measured thermodynamic properties in solution, *viz.* heat of adsorption, free energy of adsorption, etc., are the differences for the adsorption of organic and water, unlike in the gas phase where these properties simply represent those for the adsorption of the compound itself.

(3) The extent of adsorption of organic compounds from solution depends on the electric field across the metal–solution interface. Thus this factor gives an additional variable for the study of adsorption from solution. Such studies are also useful from the point of view of gaining knowledge on the structure of the double layer. Further, the region of electric potential on which adsorption takes place is quite useful to evaluate the usefulness, or otherwise, of the compound, in electrochemical energy conversion or as a corrosion inhibitor.

(b) *Methods used to determine extent of adsorption.* Most of the early work on electroadsorption of organic compounds was carried out on mercury, using the electrocapillary method. Two radiotracer methods[24,25] proved successful in the study of the adsorption of organic compounds on solid electrodes. In the first method[24], the radiation through a thin metal foil, placed over the end window of a proportional counter is measured. The thin metal foil serves as the test electrode and its potential is measured with respect to a reference electrode in the same solution. This method is satisfactory for the measurement of adsorption of organic compounds which are sparingly soluble.

In the second method[25], a moving tape arrangement is used. The tape first passes through the electrolyte containing the dissolved organic compound, an auxiliary electrode and a reference electrode. It then leaves the cell and is passed between two proportional counters. Although the tape carries a small quantity of the electrolyte (1-μ thick), the background count is small even if the activity in solution is relatively high.

The accuracy of the two methods is to within 10%. The first method has been used to study the adsorption of benzene[26], naphthalene[27] on Au, and ethylene on Pt[28], and the second method to the adsorption of naphthalene and *n*-decylamine on a number of metals[29,30].

(c) *Adsorption of ethylene on Pt in 1 N H_2SO_4*[28]. As in the gas phase, there are two possible modes for the electroadsorption of ethylene

Associative $$H_2C=CH_2 \rightarrow \begin{matrix} H_2C-CH_2 \\ | \quad | \\ M \quad M \end{matrix} \qquad (57)$$

Dissociative $$H_2C=CH_2 \rightarrow \begin{matrix} HC=CH \\ | \quad | \\ M \quad M \end{matrix} + 2\,H^+ + 2\,e_M \qquad (58)$$

From energetic considerations, associative adsorption is more favorable.

The coverage–potential relations have been obtained for different bulk concentrations of ethylene in solution (Fig. 15). The characteristic bell-shaped form of the θ–V curves was explained on the basis of a competition between organic and water molecules for sites on the surface and the field-dependence of the free energy of adsorption of water. The symmetrical nature of the curves with ethylene indicate that lateral interaction of the adsorbed species is negligible.

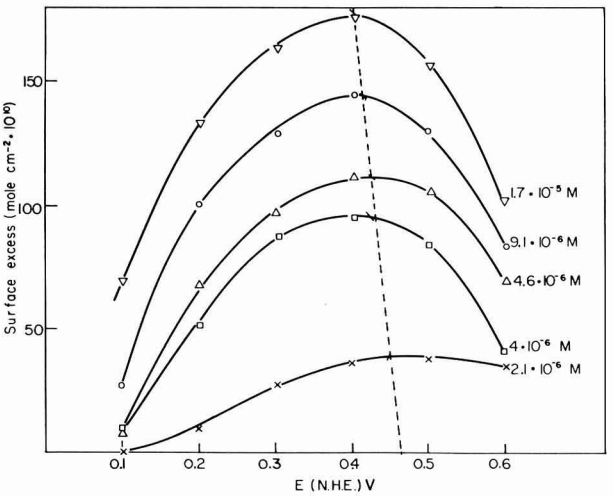

Fig. 15. Coverage–potential relation in the adsorption of ethylene on Pt in 1 N H_2SO_4 for varying bulk concns. of ethylene, (×), 2.1; (□), 4; (△), 4.6; (○), 9.1; (▽), 17 × 10^{-6} M.

The adsorption maximum occurs at 0.4 V for high ethylene bulk concentrations but for lower concentrations changes to 0.46 V.

The adsorption isotherm obtained at 0.4 V and at 30° is shown in Fig. 16. Adsorption reaches a saturation value at around $2 \cdot 10^{-5}$ ml^{-1}. The adsorption isotherms are relatively insensitive to temperature.

Evidence for a simple Langmuir adsorption behavior was obtained from a plot of $[\theta/(1-\theta)]$ *vs.* c, which was linear and passed through the origin. It was further confirmed by a plot of c/θ *vs.* c which yielded a straight line of slope, unity. Because of the large size of the ethylene molecule, one would expect n in the equation:

$$\frac{\theta}{(1-\theta)^n} = K \qquad (59)$$

to be greater than unity (a value of 4 was suggested from studies of electro-oxidation of ethylene[31]). The value of unity obtained, is probably due to the higher mobility of ethylene on the surface at lower coverages. The equilibrium constant, K, was obtained by 3 methods: (1) from the slope of the plot of $[\theta/(1-\theta)]$ *vs.* c; (2) the intercept of c/θ *vs.* c; and (3) from the coverage–time relationship which depends on the adsorption kinetics. For an adsorption process controlled by the diffusion of ethylene from the bulk of the solution to the surface of the electrode, the coverage–time relationship is given by[32,33]:

$$\theta_t = \frac{2D^{\frac{1}{2}}\theta_{eq}}{\pi^{\frac{1}{2}} K \Gamma_{\max}} t^{\frac{1}{2}} \tag{60}$$

where D is the diffusion coefficient for C_2H_4 in solution and $\Gamma_{\max}$ is the coverage at $\theta = 1$. K may thus be calculated from the slope of the θ *vs.* $t^{\frac{1}{2}}$ plots. Good agreement

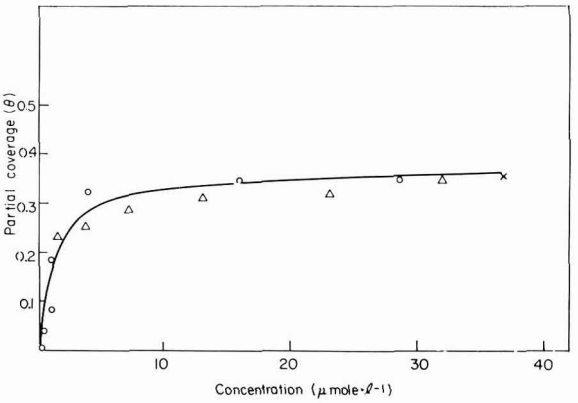

Fig. 16. Isotherm for adsorption of ethylene on Pt in 1 N H_2SO_4 at 30°. Potential 0.4 (N.H.E.).

was obtained for the three methods. K was found to be essentially independent of temperature, having an average value of $(7.5 \pm 2.5) \cdot 10^8$ cm^3 mole^{-1}. Thus, the heat of adsorption is practically zero and is given by $\Delta H^0 = 0 \pm 4$ kcal mole^{-1}. Using a Born-Haber cycle, a value of $\Delta H^0 = -2$ kcal mole^{-1} was calculated for the heat of adsorption, which is good confirmation of the experimentally obtained value. Using these values for K and ΔH^0, the entropy of adsorption is 16 ± 1 e.u. The positive value of ΔS^0 is not anomalous since the adsorption process is a replacement reaction of water by the organic.

(iii) *Mechanism determinations in electro-organic oxidation*

Studies on the kinetics of oxidation of organic compounds is a relatively new field. One of the complexities of these mechanism determination studies is that even the simplest hydrocarbon oxidation is an 8-electron transfer, thus making a complete analysis difficult. Systematic studies have been carried out so far only on the oxidation of a number of unsaturated hydrocarbons on platinum electrodes in acid and alkaline medium[31,34].

In most cases, it was established that the oxidation of the unsaturated hydrocarbon to CO_2 is 100%. For example, on ethylene, the overall reaction in acid is

$$C_2H_4 + 4\ H_2O \rightarrow CO_2 + 12\ H^+ + 12\ e_0^- \qquad (61)$$

With benzene, the coulombic efficiency for CO_2-production increases with potential. With butadiene, the opposite behavior is observed. Thus, parallel reactions occur in these cases[35].

(a) *Methods used to determine mechanism.* Studies have been carried out using potentiostatic, galvanostatic and transient methods in solutions of varying pH, from that of 1 *N* H_2SO_4 to that of 1 *N* NaOH on anodically-activated Pt electrodes at 80°[31,34].

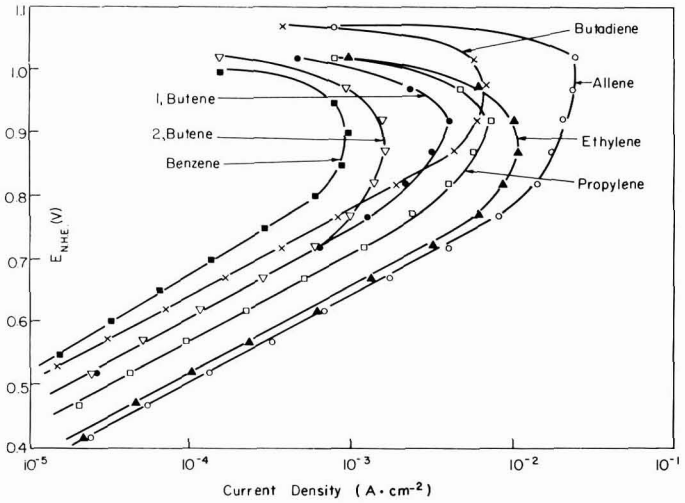

Fig. 17. Current–potential relation for oxidation of some unsaturated hydrocarbons on activated Pt electrodes in 1 *N* H_2SO_4 at 80°. (■), benzene; (▽), 2-butene; (●), 1-butene; (□), propylene; (▲), ethylene; (×) butadiene; (○), allene.

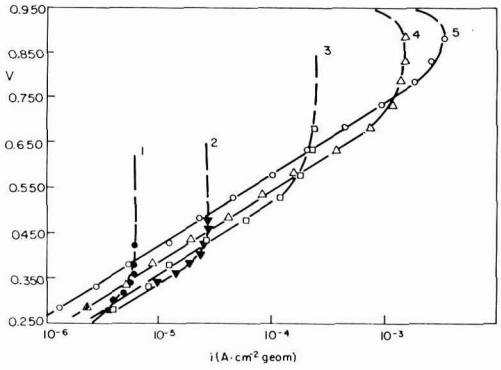

Fig. 18. Current–potential relations for the oxidation of ethylene on activated Pt electrode at ethylene partial-pressures of (1), 10^{-4}; (2), 10^{-3}; (3), 10^{-2}; (4) 10^{-1}; (5) 1 atmos.

TABLE 6

KINETIC PARAMETERS IN THE OXIDATION OF SOME UNSATURATED HYDROCARBONS ON ACTIVATED Pt IN 1 N H_2SO_4 AT 80°

Kinetic parameter	*Hydrocarbon*						
	Ethylene	*Allene*	*Propylene*	*1,3-Butadiene*	*1-Butene*	*2-Butene*	*Benzene*
Reversible potential (V, N.H.E.)	0.06	−0.01	0.07	0.04	0.07	0.07	0.07
Rest potential at 80° (V, N.H.E.)	0.25	0.29	0.26	0.25	0.25	0.24	0.31–0.37
$i_o \cdot 10^8$(A cm^{-2})	5.0	2.1	2.0	0.5	1.2	1.2	0.2
$(dV/dpH)_i$ (V)	−0.065	−0.052	−0.065	−0.067	−0.067	−0.008	−0.051
$(d\log i/d\log p)_V$	−0.2	−0.17	−0.14	−0.13	−0.16	−0.20	−0.11
$\Delta H_\eta^{\neq}$ apparent (kcal mole^{-1})	21±1	20±5	24±2	20±4	23±5	23±5	23±1

The current–potential curve for the oxidation of an unsaturated hydrocarbon shows four distinct regions: (1) low current density region where the i–V relation is nearly linear; (2) the Tafel region which extends over about 2–3 decades in current density; (3) the limiting-current region; and (4) passivation region in which the current decreases with increase of potential (Fig. 17).

A negative partial-pressure effect was observed in the oxidation of all the hydrocarbons (Fig. 18). The potential decreases by about 70 mV/decade increase of pressure at constant current density. At constant potential, $\partial \log i/\partial \mathrm{pH} = 0.5$. The usual Arrhenius temperature-dependence was observed with an apparent activation energy of 22 kcal mole^{-1} at the reversible potential, calculated by extrapolation from the Tafel region.

(b) *Mechanistic conclusions.* In Table 6, are given the various kinetic parameters observed in the oxidation of several unsaturated hydrocarbons on anodically-activated Pt. From these data, it is possible to express the rate by the empirical relation

$$i = k c_{\mathrm{org}}{}^{-\gamma} c_{\mathrm{H}^+}{}^{-0.5} e^{FV/2RT}, \tag{62}$$

where $0.1 < \gamma < 0.3$, and the following reaction sequence:

$$\mathrm{R_{soln}} \rightleftharpoons \mathrm{R_{ads}} \tag{63}$$

$$\mathrm{H_2O} \xrightarrow{\text{slow}} \mathrm{OH} + \mathrm{H^+} + e_0{}^- \tag{64}$$

$$\mathrm{OH_{ads}} + \mathrm{R_{ads}} \rightarrow \text{Intermediate} \tag{65}$$

$$\text{Intermediate} \rightarrow \mathrm{CO_2} \tag{66}$$

where R represents the hydrocarbon.

It must be pointed out that the above reaction scheme applies only to activated platinum electrodes. On unactivated Pt electrodes, as well as on other metals, the mechanism appears to be different. Mechanism studies on such substrates are still in progress[10].

6. SOME MODELS OF ELECTRODES FOR IMPROVING PERFORMANCE

(i) *General*

In most of the fuel-cell systems, which are attractive from maximum feasible performance and economic considerations, the reactants are gases or rather insoluble liquids. The electroactivity of these species on smooth or rough planar electrodes is low at practical cell voltages. Electrode designs should be such that practical current densities (current/geometric area) are attained at reasonable cell voltages, *i.e.*, activation and concentration polarization should be considerably reduced. The other important factors are decrease of the internal resistance of the cell, and increase of power/weight and power/volume ratio. Some models for improving the performance, which are either presently used or proposed, will be dealt with in the following sections.

(ii) *Porous electrodes*

Several models have been proposed for the mode of operation of porous

electrodes[36–39]. Any proposed model must serve two purposes. It should be simple but as close as possible to reality. Secondly, it must explain the current–potential behavior, limiting currents, etc., observed experimentally. Some of the recent models proposed will be considered in the following sections. In the analysis of the behavior of the single pore, a comparison with experiment will be made.

(a) *Thin film model.* A theoretical and experimental analysis of the current–potential relation at a thin film formed on the external surface of a Pt cylinder was made in the study of the hydrogen dissolution reaction[36,37]. AUSTIN *et al.* extended this treatment to porous gas diffusion electrodes[38] (Fig. 19). Such a model applies to

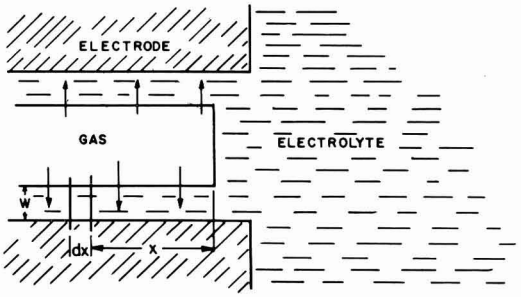

Fig. 19. Thin film model of porous electrode.

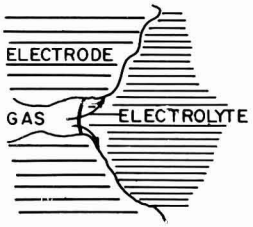

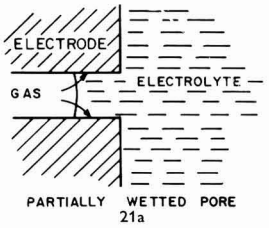

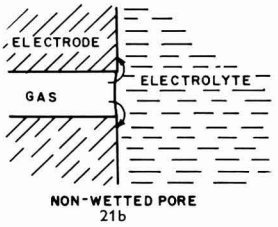

Fig. 20. Simple pore model for porous electrode.

Fig. 21. Idealized form of simple pore model.

wetted electrodes of a double-porosity structure. It is difficult to use this model for non-wetting electrodes unless one assumes that the micropores and channels will wet while the bulk surface will not. It is necessary to assume that the film is long compared to its thickness. The model has been analyzed, taking into account all forms of polarization losses. It was necessary to distinguish three regions: (a) low current density region where ohmic and mass transfer effects are small; (b) limiting current region where the potential changes rapidly for small changes of current; and (c) intermediate region where all effects are important. On this model, AUSTIN *et al.* showed that the limiting current is given by

$$i_L = DnF\, c_o \frac{At}{W} \tag{67}$$

where c_o is the concentration of the reactant in the film and t is the length of the film.

To have i_L as high as possible, t should be large and W small. With $n=2$ (say for H_2 as reactant), $D=10^{-4}$ cm^2 sec^{-1}, $c_o=10^{-6}$ g moles cm^{-3} and $i_L=2\,t/W$ mA cm^{-2}. Thus, taking a film length of 0.05 cm and a film thickness of 1 μ, a current of 1 A cm^{-2} can be maintained.

(b) *The simple pore model.* For non-wetted pores, the more appropriate model is the simple pore model[38] (Fig. 20). An idealized form of this model for simplifying the mathematical solution of the current–potential relation is given in Fig. 21. The mode of operation of this model is as follows: The gas diffuses through the pores to the electrolyte surface, dissolves in the electrolyte and reaches the active sites, where reaction occurs. A limiting current is reached when the concentration of reactant gas is zero at the electrode surface. The limiting current density is given by

$$i_L = \frac{12\,n\,F\theta DKP}{R} \text{ A cm}^{-2} \tag{68}$$

where K is Henry's constant for the dissolution of the reactant in the reactant, P is the reactant pressure, n is the number of electrons transferred in the overall reaction, θ is the fraction of open area/cm^2 of geometric area of the electrode and R is the pore radius. Using $KP=10^{-6}$ g moles cm^{-2}, $n=2$, $\theta=1/4$ and $D=10^{-4}$ cm^2 sec^{-1}, for a current density of 1 A cm^{-2} or greater, R must be 0.5 μ or less.

(c) *The intersecting pore model.* The above models are in some respects over-simplified. For example, parallel cylindrical pores of uniform size are assumed. The real structure of a porous electrode is considerably more complex. BURSHTEIN *et al.*[39] proposed a model in which there are intersections of micropores with macropores (Fig. 22). Due to the multitude of intersections of micropores with macropores, the whole surface of the macropore can be assumed to be covered with a thin electrolyte film. The reactant gas (*e.g.*, H_2) free of electrolyte enters the macropores. It then diffuses through the thin film and adsorbs on the electrode dissociatively; this is

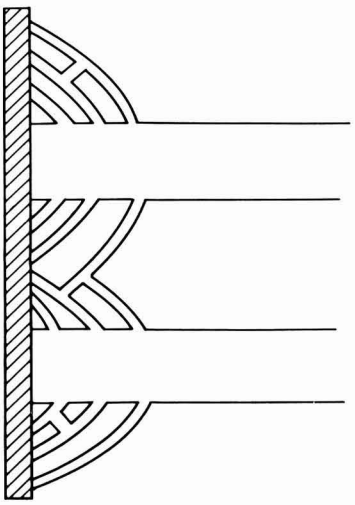

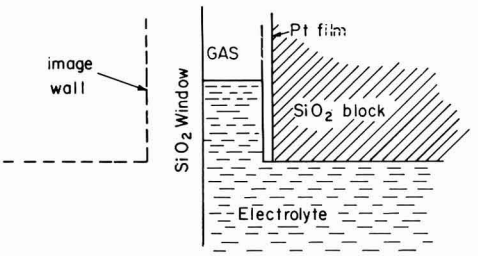

Fig. 22. Model of intersecting micro- and macro-pores.

Fig. 23. Cell for study of single pore.

followed by ionization of the adsorbed atoms (*e.g.*, H atoms). These ions are then conducted through the micropores containing the electrolyte to the bulk of the electrolyte. To obtain optimum electrochemical activity, it is necessary to have a critical ratio of the total cross-section of the micropores to the surface area of the macropores.

The current was expressed in terms of the effective electric conductivity (ϱ_e) and the specific reaction area (S_e). It was assumed that diffusion of reactants in the gas phase and migration of ions in solution are fast. ϱ_e and S_e were expressed in terms of the pore radii using a statistical method. The maximum current density is given by

$$i_m = k \sqrt{\frac{\delta v_1^2 v_2}{\beta r_2}} \tag{69}$$

where δ is the length of the reaction zone, v_1 and v_2 are the liquid and gas porosities, respectively, β is the mean tortuosity factor in the micropores, r_2 is the mean radius of the gas pores and k is a constant.

Suppose $v_2 = v_1 = v$, the electrochemical rate is proportional to $v^{3/2}$. The current is also inversely proportional to the square-root of the mean radius of the gas pores. Using eqn. (69) BURSHTEIN *et al.* arrived at values of current densities ranging from 10^{-3}–3 A cm^{-2} when r decreases from 10 to $10^{-2}\,\mu$.

(d) *Analysis of behavior of single pore.* Because of the complexity of structure of the porous electrodes commonly used, an exact theoretical analysis appears rather difficult. In the elucidation of the mode of operation of a porous electrode, two types of study are essential—the behavior of single pores and that of the complex porous electrode itself. From the first alone, useful information can be obtained concerning the mode of operation of the complex structure. The study of the behavior of a single pore is being carried out by BOCKRIS, NANIS AND CAHAN[40] using the following arrangement. A narrow gap is introduced between a working planar electrode and a non-conductive plane which is the axis of symmetry (Fig. 23). The reactant is introduced at the top of the slit and the electrolyte joins a large reservoir at the bottom. The reservoir compartment contains the counter electrode and the reference electrode. The volume in the reservoir compartment is so controllable that the height in the slit can be varied to any desired value (to within 0.1 mm).

The working electrode and the plane opposite it are optical flats and the width between them can be controlled and reproduced. The widths may vary from 0.003 mm upwards which correspond to equivalent pore sizes. The reaction being studied is the dissolution of hydrogen on Pt in sulfuric acid. Platinum sputtered on to a tantalum film on an optical flat glass (thickness of Pt, 1 μ), serves as the working electrode. This model can be used for study under a variety of experimental conditions. For example, the pore width and the depth of electrolyte penetration can be varied simultaneously. Further, it is possible to study both wetted and non-wetted electrodes, since the electrolyte can be forced into or withdrawn from the pores. Because of the one-dimensional configuration of the electrode, a considerably higher current can be drawn from it than from a cylindrical pore. Steady-state current–potential measurement and non steady-state potentiostatic measurements have been carried out for the hydrogen dissolution reaction varying the height and width of the pore.

Optical examination of the meniscus indicates a finite contact angle. Microscopical examination of the meniscus in the pore showed an unusual behavior. The gas–solution–electrode boundary shifted and microscopical droplets covered the electrode; they subsequently grew in size and moved downwards to join the main liquid. Had a film been present on the electrode, it would not have been possible to make this observation. This behavior was interpreted as due to local heating effects. These effects would arise from the fact that the current is localized in a very small area near the meniscus and hence sufficient heat is generated in this area to cause water evaporation and condensation on the wider part of the electrode above the meniscus.

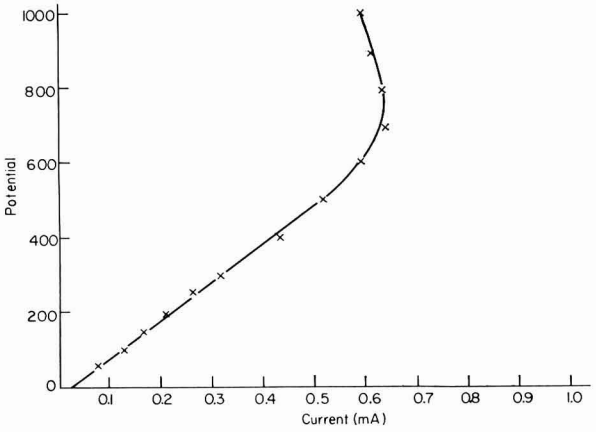

Fig. 24. Current–potential behavior on an unactivated Pt electrode in the single pore.

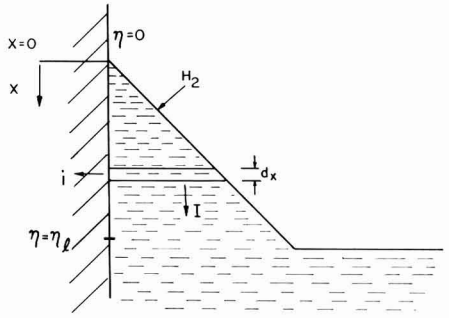

Fig. 25. Model for mathematical analysis of expected current–potential relation in single pore.

Steady-state measurements on non-activated electrodes show that the current–potential relation is linear from very low potentials to about 600 mV (Fig. 24). CAHAN[41] has carried out a mathematical analysis for the expected current-potential behavior, assuming that the meniscus makes an angle of 45° with the electrode (Fig. 25). It was also assumed that activation processes are fast compared to the diffusion of the dissolved gas and the transport of ions through the electrolyte. Under

steady-state conditions, the applied potential is η_l at $x=l$. The potential decreases from $x=l$ to $x=0$ and may be assumed to be zero at $x=0$. The total current (I_t) that leaves the electrode is the sum of the currents due to hydrogen dissolution on the electrode from $x=0$ to $x=l$. The potential drop ($d\eta$) across a thin slice of thickness dx (Fig. 25)is given by

$$d\eta = I\, dR = I\varrho(dx/x) \tag{70}$$

where I is the total current from $x=0$ to $x=x$, ϱ is the specific resistivity of the solution and $x \times 1$ is the area of the thin slice.

Since I is the integral of the local current from $x=0$ to $x=x$, it is possible to write

$$dI/dx = i \tag{71}$$

Since the activation processes were assumed to be fast, it is possible to express the local current, i, which is due to the hydrogen dissolution reaction between $x=x$ and $x=x+dx$, by the rate of hydrogen diffusion to the electrode from the gas–solution interface. Assuming the diffusion-layer thickness is equal to the shortest distance from the gas–solution interface to the electrode at $x=x$, the local current, i, is given by

$$i = 2\sqrt{2}\,\frac{DFc_o}{x}\,[1-\exp(-2\,\eta F/RT)] \tag{72}$$

Using eqns. (70) to (72), it follows that

$$\frac{x^2 d^2\eta}{dx^2} + x\,\frac{d\eta}{dx} = 2\sqrt{2}\,DFc_o\varrho[1-\exp(-2\,\eta F/RT)] \tag{73}$$

It is necessary to solve this differential equation in order that the local current or total current (I_T at $x=l$) may be evaluated. An analytical solution of this equation is possible only if the exponential term is approximated. A suitable approximation is

$$\exp(-2\,\eta F/RT) \simeq 1 - \frac{2\eta F}{RT} + b\left(\frac{2\eta F}{RT}\right)^2 \tag{74}$$

where with $b=0.3925$, the approximation is valid for $2\,F\eta/RT \leqslant 1$.

Using eqn. (74) in eqn. (73) and assuming the boundary conditions that at $x=0$, $\eta=0$, and at $x=l$, $\eta=\eta_l$.

$$\eta = \eta_l \left(\frac{x}{l}\right)^{1/s} \tag{75}$$

where

$$S = \frac{8\sqrt{2}\,DFc_o\varrho\eta}{bRT} \tag{76}$$

Using eqns. (70) and (75),

$$I = \frac{x}{\varrho}\cdot\frac{d\eta}{dx}$$

$$= \frac{\sqrt{S}}{\varrho}\cdot\eta_l\cdot\left(\frac{x}{l}\right)^{1/s} \tag{77}$$

The total current is obtained by putting $x=l$ in the last equation. Thus,

$$I_t = \frac{\sqrt{S}}{\varrho} \cdot \eta_t \,. \tag{78}$$

The local current at $x=x$, is given from eqns. (71) and (77) by

$$i = \frac{S}{\varrho} \frac{\eta_t}{l\sqrt{S}} \frac{x\sqrt{S}}{x} \tag{79}$$

With $D=10^{-5}$ cm^2 sec^{-1}, $F=10^5$ C, $c_o=10^{-6}$, $\varrho=1$ Ω cm and $F/RT=40$, S is of the order of 10^{-3}. Thus the above analysis shows that (a) the total current (I_t) varies linearly with the applied potential (η_t) as is observed experimentally and (b) the local current (i) tends to very large values as $x\to 0$. However, due to activation limitations, which were assumed to be absent in the present analysis, the current does not rise very high.

The work of WILL[37] showed that the current density is spread out over a considerable range in a thin film when the electrodes of high roughness factor were used and when they were pre-wetted. However, when smooth unwetted electrodes were used, the current–potential observed by WILL was similar to that of the present work.

(iii) *Jet electrode*

(a) *Model.* A second possible arrangement to facilitate mass transport conditions to the electrode is the use of a jet-electrode system. This method, also, should prove useful in the case of liquid hydrocarbons. The model suggested is as follows. The electrolyte saturated with the hydrocarbon is forced through a jet at high speeds

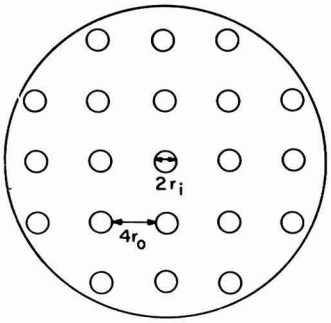

Fig. 26. Cross section of model of jet electrode.

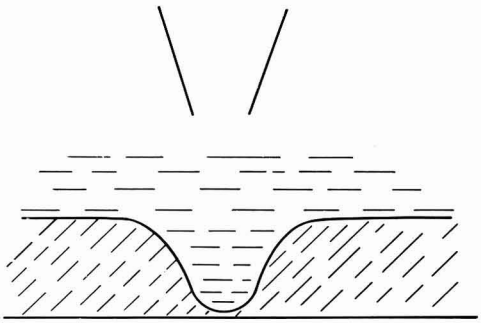

Fig. 27. Variation of diffusion-layer thickness with distance from center of projection of jet on metal plate.

on a metal plate which acts as the anode. Alternate tubes are the jets while the remaining tubes also contain the electrolyte, oxidant (*e.g.*, O_2) and the electrocatalyst for the reduction process. A horizontal cross-section of the jet electrode model is shown in Fig. 26. This arrangement should minimize ohmic polarization losses.

The diffusion layer for the transfer of the hydrocarbon to the metal electrode

is considerably reduced, due to the high velocity of the impinging electrolyte through the jet. A layer adjacent to the metal electrode plane is not affected by the turbulence caused by the streaming jet. This layer is more or less stationary. The thickness of this layer depends on the velocity of the streaming jet. Beyond this layer, there is perfect turbulence and the concentration of the hydrocarbon can be assumed to be effectively constant and equal to the saturation value. The diffusion-layer thickness may therefore be assumed to be equal to the thickness of the stationary sublayer. The thickness of this sublayer is not altered by rotating the metal electrode.

(b) *Calculation of limiting current.* Suppose the inner radius of the tubes is r_i and the outer radius r_o. Let the distance between the centers of two adjacent tubes be equal to $4\,r_o$. Thus the closest distance between the centers of two fuel jets or two cathode compartments is $8\,r_o$. A cross-section of the tubes is in the form of a cubic array.

It is assumed that the effective anodic area caused by one jet is the projection of the inner area of the tube on the metal plate, *i.e.*, πr_i^2. This assumption is valid, since the stationary layer outside this area on the metal plate increases rapidly (Fig. 27). The number of jets (N), which may be arranged at a closest distance of $8\,r_i$ apart, to cover a metal electrode of radius R is given by

$$N = \frac{2\pi R^2}{64\,r_o^2} \tag{85}$$

Thus, the effective anodic area (A_a) is

$$A_a = \frac{2\pi R^2}{64\,r_o^2} \cdot \pi r_i^2$$

$$= \frac{2\pi^2 R^2 r_i^2}{64\,r_o^2} \tag{86}$$

The limiting current for the jet model is therefore given by

$$I_{L,j} = \frac{2DZFc_0}{\delta_j} \cdot \frac{\pi^2 R^2 r_i^2}{64\,r_o^2} \tag{87}$$

The limiting current for a planar electrode of area equal to that of the disk in the presence of stirring is

$$I_{L\,p} = \frac{DzFc_o}{\delta_p} \cdot \pi R^2 \tag{88}$$

Thus, the ratio of the currents obtainable from a jet model to those from a planar model is

$$\frac{I_{L,j}}{I_{L,p}} = \frac{2\pi}{64} \frac{r_i^2}{r_o^2} \cdot \frac{\delta_p}{\delta_j} \tag{89}$$

Assuming $r_1 \simeq r_o$, $\delta_p = 10^{-3}$ cm, $\delta_j = 10^{-6}$ cm

$$I_{L,j} \simeq 100\, I_{L,p} \tag{90}$$

An improvement of about 100 times over the planar situation is obtained. A further increase by a factor of four may be obtained by having the tubes practically touching each other.

(v) *Spaghetti tube model*

The model consists of a number of parallel tubes, through which the fuel and oxidant flow in adjacent tubes (Fig. 28). On the outside of each tube is a catalyst. At present, these permeable spaghetti sticks with metallic conduction are not available. However, research is directed at obtaining them.

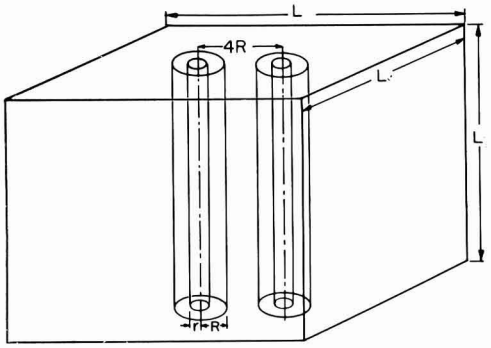

Fig. 28. The spaghetti tube model.

The outer diameter of the tubes is R, and the inner diameter is r. The current drawn from each pair of tubes is $2\pi RLi$ where i is the current density of operation at a reasonably small polarization loss and L is the length of the cubic module. The number of electrode pairs/nodule (N) is given by

$$N = L^2/32\,R^2 \tag{91}$$

Thus, the total current drawn from the nodule (I_T) is

$$I_T = \frac{2\pi RL^3}{32\,R^2} \cdot i$$

$$= i\,\frac{\pi L^3 i}{16\,R} \tag{92}$$

Thus, the current/cm^3 (i_v) is

$$i_v = \pi i/16\,R \tag{93}$$

Using $i = 10^{-2}$ A cm^{-2} and $R = 10^{-2}$ cm, $i_v \triangleq 2 \cdot 10^{-1}$ cm$^3 \triangleq 5 \cdot 10^3$ amp ft.$^{-3}$. This value of i_v compares favorably with almost the best available fuel-cell systems. Losses due to ohmic polarization in the solution and in the electrodes were considered but shown to be negligible for this arrangement. To maintain the assumed value of current density, it is necessary to have a pressure differential of about 3 atm for a tube of length 10 cm.

ACKNOWLEDGEMENTS

Financial support from the National Aeronautics and Space Administration (NsG 325) is gratefully acknowledged. The authors thank Drs. H. WROBLOWA, H. D. HURWITZ and Messrs. M. GENSHAW AND B. CAHAN for helpful discussions and suggestions. The authors much appreciate the valuable comments made by Mr. E. M. COHN.

SUMMARY

The basic similarities and dissimilarities among the three electrochemical devices—electrochemical substance producer, electrochemical electricity producer and electrochemical electricity storer— are presented. Expressions are derived for the terminal cell potential, differential resistance, efficiency and power of an electrochemical electricity producer as a function of the current drawn from it. These expressions have been used in numerical calculations to examine the effect of the various factors (*e.g.*, exchange currents, limiting currents, ohmic internal resistance) on the performance of the electrochemical energy converter. Analytical expressions for the maximum power, the terminal cell potential and the current, when the power is a maximum, are derived for two special cases.

The importance of electrocatalysis from the point of view of improving the performance of electrochemical electricity producers is stressed. Recent work on the kinetics of the important oxygen electrode reaction and on the mechanism of electro-organic oxidation is discussed. Some models of electrode design for increasing the apparent current density (and thereby reduce efficiency and power losses) are dealt with theoretically.

REFERENCES

1 D. B. MATTHEWS, Ph.D. Thesis, University of Pennsylvania, 1965.
2 B. E. CONWAY AND J. O'M. BOCKRIS, *J. Chem. Phys.*, 26 (1957) 532.
3 A. DAMJANOVIC, J. O'M. BOCKRIS AND R. JAHAN, to be published.
4 B. E. CONWAY, E. M. BEATTY AND P. A. D. DEMAINE, *Electrochim. Acta*, 7 (1962) 39.
5 R. PIONTELLI, L. PERALDO BICELLI AND A. LAVECCHIA, *Rend. Accad. Naz. Lincei, VIII*, 27 (1959) 312.
6 A. K. N. REDDY, A. PAUNOVIC AND J. O'M. BOCKRIS, University of Pennsylvania Report (NASA Contract No. NsG 325).
7 M. L. B. RAO, A. DAMJANOVIC AND J. O'M. BOCKRIS, *J. Phys. Chem.*, 67 (1963) 2508.
8 A. DAMJANOVIC, V. BRUSIC AND J. O'M. BOCKRIS, to be published.
9 H. DAHMS AND J. O'M. BOCKRIS, *J. Electrochem. Soc.*, 111 (1964) 728.
10 A. T. KUHN AND J. O'M. BOCKRIS, to be published.
11 J. O'M. BOCKRIS AND A. K. M. S. HUQ, *Proc. Roy. Soc. London*, A237 (1956) 277.
12 N. WATANABE AND M. A. V. DEVANATHAN, *J. Electrochem. Soc.*, 111 (1965) 615.
13 M. GENSHAW, to be published.
14 J. P. HOARE, *J. Electrochem. Soc.*, 110 (1964) 1019.
15 H. WROBLOWA, M. L. B. RAO, A. DAMJANOVIC AND J. O'M. BOCKRIS, to be published.
16 W. VISSCHER AND M. A. V. DEVANATHAN, *J. Electroanal. Chem.*, 8 (1964) 127.
17 H. A. LAITENEN AND C. A. ENKE, *J. Electrochem. Soc.*, 107 (1960) 773.
18 M. D. MORRIS, *J. Electroanal. Chem.*, 8 (1964) 305.
19 A. K. N. REDDY, M. GENSHAW AND J. O'M. BOCKRIS, *J. Electroanal. Chem.*, 7 (1964) 487.
20 L. NEKRASSOV AND L. MÜLLER, *Electrochim. Acta*, 9 (1964) 1015.
21 M. GENSHAW, A. DAMJANOVIC AND J. O'M. BOCKRIS, to be published.
22 V. G. LEVICH, *Physicochemical Hydrodynamics*, translation by Prentice Hall, Inc., Englewood Cliffs, N. J., 1962.
23 J. O'M. BOCKRIS, M. A. V. DEVANATHAN AND K. MÜLLER, *Proc. Roy. Soc. London*, A274 (1963) 55.

24 E. BLOMGREN AND J. O'M. BOCKRIS, *Nature*, 186 (1960) 305.
25 J. O'M. BOCKRIS, M. GREEN AND D. A. J. SWINKELS, *Rev. Sci. Inst.*, in press.
26 W. N. HEILAND, E. GILEADI AND J. O'M. BOCKRIS, to be published.
27 H. DAHMS AND M. GREEN, *J. Electrochem. Soc.*, 110 (1963) 466.
28 E. GILEADI, B. T. RUBIN AND J. O'M. BOCKRIS, *J. Phys. Chem.*, to be published.
29 J. O'M. BOCKRIS, D. A. J. SWINKELS AND M. GREEN, *J. Electrochem. Soc.*, 111 (1964) 743.
30 J. O'M. BOCKRIS AND D. A. J. SWINKELS, *J. Electrochem. Soc.*, 111 (1964) 736.
31 H. WROBLOWA, B. J. PIERSMA AND J. O'M. BOCKRIS, *J. Electroanal. Chem.*, 6 (1963) 401.
32 P. DELAHAY AND I. TRACHTENBERG, *J. Am. Chem. Soc.*, 79 (1957) 2355.
33 E. A. BLOMGREN, J. O'M. BOCKRIS AND C. JESCH, *J. Phys. Chem.*, 65 (1961) 2000.
34 H. WROBLOWA, E. GILEADI, J. O'M. BOCKRIS AND B. J. PIERSMA, *Trans. Faraday Soc.*, to be published.
35 E. GILEADI AND S. SRINIVASAN, *J. Electroanal. Chem.*, 7 (1964) 452.
36 F. G. WILL, *J. Electrochem. Soc.*, 110 (1963) 145.
37 *Ibid.*, 110 (1963) 152.
38 L. G. AUSTIN, M. ARIET, R. D. WALKER, G. B. WOOD AND R. H. COMYN, Penn. State University, Report No. 7 to HDL (Contract No. DA 49-186-AMC-146(D)).
39 R. KH. BURSHTEIN, V. S. MARKIN, A. G. PSHENICHNIKOV, YU. A. CHISMADZHEV AND YU. G. CHIRKOV, Paper presented at 14th C.I.T.C.E. Meeting.
40 J. O'M. BOCKRIS, L. NANIS AND B. CAHAN, *J. Electroanal. Chem.*, 9 (1965) 474.
41 B. CAHAN, to be published.
42 K. SCHWABE, *Z. Elektrochem.*, 61 (1957) 744.
43 M. P. BOUTRY, O. BLOCH AND J. C. BALACENU, *Compt. Rend. Sci.*, 254 (1962) 2583.
44 H. GERISCHER, *Ber. Bunsengess.*, 67 (1963) 164.
45 J. VAN HELD AND H. GERISCHER, *ibid.*, 67 (1963) 921.
46 H. D. HURWITZ, S. SRINIVASAN AND J. O'M. BOCKRIS, to be published.

SHORT COMMUNICATIONS

Polarography of europium in formamide

The polarographic reduction process of the rare earths is of two types. The rare earths in one group are directly reduced to the metallic state in a three-electron reaction and those of the other group (samarium, europium and ytterbium) are characterised by a single-electron reduction. HOLLECK[1] and LAITINEN[2] have demonstrated that the reduction of Eu^{3+} in 0.1 *M* ammonium chloride gives a well-defined single wave with a half-wave potential of −0.67 V *vs.* S.C.E. Similar results have been obtained by HIBBITS *et al.*[3] in a polarographic study of Eu^{3+} in lithium chloride, ammonium chloride and tetramethylammonium bromide supporting electrolytes. MISUMI AND IDE[4] have studied the polarography of europium in lithium iodide, lithium chloride and lithium perchlorate solutions. In all these cases, they obtained two irreversible waves, the first for a one-electron and the second for a two-electron reduction. The aqueous polarography of Eu^{3+} has been carried out in these laboratories in sodium chloride, ammonium chloride and sodium perchlorate supporting electrolytes. In the pH range 2.9–4, two waves were obtained in every case. The first wave indicated a one-electron reduction from Eu^{3+} to Eu^{2+} with a half-wave potential of −0.67 V *vs.* S.C.E. The second wave was found to be a hydrogen wave which disappeared above pH 4.0.

A study of the literature and our own results indicate that there is little evidence for reduction to the metallic state and that reproducible results are difficult to obtain. In view of the conflicting results in aqueous medium, the polarography of Eu^{3+} has been studied in non-aqueous media.

The polarography of Eu^{3+} in acetonitrile and acetone media has been studied by KOLTHOFF AND COETZEE[5] and by COETZEE AND SIAO[6] in various supporting electrolytes. The present paper reports the results of the polarographic study of Eu^{3+} in formamide medium at the D.M.E.

Experimental

The polarographic set-up used was the same as described earlier[7]. The D.M.E. had the following characteristics: $m = 1.76$ mg/sec and $t = 4.7$ sec. The diffusion currents were corrected for the residual currents. The iR drop correction was made by measuring the resistance of the cell with the help of a L.P. 024 conduscope. All experiments were carried out at a temperature of $25 \pm 0.2°$ by means of Haake-type N6114/ultra thermostat. The temperature coefficient was determined by raising the temperature from 25° to 35°. Purified nitrogen was used for removing the dissolved oxygen. The gas was pre-saturated by passing it through a solution of the same composition as that of the experimental mixture.

The europium solution was prepared by dissolving 99.99% europium oxide (Eu_2O_3) in the minimum quantity of A.R.-grade perchloric acid; pure sodium perchlorate was used as supporting electrolyte. A maxima suppressor was found to be unnecessary. Formamide (E. Merck) dried with sodium sulphate was used in all cases. Solutions containing 0, 10, 20, 40, 60, 80 and 100% formamide were prepared. The

diffusion current (i_d) was plotted against $\sqrt{h}$ after making correction for the back pressure.

Results and discussion

Europium gives a single well-defined wave in aqueous solution and in mixtures containing 20, 40, 60, 80 and 100% of formamide. The half-wave potential shifts to the negative side with increasing concentration of formamide up to 60% and then decreases in 80% formamide. The wave height decreases as the concentration of formamide is increased. The plot of the wave height (i_d) *vs.* $\sqrt{h}$ is linear and passes through the origin indicating that the current is diffusion-controlled. This is further confirmed by the temperature coefficient determination. The plot of $\log i/(i_d - i)$ *vs.* $E_{\text{d.e.}}$ is linear in all cases. The values of the slopes indicate that the reduction is irreversible in mixtures containing 0–60% formamide. At higher concentrations of formamide the reduction is reversible.

TABLE 1

Formamide (% *v/v*)	i_d (μA)	$E_{\frac{1}{2}}$ (*V vs. S.C.E.*)	*Slope* (*V*)	αn	* K_s (*cm sec*$^{-1}$)	* K_f^0 (*cm sec*$^{-1}$)
1 m*M* Eu^{3+} in 0.2 *M* $NaClO_4$						
0	5.34	−0.68	0.085	0.258	1.738×10^{-3}	2.344×10^{-5}
20	5.14	−0.698	0.082	0.230	7.762×10^{-4}	3.388×10^{-5}
40	4.339	−0.706	0.07	0.255	6.109×10^{-4}	2.818×10^{-5}
60	4.005	−0.717	0.065	0.33	4.634×10^{-4}	2.818×10^{-6}
80	3.471	−0.713	0.064	0.317	2.754×10^{-4}	1.622×10^{-5}
100	2.937	−0.74	0.063	0.265	1.698×10^{-4}	8.318×10^{-5}
1.5 m*M* Eu^{3+} in 0.1 *M* $NaClO_4$						
0	8.41	−0.695	0.087	0.206	1.603×10^{-3}	6.166×10^{-5}
20	8.345	−0.685	0.085	0.183	1.429×10^{-3}	9.772×10^{-5}
40	6.209	−0.690	0.069	0.283	9.55×10^{-4}	1.66×10^{-5}
60	5.474	−0.721	0.065	0.371	6.607×10^{-4}	5.623×10^{-6}
80	5.074	−0.718	0.062	0.298	8.590×10^{-4}	1.259×10^{-5}
100	4.539	−0.725	0.062	0.280	6.310×10^{-4}	1.023×10^{-5}

* K_s- and K_f^0-values reported are *vs.* N.H.E.

The kinetic parameters for the reaction at the D.M.E. have been calculated by Koutecký's method for irreversible processes. The mathematical solution for the electrode reactions at the D.M.E. which are controlled by the kinetics of electron transfer, is given in the form

$$i_l/i_d = F(x) - \xi H_c(x) = F'(x) \qquad (1)$$

where $x = K_f(12t/7D)^{1/2}$, $\xi = 50.4\ D^{1/2}m^{-1/3}t^{1/6}$, i_l the maximum limiting current along the polarogram, i_d the maximum diffusion current, t the drop time, D the diffusion coefficient and K_f the rate constant for the forward reaction in the irreversible process which varies with the electrode potential, E, according to the equation

$$K_f = K_f^0 \exp\left(-\frac{\alpha n F E}{RT}\right)$$

where α is the transfer coefficient, n the number of electrons involved in the

rate-determining step and K_f^0 the rate constant of the electron transfer at zero volts *vs.* N.H.E.

The plot of $-\log K_f$ *vs.* E ($-$volt N.H.E.) gave a straight line the slope of which is equal to $\alpha nF/2.303RT$ from which the αn-values have been calculated. Extrapolation to the values of $E_{\frac{1}{2}}$ and o V gave the values of K_s and K_f^0, respectively, where K_s is the standard rate constant. The results have been summarised in Table 1.

The decrease in i_d with the increasing concentration of formamide is due to the increase in the viscosity. The polarographic reduction of Eu^{3+} in formamide affords an interesting method for the determination of europium.

Chemical Laboratories, J. N. GAUR
University of Rajasthan, K. ZUTSHI
Jaipur (India)

1 L. HOLLECK, *Z. Naturforsch.*, 2b (1947) 81.
2 H. A. LAITINEN AND W. A. TAEBEL, *Ind. Eng. Chem., Anal. Ed.*, 13 (1941) 825.
3 J. O. HIBBITS, M. R. MENKE AND W. F. DAVIS, *At. Energy Rept., Apex-405 (1958)*, Office of Technical Services, U.S. Department of Commerce.
4 SEIZO MISUMI AND YASUSHI IDE, *Bull. Chem. Soc. Japan*, 32 (1959) 1159.
5 I. M. KOLTHOFF AND J. F. COETZEE, *J. Am. Chem. Soc.*, 79 (1957) 1852.
6 J. F. COETZEE AND W.-S. SIAO, *Inorg. Chem.*, 2 (1963) 14.
7 K. ZUTSHI, *J. Electroanal. Chem.*, 6 (1963) 198.
8 J. KOUTECKY AND J. ČÍŽEK, *Collection Czech. Chem. Commun.*, 21 (1956) 836.

Received July 3rd, 1965

J. Electroanal. Chem., 11 (1966) 390–392

Polarographisches Halbstufenpotential des 1. angeregten Singulettzustandes

In der Natur spielen Redoxreaktionen angeregter Moleküle eine bedeutende Rolle, so dass ein grosses Interesse an der Ermittlung des Halbstufenpotentials in den verschiedenen Anregungszuständen besteht. Obwohl bis zu den kurzen Lebenszeiten des 1. angeregten Singulettzustandes (10^{-9}–10^{-8} sec) diffusionsbedingte Reaktionen durchaus möglich sind[1], ist schon bei den wesentlich längerlebigen Triplettmolekülen (10^{-3} sec bis einige Sekunden) eine experimentelle polarographische Ermittlung nicht einfach[2,3]. Niedrige Konzentrationen angeregter Moleküle, Sekundärreaktionen mit dem Lösungsmittel und dynamische Löschung an der Quecksilbertropfelektrode[4] er-

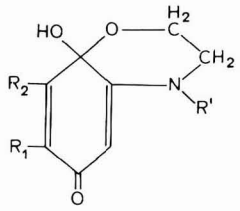

(I)

schweren die Messbedingungen. Für angeregte Singulettzustände ist eine direkte, polarographische Ermittlung unseres Wissens nach noch nicht möglich gewesen, so dass man auf indirekte Methoden, insbesondere in Verbindung mit der Spektroskopie, angewiesen ist.

Bereits in anderen Mitteilungen[5,6] wurde gezeigt, dass zwischen der Desaktivierung des Anregungszustandes und dem polarographischen Halbstufenpotential einer Reihe von Chinolderivaten mit Merocyaningruppierung (I) eine Beziehung besteht. Dieser Zusammenhang kann jedoch, wie aus den Abb. 1 und 2 zu entnehmen ist, nicht einfacher Art sein. Während nämlich nach Abb. 2 der Desaktivierungsprozess, ausgedrückt durch dessen Aktivierungsenergie, vorwiegend von der veränderten Elektronenverteilung des Anregungszustandes abhängig ist, wird das polarographische Halbstufenpotential zumindest durch einen elektronischen und einen sterischen Anteil bedingt[7]. Der elektronische Anteil überwiegt bei der Kernsubstitution. Zur Interpretation wurde vorgeschlagen, dem Chinol mit seinem Aminosubstituenten eine Reaktionskonstante zuzuordnen und die Veränderung der $\pi_{\frac{1}{2}}$-Werte bei Kernsubstitution durch induktiven Einfluss der Methylgruppen zu deuten[5]. Dafür spricht, dass die Verbindungen I, II und III und IV, V und VI auf annähernd parallel zueinander verlaufenden Geraden liegen. Beide Gruppen haben Seitenkettensubstituenten extrem verschiedener Länge (Verbindungen mit Phenylresten in der Seitenkette liegen nicht auf den Geraden). Ein qualitativer Vergleich der in Abb. 1 gegeneinander auf-

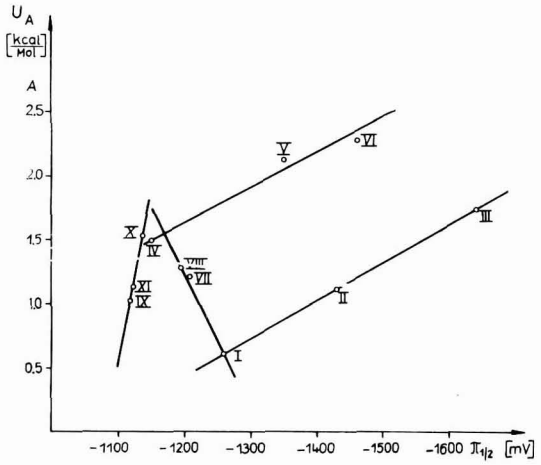

R_1, R_2, R'

I:	H,	H,	CH_3	IV:	H, H, $CH_2—CH_2—OH$
II:	CH_3,	H,	CH_3	V:	CH_3, H, $CH_2—CH_2—OH$
III:	CH_3,	CH_3,	CH_3	VI:	CH_3, CH_3, $CH_2—CH_2—OH$
VII:	H,	H,	C_2H_5	X:	H, H, $CH_2—C_6H_5$
VIII:	H,	H,	C_3H_7	XI:	H, H, $CH_2—CH_2—C_6H_5$
IX:	H,	H,	C_6H_5		

Abb. 1. U_A als Funktion von $\pi_{\frac{1}{2}}$; Lösungsmittel: Äthylalkohol (Fluoreszenz) bzs. 60% Äthylalkohol + 40% Phosphatpuffer 0.1 *M*, pH 7 (Polarographie); $c = 5 \cdot 10^{-4}$ *M* (F) und $c = 1 \cdot 10^{-4}$ *M* (P).

getragenen Messgrössen $\pi_{\frac{1}{2}}$ und U_A (Aktivierungsenergie des strahlungslosen Prozesses, Definition nach BOWEN UND SAHU[8]) erscheint zunächst sinnvoll, da sowohl die Desaktivierung des Anregungszustandes als auch die Reduktion der Carbonylgruppe durch die Elektronenverteilung in der Merocyaningruppierung bestimmt werden. $\pi_{\frac{1}{2}}$- und U_A-Werte beziehen sich jedoch auf verschiedene Energiezustände des Mole-

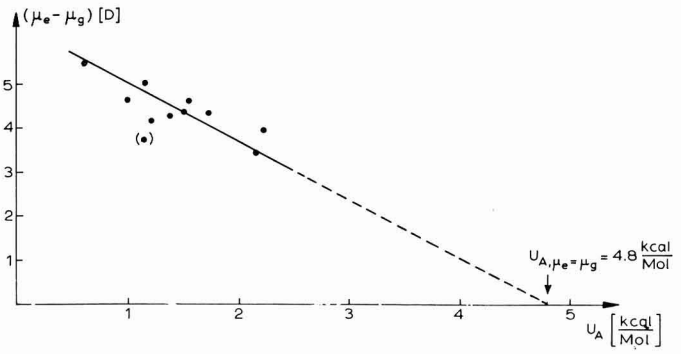

Abb. 2. $(\mu_e-\mu_g)$ als Funktion von U_A; μ_e = Dipolmoment des Anregungszustandes, μ_g = Dipolmoment des Grundzustandes[11,12].

küls und der nachgewiesene, stärker polare Charakter des ersten angeregten Singulettzustandes[9] lässt eine Positivierung des Halbstufenpotentials $\pi^*_{\frac{1}{2}}$ gegenüber $\pi_{\frac{1}{2}}$ erwarten. Es kann nun in folgender Weise auf die $\pi^*_{\frac{1}{2}}$-Werte geschlossen werden:
Nach Abb. 1 gilt für die Geraden I, II, III bzw. IV, V, VI

$$\frac{dU_A}{d\pi_{\frac{1}{2}}} = a; \quad a<0 \tag{1}$$

Wenn der sterische Einfluss auf die Halbstufenpotentiale des Grund- und Anregungszustandes gleich ist, so folgt einfach

$$\int_{U_{A,\mu_e=\mu_g}}^{U_A} dU_A = a \int_{\pi_{\frac{1}{2}}}^{\pi_{\frac{1}{2}}^*} d\pi_{\frac{1}{2}} \tag{3}$$

oder ausgerechnet

$$\pi_{\frac{1}{2}}^* = \pi_{\frac{1}{2}} + \frac{U_A - U_{A,\mu_e=\mu_g}}{a} \tag{4}$$

Dabei ist $U_{A,\mu_e=\mu_g}$ die Aktivierungsenergie für den Fall, wenn das Dipolmoment sich beim Übergang in den Anregungszustand nicht ändert. Diese hypothetische Grösse kann bei Gültigkeit einer linearen Beziehung zwischen $(\mu_e-\mu_g)$ und U_A durch Extrapolation bestimmt werden. (Näheres hierzu in[10].)

Tabelle 1 enthält eine Zusammenstellung der Ergebnisse. Folgende Abschätzung zeigt, dass die so ermittelten $\Delta\pi_{\frac{1}{2}}$-Werte zu erwarten sind. Wird nämlich die Änderung der freien Enthalpie allein durch die zugeführte Lichtenergie bedingt, so lässt sich für den reversiblen und isentropen Prozess $\Delta\pi_{\frac{1}{2}}$ nach (5) berechnen.

$$\Delta G = n \cdot F \cdot \Delta\pi_{\frac{1}{2}} \tag{5}$$

Da der O–O-Übergang aller hier untersuchten Substanzen zwischen 24 und $25 \cdot 10^3$

cm^{-1} liegt, ergibt sich dementsprechend für $n=2$ eine Positivierung um 1.5–1.6 V. Die Werte der Tabelle 1 liegen etwas niedriger, da die Annahme der Reversibilität nicht für den gesamten Reduktionsvorgang gültig ist. Versuche an einfacheren, reversiblen Systemen sind vorgesehen.

TABELLE 1

$\pi_{\frac{1}{2}}$ und $\Delta\pi_{\frac{1}{2}} = \pi_{\frac{1}{2}}^* - \pi_{\frac{1}{2}}$ für eine Reihe von Verbindungen der angegebenen Formel; zur Berechnung von $\Delta\pi_{\frac{1}{2}}$ nach Gl. 4 wurden folgende Daten verwendet:

$$a = -\frac{3 \text{ kcal}}{V \cdot M}; \quad U_{A,\mu_e-\mu_g} = (4.8 \pm 0.8)\frac{\text{kcal}}{M}$$

Nr.	$\pi_{\frac{1}{2}}$ *(V)*	$\Delta\pi_{\frac{1}{2}}$*(V)*	*Nr.*	$\pi_{\frac{1}{2}}$ *(V)*	$\Delta\pi_{\frac{1}{2}}$*(V)*
I	−1.36	1.40 ± 0,27	VII	−1.20	1.20
II	−1.43	1.22	VIII	−1.30	1.17
III	−1.63	1.01	IX	−1.04	1.25
IV	−1.15	1.10	X	−1.54	1.08
V	−1.35	0.89	XI	−1.14	1.22
VI	−1.45	0.84			

Die Polarogramme zur Bestimmung der Halbstufenpotentiale des Grundzustandes wurden mit dem Heyrovský-Polarographen LP 55 gegen NCE aufgenommen. Eine ausführliche Mitteilung, vor allem der spektroskopischen Versuche, wird an anderen Stelle erfolgen[10].

Herrn Dr. H. BERG sei für Diskussionen herzlich gedankt.

Institut für Mikrobiologie und experimentelle Therapie der Deutschen Akademie der Wissenschaften zu Berlin, Abteilung Biophysikochemie, Jena

G. LÖBER

1 A. WELLER, *Z. Physik. Chem. (Frankfurt)*, 15 (1958) 438.
2 H. BERG, *Naturwissenschaften*, 49 (1962) 11.
3 H. BERG, *Z. Chem.*, 2 (1962) 237.
4 F. GOLLMICK, Diplomarbeit, Jena, 1964.
5 G. LÖBER UND D. OSE, *Acta Phys. Polon.*, 26 (1964) 469.
6 G. LÖBER, *Z. Physik. Chem. (Leipzig)*, im Druck.
7 P. ZUMAN, *Z. Chem.*, 3 (1963) 161.
8 E. J. BOWEN UND J. SAHU, *Photochemistry in the Liquid and Solid States*, Wiley, New York–London, 1960.
9 G. LÖBER, *Z. Chem.*, 3 (1963) 399.
10 G. LÖBER, *Z. Elektrochem.*, in Vorbereitung.
11 E. LIPPERT, *Z. Elektrochem.*, 61 (1957) 957.
12 N. MATAGA, Y. KAIFU UND M. KOIZUMI, *Bull. Chem. Soc. Japan*, 29 (1956) 465.

(Eingegangen den 30 September 1965)

BOOK REVIEW

Introduction to Electroanalysis by L. L. LEVESON, Butterworths, London, 1964, 120 pages, 15 s.

This small paperback aims at providing an elementary introduction, at the undergraduate level, to the various electrochemical methods of analysis. The scope of its 120 pages, covering potentiometry, voltammetry, amperometric titrations, coulometry and conductometry, is a fair indication of the conciseness of presentation. It doubtless fulfils a need for an inexpensive text in this area but suffers unduly from the compression of material, from a considerable amount of incorrect (*e.g.*, the account of polarographic charging currents) or misleading (*e.g.*, the paragraph headed "Voltammetry with continuously changing voltage or anodic dissolution voltammetry") information and from a lack of the clear, accurate outlines of the principles of each method that one would expect to find in a work of this nature. Some of the diagrams, such as that showing a polarographic maximum leaning over, are carelessly drawn; others, including one of a dropping mercury electrode, convey the sense poorly. An unhelpful bibliography contains nearly every text-book of electrochemistry in the English language.

T. BIEGLER, University of Bristol

J. Electroanal. Chem., 11 (1966) 396

ANNOUNCEMENT

CHEMICAL INSTRUMENTATION COURSE

A course entitled "Introduction to Chemical Instrumentation" is being offered in the Department of Chemistry at Purdue University, July 10–30, 1966. The course is designed to give research scientists in chemistry and related areas a working knowledge of electronic circuits and their application in instruments. Additional information is available from Professor H. L. PARDUE, Department of Chemistry, Purdue University, Lafayette, Ind., 47907.

J. Electroanal. Chem., 11 (1966) 396

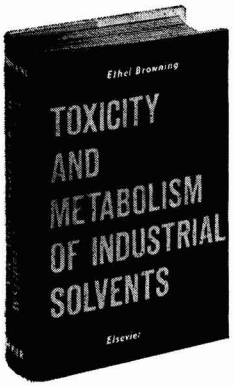

TOXICITY AND METABOLISM OF INDUSTRIAL SOLVENTS

by ETHEL BROWNING,

M. D., formerly H. M. Medical Inspector of Factories, Ministry of Labour and National Service, London

7 x 10″, xi + 739 pages, 4 tables, 1922 lit. refs., 1965, £ 9.10.0, Dfl. 95.00 or $ 32.50

Since the publication of the second edition of The Toxicity of Industrial Organic Solvents in 1953, under the auspices of the Medical Research Council of Great Britain, many new solvents have come into world-wide use, and many new investigations of their toxic effects have been made. It was therefore thought advisable to make a new assessment of this mass of new data.

With the permission of the Medical Research Council, the original publication (now out of print) has formed the basis of the present volume. But this is by no means merely a revised edition; it is, as agreed with the M.R.C., an entirely new book with an entirely new title. The introduction of the word metabolism in the new section headings draws attention to the importance of this aspect of the subject, since it is now universally recognised that the toxic effects of certain chemical substances depend almost entirely on their fate in the organism under the influence of enzymes.

The main purpose of this book is to make available a comprehensive account of the nature, uses and potential and actual toxicity of well-known and lesser-known solvents used in industry as judged from animal experiments and human experience. Recording the Threshold Limit Values as recommended in the 1965 Official List, the detailed and fully documented bibliography should also make it an useful adjunct to reference libraries.

CONTENTS:

ELSEVIER PUBLISHING COMPANY
AMSTERDAM LONDON NEW YORK

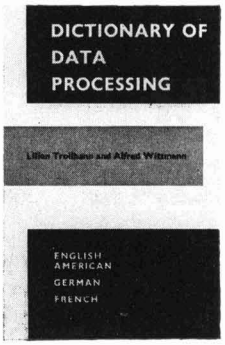

DICTIONARY OF DATA PROCESSING

compiled by **LILIAN TROLLHANN**, Munich
and **ALFRED WITTMANN**, Munich

6 x 9″, viii + 300 pages, 4533 entries, 1964, Dfl. 47.50, 95s, $17.00

The rapid spread of automatic data processing throughout the world has resulted in the steady growth of relevant literature with which scientists, technicians and linguists are confronted. The literary output of the English-, French- and Germanspeaking areas is particularly noteworthy and the present volume was conceived as the key to understanding and translation within the bounds of these three most important languages.

The Dictionary of Data Processing contains approximately 5,000 entries in English/American, German and French relating to: digital and analog computers and their most important components; mathematical terms in constant use; office automation and organization relative to commercial data processing; technical and scientific applications of computers; and civil and military data transmission terms. Listed alphabetically in English/American, each term is followed by its German and French equivalent and a reference to usage. Where this is felt to be insufficient an actual working example is given. The subsidiary part of the volume contains separate German and French cross-reference indexes allowing the user to locate rapidly the corresponding term in the basic section.

This comprehensive volume will be of immediate interest and benefit to all concerned with computers, their design, applications and programming.

ELSEVIER PUBLISHING COMPANY
AMSTERDAM LONDON NEW YORK

CONTENTS

SUBMICRO METHODS OF ORGANIC ANALYSIS

by R. BELCHER
Professor of Analytical Chemistry,
The University of Birmingham, Great Britain

6 × 9″, ix + 173 pages, 12 tables, 35 illus., 186 lit. refs., 1966, Dfl.27.50, 55s., $10.00

Contents: 1. Introduction. 2. The balance. 3. General apparatus. 4. The determination of nitrogen. 5. Carbon and hydrogen. 6. Chlorine. 7. Bromine and iodine. 8. Fluorine. 9. Sulphur. 10. Phosphorus and arsenic. 11. Carboxyl groups. 12. Organic bases in non-aqueous media. 13. Alkoxyl and N-methyl groups. 14. Acetyl groups. 15. The carbonyl group. 16. Olefinic unsaturation. 17. Oxidation with periodate. 18. The determination of nitro and nitroso groups. 19. Thiol groups. 20. The cryoscopic determination of molecular weight. Index.

TECHNIQUES OF OSCILLOGRAPHIC POLAROGRAPHY

Second Edition, completely revised and enlarged
by R. KALVODA
Institute of Polarography, Czechoslovak Academy of Sciences, Prague, Czechoslovakia
with a preface by Professor J. Heyrovský

6 × 9″, 213 pages, 3 tables, 90 illus., 263 lit. refs., 1965, Dfl. 30.00, 60s., $11.00

Contents: Preface (J. Heyrovský); Author's Preface; 1. Introduction. 2. Examples of application of the oscillopolarographic method. 3. Practical oscillopolarographic exercises. 4. Maintenance of apparatus and construction of auxiliary electrical circuits. Index.

TABLE OF META-STABLE TRANSITIONS FOR USE IN MASS SPECTROMETRY

by J. H. BEYNON, R. A. SAUNDERS AND A. E. WILLIAMS
Research Department, Imperial Chemical Industries Ltd.,
Manchester, Great Britain

9½ × 6½″, xix + 392 pages, 1965, Dfl. 45.00, 90s., $16.50

These tables are intended to make it easy to determine the ionic reaction which gives rise to any meta-stable peak in a mass spectrometer, and will prove indispensable to any laboratory possessing this equipment. The introduction is given in English, German, French and Russian, to make the tables more generally useful.

STATIONARY PHASE IN PAPER AND THIN-LAYER CHROMATOGRAPHY

Second International Symposium organized by the Chromatography Group of the Czechoslovak Chemical Society, at Liblice
by K. MACEK AND I.M.HAIS

7 × 10″, 358 pages, 69 tables, 135 illus., 494 lit. refs., 3 coloured plates, 1965, Dfl. 42.50, 85s., $16.00

Contents: List of participants in the discussion. Introduction. Opening speech. I. Chromatography papers. II. Thin-layer materials. III. Stationary liquids and adsorbents in paper chromatography. IV. Stationary liquids and impregnations for thin layers. V. General problems of the stationary phase. Discussion. Closing remarks. Author index. Subject index.

ELSEVIER PUBLISHING COMPANY
AMSTERDAM LONDON NEW YORK